University of Calabria
Department of Physics
FIS/02 – Fisica Teorica Modelli e Metodi Matematici

PhD School "Archimede"
Curriculum in Physics and Quantum Technologies
Cycle XXV

Forward jets at LHC in pQCD

PhD Candidate: Beatrice MURDACA

Beatrice Murdaca

Supervisor

Prof. Alessandro PAPA

Curriculum Coordinator

Prof. Roberto FIORE

December 2012

To my family

Contents

Introduction

The standard model (SM) of the fundamental interactions and particles represents the framework of our present knowledge about the world. So far it passed all the experimental tests, but there are some sectors of the model which still wait for an experimental confirmation. The Large Hadron Collider (LHC) not only will give us the possibility to test the SM at energies never reached before, but also provided the possibility to investigate with good precision parton-parton scattering in a regime where the energy of hard partonic subprocess is much bigger than the hard scale involved. This corresponds to the kinematics where produced hadrons are separated by the large interval of rapidity, $\Delta y \gg 1$.
The understanding of the parton dynamics in this, semihard kinematic region is an important issue in strong interaction physics, it is also essential for the control over multijet background in the Higgs and electroweak boson production physics at LHC.

At $\alpha_s \Delta y \geq 1$ (α_s is a strong coupling) the cross sections of the partonic subprocesses receives large higher order corrections $\sim \alpha_s^n \left(\Delta y\right)^n$, which can be accounted for in the Balitsky-Fadin-Kuraev-Lipatov (BFKL) approach.
The $\gamma^*\gamma^*$ total cross section in e^+e^- scattering is considered to be the gold-plated BFKL measurement, but also LHC can provide an ideal opportunity to test BFKL-driven observable.
The candidate processes for this purpose are both central production processes, such as heavy quark productions and forward production of different systems such as high transverse momentum jets, heavy quark pairs or Drell-Yan pairs. In the case of two tagged forward/backward jets with a rapidity gap between

them, there could be no particular production between them ("Mueller-Tang") or not ("Mueller-Navelet"). These jet events allow then to test the forward (Mueller-Navelet) and non-forward (Mueller-Tang) BFKL kernel. In particular the Mueller-Navelet jets are one of the most famous testing ground for the BFKL and different description are proposed. For the Mueller-Tang jets so far we have at NLO accuracy the non-forward BFKL kernel, while impact factors are known only at leading order (LO). The limitation to LO impact factors is currently one of the main drawbacks of BFKL phenomenology. A promising tool to overcome this limitation is given by Lipatov's effective action. So far this action has been mainly applied for the determination of LO transition kernels.

The thesis is organized as follows. In the first two Chapters there is a brief overview on the BFKL approach and the Lipatov's effective action, respectively. In the second Chapter we will present the work in progress on the calculation of Mueller-Tang impact factor.
The last two Chapters are devoted to the derivation of impact factor for Mueller-Navelet jets and for the cross section of the process $p(p_1) + p(p_2) \to J(k_{J_1}) + J(k_{J_2}) + X$.

Chapter 1

The BFKL approach

1.1 Regge theory

In 1959 *Regge* [1] showed that, when discussing solutions of the Schrödinger equation for non-relativistic potential scattering, it is useful to regard the angular momentum, l, as a complex variable. He proved that for a wide class of potentials the only singularities of the scattering amplitude in the complex l plane were poles, now called "*Regge poles*" [2, 3]. If these poles occur for positive integer values of l they correspond to bound states or resonances, and they are also important for determining certain technical aspects of the dispersion properties of the amplitudes. They are located at values defined by a relation of the kind

$$l = \alpha(k) \ , \tag{1.1}$$

where $\alpha(k)$ is a function of the energy called *Regge trajectory*. Each family of bound states or resonances corresponds to a single trajectory like (1.1). The energies of these states are obtained from Eq. (1.1), assigning physical (i.e., integer) values to the angular momentum l.

The extension of Regge's technique to high-energy particle physics is originally due to Clew and Frautschi [4] (1961) and Gribov [5] (1961), but many more authors contributed to the theory and its applications. Under some hypotheses and using the general properties of the S-matrix, the relativistic partial wave amplitude $\mathcal{A}_l(t)$ can be analytically continued to complex l values in a unique

way. The resulting function, $\mathcal{A}(l,t)$, has simple poles at

$$l = \alpha(t) \ .$$

Each pole contributes to the scattering amplitude with a term which behaves asymptotically (i.e. for $s \to \infty$ and t fixed) as

$$A(s,t) \sim s^{\alpha(t)} \,, \tag{1.2}$$

where s and $-t$ are the square of the centre-of-mass energy and of the momentum transferred, respectively.
The leading singularity (i.e. the singularity with the largest real part) in the t-channel determines the asymptotic behavior of the scattering amplitude in the s-channel.
What is surprising is the wide success of Regge theory in its simplest form, namely the fact that a large class of processes is accurately described by such simple predictions as (1.2). That is why people tend to believe that Regge theory must contain at least a grain of truth.

1.1.1 The Pomeron

Regge theory belongs to the class of the so-called t-channel models. These models describe hadronic processes in terms of the t-channel exchange of "something".
In the simplest case of t-channel models, this "something" is a *virtual particle*. In the Regge theory is a *Regge trajectory*, i.e. a whole family of resonances. The large s-limit of a hadronic process is determined by the exchange of one or more Regge trajectories in the t-channel which are often called *Reggeons*. Exchanging Reggeons instead of particles leads to scattering amplitudes of the type of (1.2).
Via the optical theorem and from (1.2) the total cross sections in the Regge theory is:

$$\sigma_{tot} \simeq \frac{1}{s}\mathcal{I}mA(s,t=0) \sim s^{\alpha(0)-1} \,. \tag{1.3}$$

It is experimentally known that hadronic total cross sections, as a function of s, are rather flat around $\sqrt{s} \sim (10-20)$ GeV and increase at higher energies.

In order to account for asymptotically constant total cross sections, Chew, Frautschi and Gribov (1961) introduced a Regge trajectory with intercept one. This Reggeon was named *Pomeron*, after I.Ya. Pomeranchuk [6], and is denoted by $\mathbb{P}$. The Pomeron trajectory [7] does not correspond to any known particle; it results from a complicated exchange of gluons (at least two). It is the dominant trajectory in the elastic and diffractive processes, which are known to proceed via the exchange of vacuum quantum numbers in the t-channel.
Evidently the power growth of cross sections (1.3) violates the Froissart bound [8] $\sigma_{tot} < \text{const}\,(\ln s)^2$, which follows from unitarity. The violation of Froissart bound cannot be removed by calculation of relative corrections at any fixed order. A general approach to the unitarization problem is the reformulation of QCD in terms of a gauge-invariant affective field theory for the Reggeized gluon interactions [9, 10] (see Chapter 2).

1.2 BFKL equation

The BFKL equation [11, 12, 13, 14] became famous when the rapid growth of the $\gamma^* p$ cross section at increasing energy, predicted by Balitsky, Fadin, Kuraev and Lipatov (BFKL), was discovered at HERA. Therefore this equation is usually associated with the evolution of the unintegrated gluon distribution. The parton distributions serve as the inherent part in the theoretical description of hard QCD processes.
Evolution of the parton distributions with $\tau = \ln\left(Q^2/\Lambda^2_{QCD}\right)$ is determined by the DGLAP equations [15, 16, 17, 18, 19]. These equations permit to sum the perturbation series by powers of collinear logarithms $\ln Q^2$ so called because they are picked up from the region of small angles between parton momenta. There is another kind of logarithms: soft logarithms come from the ratios of parton energies. These logarithms are present both in parton distributions and in partonic cross sections. At small values of the ratio $x = \ln Q^2/s$ soft logarithms appear to be even more important than collinear ones.
For small values of x, large s, and fixed momentum transfer t, $s \gg |t|$ (Regge region), with various color states in the t-channel, the BFKL approach gives the description of QCD scattering amplitudes. The evolution equation for the

unintegrated gluon distribution appears in this approach as a particular result for the imaginary part of the forward scattering amplitude ($t = 0$ and vacuum quantum numbers in the t-channel). This approach was developed, and is more suitable, for the description of processes with only one hard scale, such as $\gamma^*\gamma^*$ scattering with both photon virtualities of the same order, where the DGLAP evolution (i.e. evolution in Q^2) is not appropriate.
The basis of the BFKL approach is the gluon reggeization, which can be described in oversimplified terms as the appearance of a modified propagator of the form (in Feynman gauge) (see, for instance, Ref. [7])

$$D_{\mu\nu}\left(s, q^2\right) \; = \; -\imath \frac{g_{\mu\nu}}{q^2} \left(\frac{s}{s_0}\right)^{\alpha_g\left(q^2\right)-1} \; ,$$

where $\alpha_g\left(q^2\right) = 1 + \epsilon\left(q^2\right)$ is the Regge trajectory of the gluon.

1.2.1 Gluon reggeization

The reggeization of an elementary particle (with spin j_0 and mass m) in perturbative theory was introduced in [20] and it means [21] that at large s and fixed t Born amplitudes with exchange of this particle in the t-channel acquire a factor $s^{j(t)-j_0}$, with $j(m^2) = j_0$. This phenomenon was discovered originally in QED in the backward Compton scattering [20]. It was called reggeization because just such form of amplitudes is given by the Regge poles (moving poles in the complex angular momentum plane, j-plane, introduced by Regge [1]).
In contrast to QED, where the electron does reggeize in perturbation theory [20], but the photon remains elementary [22], in QCD the gluon does reggeize [11, 12, 23, 24, 25] as well as the quark [26, 27, 28, 29]. Therefore QCD is the unique theory where all elementary particles reggeize.

The reggeization is very important for the theoretical description of high-energy processes with fixed momentum transfer. Especially important is the gluon reggeization, because cross sections non-decreasing with energy are provided by gluon exchanges and it determines the form of QCD amplitudes at large energies and limited transverse momenta.
The simplest realization of the gluon reggeization is in the elastic process $A +$

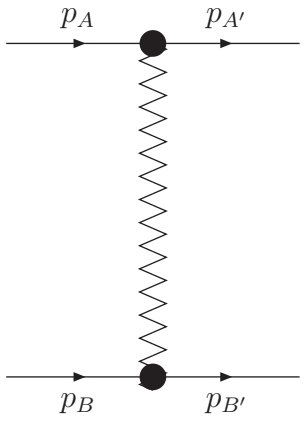

Figure 1.1: Diagrammatical rappresentation of the process $A + B \to A' + B'$ with color octet in the t-channel. The zig-zag line represent the Reggeized gluon exchange.

$B \to A' + B'$, where amplitudes with a color octet t-channel exchange and negative signature (schematically represented by the diagram of Fig. 1.1) take the form

$$(\mathcal{A}_8)^{A'B'}_{AB} = \Gamma^c_{A'A} \frac{s}{t} \left[\left(\frac{s}{-t} \right)^{\omega(t)} + \left(\frac{-s}{-t} \right)^{\omega(t)} \right] \Gamma^c_{B'B} \,, \tag{1.4}$$

where

$$s = (p_A + p_B)^2 \quad , \quad t = q^2 \quad , \quad q = p_A - p_{A'}$$

and $\omega(t)$ is the gluon trajectory, instead c is a color index and $\Gamma^c_{P'P}$ are the Particle-Particle-Reggeon (PPR) vertices which do not depend on s.

This factorization (1.4) represents correctly the analytical structure of the scattering amplitude, which is quite simple in the elastic case. It is valid in the leading logarithmic approximation (LLA), which means resummation of all terms $(\alpha_s \ln(s))^n$, and in the next-to-leading logarithmic approximation (NLA), which means resummation of all terms $\alpha_s(\alpha_s \ln(s))^n$. In particular it remains valid also for the case when any of the particles A', B' is replaced by a jet.

In general the PPR vertex can be written in the form $\Gamma^c_{P'P} = g\langle P'|T^c|P\rangle \Gamma_{P'P}$, where g is the QCD coupling and $\langle P'|T^c|P\rangle$ stands for a matrix element of the color group generator in the fundamental (adjoint) representation for quarks (gluons).

In the LLA this form of amplitude has been rigorously proved [11, 12, 13, 14].

In this approximation the helicity λ_p of the scattered particle P is conserved, so $\Gamma^{(0)}_{P'P}$ is given by $\delta_{\lambda_{P'}\lambda_P}$ and the Reggeized gluon trajectory is calculated with 1-loop accuracy (see, for instance, Ref. [30]),

$$\omega\left(t\right) \simeq \omega^{(1)}\left(t\right) = \frac{g^2 t}{\left(2\pi\right)^{(D-1)}} \frac{N_c}{2} \int \frac{d^{D-2}k_\perp}{k_\perp^2 \left(q-k\right)_\perp^2} = -\frac{g^2 N_c \Gamma\left(1-\varepsilon\right)}{\left(4\pi\right)^{D/2}} \frac{\Gamma^2\left(\varepsilon\right)}{\Gamma\left(2\varepsilon\right)} \left(\vec{q}^{\,2}\right)^{\varepsilon}$$

where $t = q^2 \approx q_\perp^2$, $D = 4+2\varepsilon$ is the space-time dimension and N_c is the number of QCD colors. The ε parameter has been introduced in order to regularize the infrared divergences and the integration is performed in a $(D-2)$-dimensional space, orthogonal to the momenta of the initial colliding particles p_A and p_B. The gluon reggeization determines also inelastic amplitudes in the multi-Regge-kinematics (MRK) where all particles are strongly ordered in the rapidity space with limited transverse momenta and the squared invariant masses $s_{ij} = \left(k_i + k_j\right)^2$ of any pair of produced particles i and j are large (increasing with s). In QCD processes this kinematic gives dominant contributions to cross section. In the LLA, there are exchanges of vector particles (i.e. gluons) in all channels. In NLLA, contrary to LLA, MRK is not a single kinematic that contributes. Any pair, but only one, of the produced particles can have a fixed (not increasing with s) invariant mass, i.e. components of this pair can have rapidities of the same order. This kinematics was called [31] quasi-multi-Regge-kinematics (QMRK).

In the next-to-leading-logarithm approximation the form (1.4) has been checked in the first three orders of perturbative theory and is only assumed to be valid to all orders [32, 33, 34, 35, 36]. A rigorous proof of gluon reggeization does not exist in the NLLA, but it is possible impose and prove some stringent self-consistency conditions (bootstrap conditions [37]).

1.2.2 The $2 \to 2$ scattering amplitude in multi-Regge kinematics.

The gluon reggeization determines amplitudes with color octet states and negative signature in the t-channels. Amplitudes with other quantum numbers are found in the BFKL approach using s-channel unitarity. In the unitarity relations the contribution of order s is given by the MRK. Large logarithms

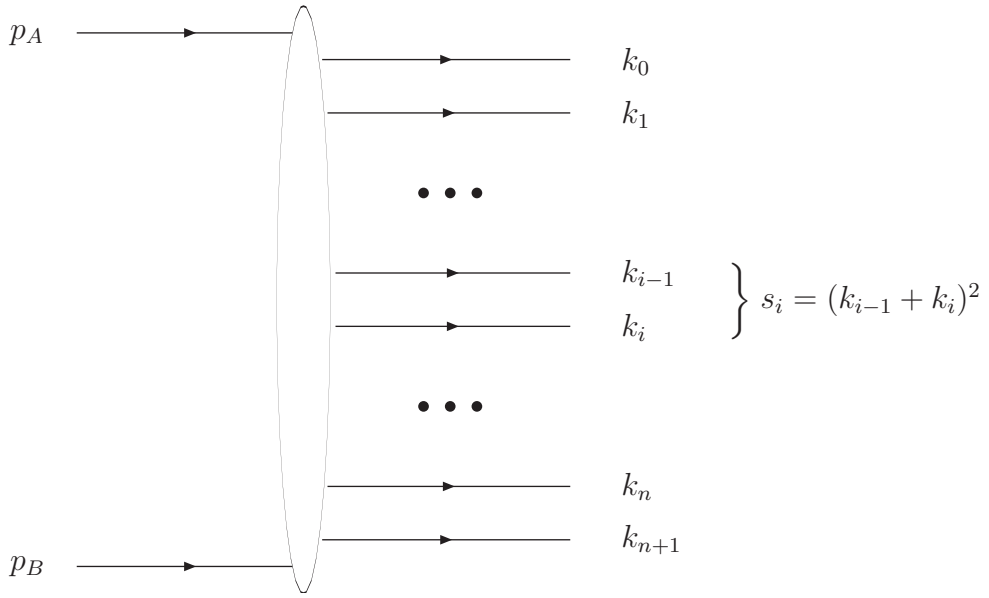

Figure 1.2: Schematic representation of the s-channel unitarity relation.

come from integration over longitudinal momenta of the produced particles.
In an elastic process $A+B \to A'+B'$, from the Cutkosky rule [38], the imaginary part of the elastic scattering amplitude $\mathcal{A}_{AB}^{A'B'}$ can be presented as (s-unitarity relation)

$$\mathcal{I}m_s \mathcal{A}_{AB}^{A'B'} = \frac{1}{2} \sum_{n=0}^{\infty} \sum_{\{f\}} \int \mathcal{A}_{AB}^{\tilde{A}\tilde{B}+n} \left(\mathcal{A}_{A'B'}^{\tilde{A}\tilde{B}+n} \right)^* d\Phi_{\tilde{A}\tilde{B}+n} \,, \tag{1.5}$$

where $\mathcal{A}_{AB}^{\tilde{A}\tilde{B}+n}$ is the amplitude of the production of $n+2$ particles (Figs. 1.2 and 1.3) with momenta $k_i \,, i = 0, 1, ..., n, n+1$ in the process $A+B \to \tilde{A}+\tilde{B}+n$, while $d\phi_{\tilde{A}\tilde{B}+n}$ is the element of intermediate state phase space and $\sum_{\{f\}}$ means sum over the discrete quantum numbers of intermediate particles.
We assume that the momenta of the initial particles A and B are equal to $p_A = p_1 + (m_A^2/s)\, p_2$ and $p_B = p_2 + (m_B^2/s)\, p_1$, respectively. For any momentum k_i the Sudakov decomposition is given by

$$k_i = \beta_i p_1 + \alpha_i p_2 + k_{i\perp} \,, \tag{1.6}$$

where p_1 and p_2 are light-like vectors ($p_1^2 = p_2^2 = 0$) and $(p_1 + p_2)^2 = 2p_1 \cdot p_2 = s$,

$$s\alpha_i\beta_i = k_i^2 - k_{i\perp}^2 = k_i^2 + \vec{k}_i^{\,2} \,,$$

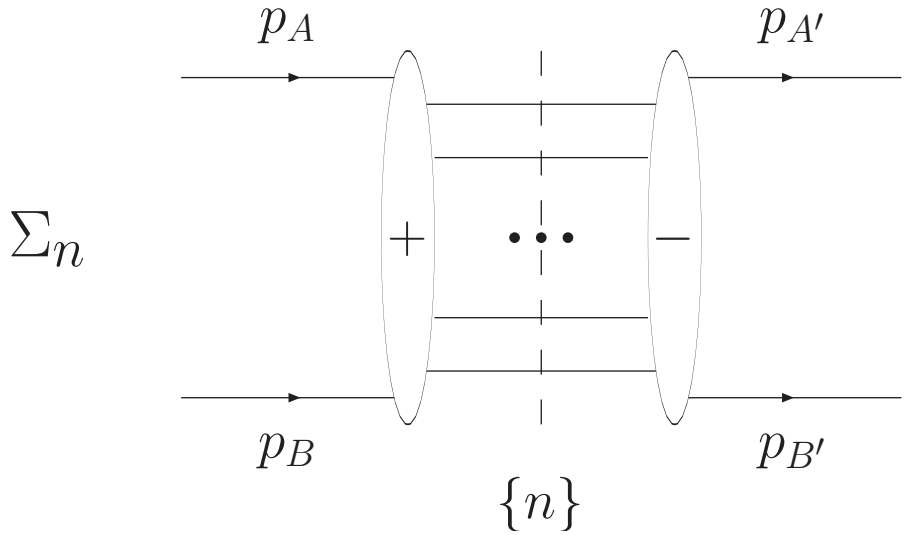

Figure 1.3: Schematic representation of the s-channel unitarity relation.

where $\vec{k}_{i\perp}$ denotes the transverse momentum and $k_{i\perp}^2 \equiv -\vec{k}_i^{\,2}$.
With this decomposition we obtain for the phase space

$$\begin{aligned} d\Phi_{\tilde{A}\tilde{B}+n} &= \frac{2}{s}(2\pi)^D \delta\left(1+\frac{m_A^2}{s}-\sum_{i=0}^{n+1}\alpha_i\right)\delta\left(1+\frac{m_B^2}{s}-\sum_{i=0}^{n+1}\beta_i\right) \\ &\times\delta^{D-2}\left(\sum_{i=0}^{n+1}k_{i\perp}\right)\frac{d\beta_{n+1}}{2\beta_{n+1}}\frac{d\alpha_0}{2\alpha_0}\prod_{i=1}^{n}\frac{d\beta_i}{2\beta_i}\prod_{i=0}^{n+1}\frac{d^{D-2}k_{i\perp}}{(2\pi)^{D-1}}\,, \end{aligned} \tag{1.7}$$

with the denotations

$$p_{\tilde{A}} = k_0\,, \qquad p_{\tilde{B}} = k_{n+1}\,.$$

In the unitarity condition (1.5) the dominant contribution (of order of s) in the LLA is given by the region of limited (not growing with s) transverse momenta of produced particles.
As we said, large logarithms come from the integration over longitudinal momenta of the produced particles. In particular we have a logarithm of s for every particle produced in a particular kinematics called multi-Regge-kinematics (MRK). By definition, in this kinematics transverse momenta of the produced particles are limited and their Sudakov variables α_i and β_i are strongly ordered in rapidity space. That means,

$$\alpha_{n+1} \gg \alpha_n \gg \alpha_{n-1}... \gg \alpha_0\,, \quad \beta_0 \gg \beta_1 \gg \beta_2... \gg \beta_{n+1}\,. \tag{1.8}$$

Eqs. (1.6) and (1.8) ensure the squared invariant masses of neighboring particles,

$$s_i = (k_{i-1} + k_i)^2 \approx s\beta_{i-1}\alpha_i = \frac{\beta_{i-1}}{\beta_i}\left(k_i^2 + \vec{k}_i^{\,2}\right) ,$$

to be large compared with the squared transverse momenta:

$$s_i \gg \vec{k}_i^{\,2} \sim |t_i| = q_i^2 ,$$

where

$$t_i = q_i^2 \approx q_{i\perp}^2 = -\vec{q}_i^{\,2} ,$$

and their product is proportional to s:

$$\prod_{i=1}^{n+1} s_i = s\prod_{i=1}^{n}\left(k_i^2 + \vec{k}_i^{\,2}\right) .$$

In order to obtain the large logarithm from the integration over β_i for each produced particle in the phase space (1.7), the amplitude in the r.h.s. in (1.5) must not decrease with the growth of the invariant masses. This is possible only in the case where there are exchanges of vector particles (i.e. gluons) in all channels with momentum transfers $q_i, i = 1 \div n+1$ with

$$q_i = p_A - \sum_{j=0}^{i-1} k_j = -\left(p_b - \sum_{l=i}^{n+1} k_l\right) \simeq \beta_i p_1 - \alpha_{i-1} p_2 - \sum_{j=0}^{i-1} k_{j\perp}, \;\; q_i^2 \simeq q_{i\perp}^2 = -\vec{q}_i^{\,2} .$$

The amplitudes dominant in each order of perturbative theory can be represented as in Fig. 1.4 . Multi-particle amplitudes have a complicated analytical structure. They are not simple even in MRK (see, for instance, Refs. [39, 40, 41, 42]). Fortunately, only real parts of these amplitudes are used in the BFKL approach in NLA as well as in LLA. Restricting ourselves to the real parts we can write (see Ref. [43])

$$\begin{aligned} \mathcal{A}_{AB}^{\tilde{A}\tilde{B}+n} &= 2s\Gamma_{\tilde{A}A}^{c_1}\left(\prod_{i=1}^{n}\gamma_{c_i c_{i+1}}^{P_i}(q_i, q_{i+1})\left(\frac{s_i}{s_R}\right)^{\omega(t_i)}\frac{1}{t_i}\right) \\ &\times \frac{1}{t_{n+1}}\left(\frac{s_{n+1}}{s_R}\right)^{\omega(t_{n+1})}\Gamma_{\tilde{B}B}^{c_{n+1}} , \end{aligned} \tag{1.9}$$

where s_R is some energy scale, which is irrelevant in LLA; $\omega(t)$ and $\Gamma_{P'P}^{a}$ are the gluon Regge trajectory and the PPR, as in (1.5); $\gamma_{c_i c_{i+1}}^{P_i}(q_i, q_{i+1})$ are the

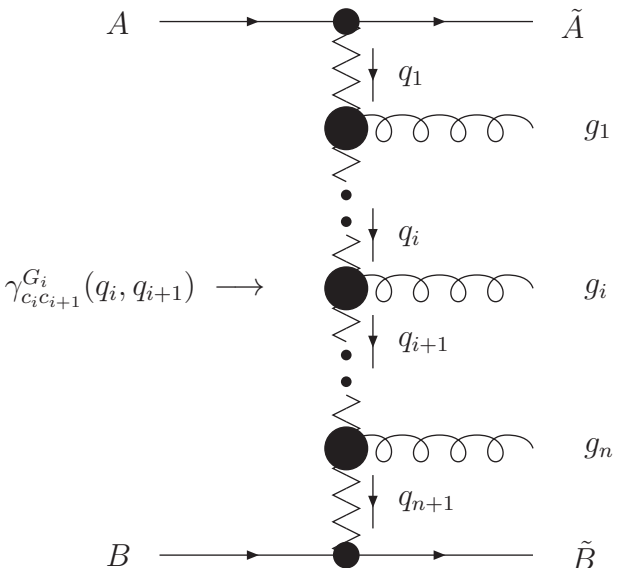

Figure 1.4: Schematic representation of the amplitude $\mathcal{A}_{AB}^{\tilde{A}\tilde{B}+n}$.

Reggeon-Reggeon-Particle (RRP) vertices, i.e. the effective vertices for the production of particles P_i with momenta $q_i - q_{i+1}$ in collisions of Reggeons (i.e. Reggeized gluons) with momenta q_i and $-q_{i+1}$ and color indices c_i and c_{i+1}, respectively. In the LLA only one gluon can be produced in the RRP vertex; therefore, the masses of the produced particles are equal to zero. The Reggeon-Reggeon-Gluon (RRG) vertex has the form [11, 12, 13, 14]

$$\gamma^{G_i}_{c_i c_{i+1}}(q_i, q_{i+1}) = g T^{d_i}_{c_i c_{i+1}} e^*_\mu(k_i)\, C^\mu(q_{i+1}, q_i)\ ,$$

where $T^{d_i}_{c_i c_{i+1}}$ are the matrix elements of the $SU(N_c)$ group generators in the adjoint representation, d_i is the color index of the produced gluon, $e^*_\mu(k_i)$ its polarization vector, $k_i = q_i - q_{i+1}$ its momentum and

$$\begin{aligned} C^\mu(q_i, q_{i+1}) &= -q_i^\mu - q_{i+1}^\mu + p_1^\mu \left(\frac{q_i^2}{k_i \cdot p_1} + 2\frac{k_i \cdot p_2}{p_1 \cdot p_2} \right) \\ &- p_2^\mu \left(\frac{q_{i+1}^2}{k_i \cdot p_2} + 2\frac{k_i \cdot p_1}{p_1 \cdot p_2} \right) . \end{aligned} \tag{1.10}$$

The Eq. (1.10) has the important property corresponding to the current conservation

$$(k_i)_\mu\, C^\mu(q_{i+1}, q_i) = 0\,,$$

which gives the possibility to choose an arbitrary gauge for each of the produced gluons. For example a possible choice can be the left (l) light-cone gauge, in which $p_A e^l(k) = 0$ that allows, together with $k e^l(k) = 0$, to write the polarization vector $e^l(k)$ as

$$e^l = e^l_\perp - \frac{k_\perp e^l_\perp}{k p_A} p_A \,.$$

Introducing in this gauge the complex components $e = e_x + \imath e_y$, $e^* = e_x + \imath e_y$ and $k = k_x + \imath k_y$, $k^* = k_x - \imath k_y$ for transverse vectors $e^l_\perp$ and $k_\perp$ [44], the RRP vertex takes a simple form

$$\Gamma^1_{2,1} = C e^* + C^* e \,, \text{ with } C = \frac{q_1^* q_2}{k_1^*} \,.$$

Let us introduce now the following decomposition

$$T^{d_i}_{c_i c_{i+1}} \left(T_{c'_i c'_{i+1}} \right)^* = \sum_R c_R \langle c_i c'_i | \hat{\mathcal{P}}_R | c_{i+1} c'_{i+1} \rangle \,, \tag{1.11}$$

where $\hat{\mathcal{P}}_R$ is the projection operator of the two-gluon color states on the irreducible representation R of the color group.
For the singlet (vacuum) and antisymmetrical octet (gluon) representations we have

$$\langle c_i c'_i | \hat{\mathcal{P}}_0 | c_{i+1} c'_{i+1} \rangle = \frac{\delta_{c_i c'_i} \delta_{c_{i+1} c'_{i+1}}}{N_c^2 - 1}$$

$$\langle c_i c'_i | \hat{\mathcal{P}}_8 | c_{i+1} c'_{i+1} \rangle = \frac{f_{a c_i c'_i} f_{a c_{i+1} c'_{i+1}}}{N_c} \,,$$

respectively, where f_{abc} are the $SU(N_c)$ structure constant. So it easy to find

$$c_0 = N_c, \quad c_8 = \frac{N_c}{2} \,.$$

Using the decomposition (1.11)

$$\begin{aligned} \sum_{G_i} \gamma^{G_i}_{c_i c_{i+1}} (q_i, q_{i+1}) \left(\gamma^{G_i}_{c'_i c'_{i+1}} (q_i, q_{i+1}) \right)^* &= \sum_R \langle c_i c'_i | \hat{\mathcal{P}}_R | c_{i+1} c'_{i+1} \rangle \\ &\times 2 (2\pi)^{D-1} \mathcal{K}^{(R)}_r (\vec{q}_i, \vec{q}_{i+1}; \vec{q}) \,, \end{aligned} \tag{1.12}$$

where the sum is taken over color and polarization states of the produced gluon and $\mathcal{K}^{(R)}_r (\vec{q}_i, \vec{q}_{i+1}; \vec{q})$ will be called *real part of the kernel*.

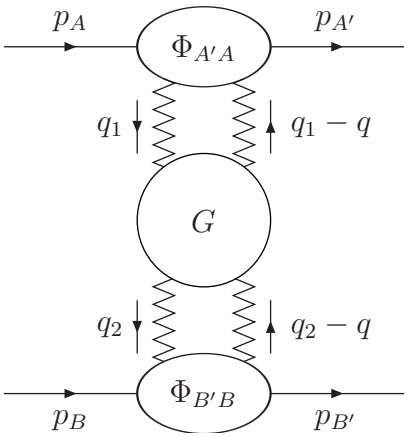

Figure 1.5: Schematic representation of the imaginary part of the BFKL elastic amplitude.

The BFKL equation It is obtained using the amplitude (1.9) in the unitarity relation (1.5) for the s-channel imaginary part of the elastic scattering amplitude.

Corrisponding to the decomposition (1.11), the elastic scattering amplitude $\mathcal{A}_{\mathcal{A}\mathcal{B}}^{\mathcal{A}'\mathcal{B}'}$ in (1.5) assumes the following form:

$$\mathcal{A}_{\mathcal{A}\mathcal{B}}^{\mathcal{A}'\mathcal{B}'} = \sum_{\mathcal{R}} \left(\mathcal{A}_{\mathcal{R}}\right)_{\mathcal{A}\mathcal{B}}^{\mathcal{A}'\mathcal{B}'} \ ,$$

where $\left(\mathcal{A}_{\mathcal{R}}\right)_{AB}^{A'B'}$ is the part of the scattering amplitude corresponding to a definite irreducible representation R of the color group in the t-channel.

Using the amplitude (1.9) in the unitarity relation (1.5) for the s-channel imaginary part of the elastic scattering amplitude, we get an expression that can be factorized [30] in the following way (see Fig. 1.5):

$$\begin{aligned} \mathcal{I}m_s \left(\mathcal{A}_{\mathcal{R}}\right)_{AB}^{A'B'} \ = \ & \frac{s}{\left(2\pi\right)^{D-2}} \int \frac{d^{D-2}q_1}{\vec{q}_1^{\,2}\left(\vec{q}_1 - \vec{q}\right)^2} \int \frac{d^{D-2}q_2}{\vec{q}_2^{\,2}\left(\vec{q}_2 - \vec{q}\right)^2} \sum_{\nu} \Phi_{A'A}^{(R,\nu)}\left(\vec{q}_1; \vec{q}; s_0\right) \\ & \times \int_{\delta - \imath\infty}^{\delta + \imath\infty} \frac{d\omega}{2\pi\imath} \left[\left(\frac{s}{s_0}\right)^{\omega} G_{\omega}^{(R)}\left(\vec{q}_1, \vec{q}_2, \vec{q}\right)\right] \Phi_{B'B}^{(R,\nu)}\left(-\vec{q}_2; -\vec{q}; s_0\right) \ , \end{aligned} \tag{1.13}$$

Here $\vec{q}_1$ and $\vec{q}_2$ are the transverse momenta of the Reggeized gluons, while s_0 is the energy scale (which can be, in principle, arbitrary) introduced in order to define the partial wave expansion of the scattering amplitudes through the Mellin

transform, the index ν enumerates the state in the irreducible representation R, $\Phi^{(R,\nu)}_{P'P}\left(\vec{q}_1;\vec{q};s_0\right)$ are the so-called impact factors, that are the convolution of two PPR vertex. $G^{(R)}_{\omega}$, which can be called Green function for scattering of two Reggeized gluons, is a Mellin transform. This function is the only quantity that determines the s-dependence of the scattering amplitude and it is universal, i.e. it does not depend on the particular process.
On the other hand, the impact factors are related to the particles on the external lines. They can be expressed through the imaginary part of the particle-Reggeon scattering amplitudes. They take the form [43]

$$\Phi^{(R,\nu)}_{P'P}\left(\vec{q}_R;\vec{q};s_0\right) = \int\frac{ds_{PR}}{2\pi s}\,\mathcal{I}m\,\mathcal{A}^{(R,\nu)}_{P'P}\left(p_P,q_R;\vec{q};s_0\right)\theta\left(s_\Lambda - s_{PR}\right) \quad (1.14)$$
$$-\frac{1}{2}\int\frac{d^{D-2}q'}{\vec{q}\,'^2\left(\vec{q}\,'-\vec{q}\right)^2}\Phi^{(R,\nu)B}_{P'P}\left(\vec{q}\,',\vec{q}\right)\mathcal{K}^{(R)B}_{r}\left(\vec{q}\,',\vec{q}_R\right)\ln\left(\frac{s^2_\Lambda}{\left(\vec{q}\,'-\vec{q}_R\right)s_0}\right),$$

where $s_{PR} = \left(q_p - q_R\right)^2$ is the squared particle-Regeon invariant mass while $\mathcal{I}m\mathcal{A}^{(\mathcal{R},\nu)}_{\mathcal{P}'\mathcal{P}}$ is the s_{PR}-channel imaginary part of the scattering amplitude of the particle P with momentum p_P off Reggeon with momentum $-q_R$, $\vec{q}$ being the momentum transfer. It can be shown that this definition is valid both in the LLA and in the NLLA.
In the former case, the second terms in the right hand side of the above equation as well as the θ function in the first term are not active. The parameter s_Λ, which limits the integration over s_{PR} is introduced in order to separate the contributions from multi-Regge and quasi-multi-Regge kinematics and is to be considered as tending to infinity. In this way the second term in the R.H.S. of (1.14) behaves as a counterterm for the large s_{PR} and it will be attribute to the quark-gluon intermediate state.

The Green's function obeys the integral equation called generalized BFKL equation (Fig. 1.6)

$$\begin{aligned}\omega G^{(R)}_{\omega}\left(\vec{q}_1,\vec{q}_2;\vec{q}\right) &= \vec{q}_1^{\,2}\left(\vec{q}_1-\vec{q}\right)^2\delta^{(D-2)}\left(\vec{q}_1-\vec{q}_2\right) + \int\frac{d^{D-2}q_1'}{\vec{q}_1'^{\,2}\left(\vec{q}_1\,'-\vec{q}\right)^2}\\ &\times\ \mathcal{K}^{(R)}\left(\vec{q}_1,\vec{q}_2;\vec{q}\right)G^{(R)}_{\omega}\left(\vec{q}_1,\vec{q}_2;\vec{q}\right), \qquad (1.15)\end{aligned}$$

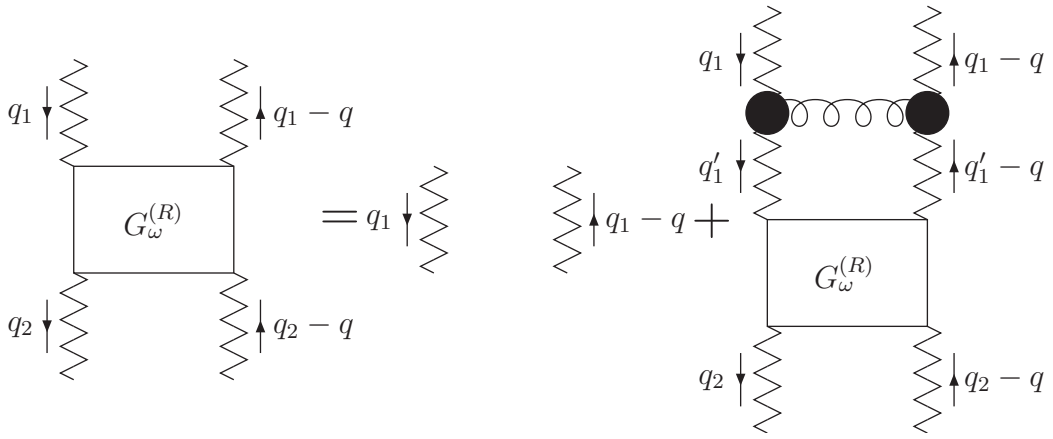

Figure 1.6: Schematic representation of integral equation for $G_\omega^{(R)}$.

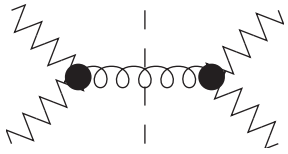

Figure 1.7: Schematic representation or real part of kernel at Born approximation.

where $\mathcal{K}^{(R)}$ is the kernel of the integral function and consists of two parts: a virtual part, which is expressed in terms of the gluon Regge trajectory and the real part $\mathcal{K}_r^{(R)}$ related to the real particle production in Reggeon-Reggeon collisions. It has the following expression:

$$\begin{aligned}\mathcal{K}^{(R)}\left(\vec{q}_1,\vec{q}_2;\vec{q}\right) &= \left[\omega\left(\vec{q}_{1\perp}^{\,2}\right)+\omega\left(\left(q_1-q\right)_\perp^2\right)\right]\vec{q}_1^{\,2}\left(\vec{q}_1-\vec{q}\right)^2\delta^{(D-2)}\left(\vec{q}_1-\vec{q}_2\right)\\ &+ \mathcal{K}_r^{(R)}\left(\vec{q}_1,\vec{q}_2;\vec{q}\right),\end{aligned}$$

where $\mathcal{K}_r^{(R)}\left(\vec{q}_1,\vec{q}_2;\vec{q}\right)$ is the real part (see Fig. 1.7) and it reads

$$\begin{aligned}\mathcal{K}_r^{(R)}\left(\vec{q}_i,\vec{q}_{i+1};\vec{q}\right) &= -\frac{g^2 c_R}{2\left(2\pi\right)^{D-1}}C^\mu\left(q_{i+1},q_i\right)C_\mu\left(q_{i+1}-q,q_i-q\right) \qquad (1.16)\\ &= \frac{g^2 c_R}{\left(2\pi\right)^{D-1}}\left(\frac{\vec{q}_i^{\,2}\left(\vec{q}_{i+1}-\vec{q}\right)^2+\vec{q}_{i+1}^{\,2}\left(\vec{q}_i-\vec{q}\right)^2}{\left(\vec{q}_i-\vec{q}_{i+1}\right)^2}-\vec{q}^{\,2}\right).\end{aligned}$$

If $R=0$ the equation (1.15) is called BFKL equation.
The integral equation (1.15) is an iterative equation; in fact, knowing the kern at Born level, it allows to obtain all the LLA terms of the Green's function. In

the same way knowing all the NLLA correction to the gluon trajectory and to the real part of the kernel, it is possible to obtain all the NLLA terms of the Green's function.
In order to obtain a full amplitude what remains to be calculated is the impact factors, which are in most cases non-perturbative objects for real processes.

The BFKL equation in NLLA In the NLLA, where all terms of the type $\alpha_s \left[\alpha_s \ln(s)\right]^n$ have to be collected, the PPR vertex in (1.4) assumes the following expression

$$\Gamma_{P'P} = \delta_{\lambda_P,\lambda_{P'}} \Gamma^{(+)}_{PP} + \delta_{\lambda_{P'},-\lambda_P} \Gamma^{(-)}_{PP} \,.$$

In this approximation here appears a term in which the helicity of the scattering particle P is not conserved.
To obtain production amplitudes in the NLLA it is sufficient to take one of the vertices or the trajectory in (1.9) in the NLO. In the LLA, the Reggeized gluon trajectory is needed at 1-loop accuracy and the only contribution to the "real" part of the kernel is from the production of one gluon at Born level in the collision of two Reggeons ($\mathcal{K}^B_{RRG}$) [30]. In the NLLA the gluon trajectory is taken in the NLO (2-loop accuracy [32, 33, 34, 35, 36]) and the real part includes the contributions coming from one-gluon ($\mathcal{K}^1_{RRG}$ [45]), two-gluon ($\mathcal{K}^B_{RRGG}$ [46, 47, 48, 49]) and quark-antiquark pair ($\mathcal{K}^B_{RRQ\bar{Q}}$ [50, 51, 52, 53]) production at Born level [30].

Cross section Due to the *Optical Theorem* (for instance [7]), the total cross section is related to the imaginary part of the forward scattering amplitude ($\vec{q} = 0$) and in particular it can be expressed by

$$\sigma_{AB}(s) \;=\; \frac{\mathcal{I}m\mathcal{A}^{AB}_{AB}}{s} \,, \tag{1.17}$$

where the $\mathcal{I}m\mathcal{A}^{AB}_{AB}$ is given in (1.13), and one can find:

$$\begin{aligned} \sigma_{AB}(s) \;=\; & \frac{1}{(2\pi)^{D-2}} \int \frac{d^{D-2}q_A}{\left(\vec{q}_A^{\,2}\right)^2} \Phi_A(\vec{q}_A) \int_{\delta-\imath\infty}^{\delta+\imath\infty} \frac{d\omega}{2\pi\imath} \left(\frac{s}{s_0}\right)^{\omega} G_\omega(\vec{q}_A, \vec{q}_B) \\ & \times \int \frac{d^{D-2}q_B}{\left(\vec{q}_B^{\,2}\right)^2} \Phi_B(-\vec{q}_B) \,. \end{aligned} \tag{1.18}$$

From this equation it is possible to see that if the Green's function $G_\omega\left(\vec{q}_A, \vec{q}_B\right)$ has a pole at ω', the cross section takes the form

$$\sigma_{tot}^{LLA} \sim \frac{s^{\omega_P^B}}{\sqrt{\ln s}}\,, \qquad \omega' \equiv \omega_P^B\,,$$

where ω_P^B is the intercept at $t = 0$ of the Regge trajectory that rules the asymptotic behaviour in s of the amplitude with exchange of vacuum quantum numbers in the t-channel. It is equal to $4N_c\left(\alpha_s/\pi\right)\ln 2$ which signifies violation of the Froissart bound [8].

The NLO corrections to the BFKL resummation of the energy logarithms were calculated, see Refs. [54, 55] and references therein.
We do not know the eigenfunctions of the kernel at NLO, but it is possible to find its action on the eigenfunctions $|\nu\rangle$ of the Born kernel

$$\begin{aligned}\hat{K}|\nu\rangle &= \bar{\alpha}_s(\mu_R)\chi(\nu)|\nu\rangle + \bar{\alpha}_s^2(\mu_R)\left(\frac{\beta_0}{4N_c}\chi(\nu)\ln(\mu_R^2)\chi^{(1)}\left(\nu\right)\right)|\nu\rangle \\ &+ \bar{\alpha}_s^2\left(\mu_R\right)\frac{\beta_0}{4N_c}\chi\left(\nu\right)\left(i\frac{\partial}{\partial\nu}\right)|\nu\rangle\,, \end{aligned} \tag{1.19}$$

where the first term represents the action of LLA kernel, the second and the third ones stand for the diagonal and the non-diagonal parts of the NLA BFKL kernel (for more details, see Section 4.2). In particular the last term comes from the renormalization of the coupling constant.
In the symmetrical case, when $\nu = 0$, corresponding to the eigenfunction of the LLA kernel with the largest eigenvalue, the correction is very large. In particular, for the Pomeron intercept, is possible to obtain (see Refs. [54, 55] and references therein)

$$\omega_P \simeq \omega_P^B\left(1 - 2.4\;\omega_P^B\right). \tag{1.20}$$

The NLO corrections to the eigenvalue of the BFKL equation turn out to be negative and even larger than the LO contribution for $\alpha_s > 0.157$.
This problem has been addressed in many papers, which suggested several ways..... We mention here only two of them: the "rapidity veto" approach [56, 57] and the "collinear improvement" method [58].

1.3 Summary

The BFKL approach [11, 12, 13, 14] is the most suitable framework for the theoretical description of the high-energy limit of hard or semi-hard processes. It provides indeed a systematic way to perform the resummation of the energy logarithms, both in the leading logarithmic approximation (LLA), which means resummation of all terms $(\alpha_s \ln(s))^n$, and in the next-to-leading logarithmic approximation (NLA), which means resummation of all terms $\alpha_s(\alpha_s \ln(s))^n$.
The total cross section is given by

$$\sigma(s) = \frac{\mathcal{I}m_s\mathcal{A}}{s} \tag{1.21}$$

where $\mathcal{I}m_s\mathcal{A}$ is the imaginary part of forward scattering amplitude and in the BFKL approach at NLA it reads

$$\begin{aligned}\mathcal{I}m_s A &= \frac{s}{(2\pi)^{D-2}} \int \frac{d^{D-2}q_A}{\left(\vec{q}_A^{\,2}\right)^2} \Phi_A(\vec{q}_A) \int_{\delta-\imath\infty}^{\delta+\imath\infty} \frac{d\omega}{2\pi\imath} \left(\frac{s}{s_0}\right)^{\omega} G_\omega(\vec{q}_A, \vec{q}_B) \\ &\quad \times \int \frac{d^{D-2}q_B}{\left(\vec{q}_B^{\,2}\right)^2} \Phi_B(-\vec{q}_B) \ . \end{aligned} \tag{1.22}$$

The energy scale parameter s_0 is arbitrary, the amplitude, indeed, does not depend on its choice within NLA accuracy due to the properties of NLO impact factors.
The $G_\omega(\vec{q}_A, \vec{q}_B)$ is called Green's function and obeys the BFKL equation (1.15), while $\Phi_A(\vec{q}_A)$ and $\Phi_B(\vec{q}_B)$ are called impact factors (1.14).
The Green's function is process-independent so, in order to obtain a full amplitude, we have to calculate the process-dependent impact factors. So far only very few have been calculated in the NLA and in particular:

- colliding partons [59, 60, 61, 62]
- the $\gamma^* \to \gamma^*$ transition [63, 64, 65, 66, 67, 68, 69]
- the γ^* to light vector meson transition at leading twist [70, 71]
- forward jet production [72, 73, 74, 75].

Chapter 2

Lipatov's high-energy effective action

The BFKL approach (see Chapter 1) is applied to describe the hadronic scattering amplitudes in the Regge kinematic ($s \to \infty$, $s \gg -t$) and the high-energy behavior of the total cross sections for semi-hard QCD processes ($Q^2 \gg \Lambda^2_{QCD}$). In the leading logarithmic approximation (LLA), the BFKL equation predicts a power-like rise of cross sections with energy, which violates the Froissart constraint $\sigma_t < c \ln^2 s$ being a consequence of the s-channel unitarity. One possible method to overcome this difficulty is to take into account the multiple Pomeron exchanges in the eikonal approximation [76]. A more consistent approach is based on the solution of the BKP (Bartels, Kwiecinski, Praszalowicz) equation [77, 78] which is a generalization of the BFKL equation for the case of composite states of several Reggeized gluons [77, 78].
For the unitarization purpose, it is also possible to use an effective Lagrangian written for the Multi-Regge-Kinematics of gluons in intermediate states of the direct s- and u-channels [44, 79]. The most general approach consists in reformulating QCD in terms of a gauge-invariant effective field theory for the Reggeized gluon interactions: this is the *effective action* [9, 10], which is based on the QCD action with the addition of an induced term.

2.1 Effective action approach

Due to the gluon reggeization it is natural to expect that QCD, at high energies, can be reformulated as an interaction theory for physical particles (quarks and gluons) and Reggeized gluons. This reformulation is given [9] by the effective action which is valid at high energies for interactions of particles having their rapidities y in a certain interval η around the rapidity y_0,

$$y = \frac{1}{2} \ln \frac{E_k + |k|}{E_k - |k|} , \quad |y - y_0| < \eta , \quad \eta \ll \ln s . \tag{2.1}$$

This means that particles which are produced in direct channels can be arranged in groups (clusters) consisting of gluons within some rapidity intervals $(y - \eta/2, y + \eta/2)$, where η is an auxiliary parameter, smaller than the relative rapidity of colliding particles $Y = \ln s$,

$$1 \ll \eta \ll Y . \tag{2.2}$$

This parameter represents an infrared or ultraviolet cut-off in the relative longitudinal momenta for interactions between the neighbouring groups and for interactions among particles inside each group, respectively.
The η-dependence should disappear in the final result analogously to the case of the normalization point dependence in hard processes. In the (LLA) all transverse momenta $k_\perp$ of gluons in the Feynman diagrams are of the same order as transverse momenta $p_\perp$ of partons inside of colliding hadrons [11, 12, 14, 25]. This means that the center-of-mass pair energy $\sqrt{s_i}$ of the neighbouring gluons in the Multi-Regge-Kinematics is significantly bigger than $p_\perp$ and the effective parameter of the perturbation theory is $g^2 \ln (s/p_\perp^2)$. Beyond LLA one should introduce the above parameter η in the analogous inequality for the pair energies of the neighbouring clusters of particles

$$\ln \frac{s_i}{p_\perp^2} . \tag{2.3}$$

In order to write the high-energy effective action we introduce the gluon and quark fields

$$v_\mu (x) = -\imath T^a v_\mu^a (x) , \quad \psi (x) , \quad \bar{\psi} (x) , \quad \left[T^a, T^b\right] = \imath f_{abc} T^c . \tag{2.4}$$

and new fields $A_\pm$

$$A^\pm = A_\mp = A^0 \pm A^3\,,\ p_A^\mu A_\mu = \frac{\sqrt{s}}{2}A^-\,,\ p_B^\mu A_\mu = \frac{\sqrt{s}}{2}A^+\,, \tag{2.5}$$

which describe the production and annihilation of the Reggeized gluons in the t-channel.
Under the global color group rotations the fields are transformed in the standard way

$$\delta v_\mu(x) = [v_\mu(x), \chi]\ ,\quad \delta\psi(x) = -\chi\psi(x)\ ,\quad \delta A(x) = [A(x), \chi]\ , \tag{2.6}$$

but under the local gauge transformations with $\chi(x) \to 0$ at $x \to \infty$ we have

$$\delta v_\mu(x) = \frac{1}{g}[D_\mu, \chi(x)]\ ,\quad \delta\psi(x) = -\chi(x)\psi(x)\ ,\quad \delta A_\pm(x) = 0\,, \tag{2.7}$$

where D_μ is the covariant derivative and χ the parameter of the gauge transformations.

2.1.1 Explicit form of the effective action

We consider the parton-parton collisions at high-energy $\sqrt{s}$ in the center-of-mass system. In Multi-Regge-Kinematics the final state particles contains several groups (clusters) with an arbitrary number of gluons or/and quarks with a fixed mass M_i $(i = 1, 2, ..., n)$ of each group and significantly different rapidities corresponding to the Multi-Regge asymptotics,

$$\begin{aligned} &p_A + p_B = k_0 + k_1 + k_2 + ... + k_n + k_{n+1}\,, \\ &s = (p_A + p_B)^2 \gg s_r = (k_{i-1} + k_i)^2 \gg \mathbf{q}_r^2\,, \end{aligned} \tag{2.8}$$

with $k_r = q_{r+1} - q_r$ and $\mathbf{q}_r$ the momentum transfers in the various t-channels which are all of the same order of magnitude (Fig. 1.2).

Introducing the light-cone vectors

$$n^+ = 2p_b/\sqrt{s}\,,\quad n^- = 2p_a/\sqrt{s}\,,\quad n^+ \cdot n^- = 2\,,\quad \left(n^\pm\right)^2 = 0 \tag{2.9}$$

the light-cone projections of momenta and derivatives read respectively

$$k^\pm = \left(n^\pm\right)_\mu \cdot k^\mu\,,\quad \partial_\pm = \left(n^\pm\right)_\mu \cdot \partial^\mu\,. \tag{2.10}$$

Moreover the derivatives that act on the particle $v(p)$ and Reggeon $A(p)$ fields in the momentum representation are the following:

$$\partial_{\pm} v(p) = -\imath p_{\pm} v(p) \ , \quad \frac{1}{\partial_{\pm}} v(p) = \frac{\imath}{p_{\pm}} v(p) \ , \quad \partial^2 A(p) = -q^2 A(q) \ , \quad q^2 = -\mathbf{q}_{\perp}^2 \ . \tag{2.11}$$

Strong ordering of longitudinal momenta in high-energy factorized amplitudes leads to the kinematical constraint of the Reggeized gluon fields,

$$\partial_{\mp} A_{\pm} = 0 \, , \ \partial_{\pm} = n_{\pm}^{\mu} \partial_{\mu} \, , \qquad n_{\pm}^{\mu} = \delta_0^{\mu} \pm \delta_3^{\mu} \, , \tag{2.12}$$

which is always implied.

In QCD the gauge-invariant effective action local in the rapidity y is given as the sum of two terms [9]

$$S_{eff} = \int d^4x \left(L_0 + L_{ind} \right) \ , \tag{2.13}$$

in which L_0 represents the usual Yang-Mills Lagrangian, while L_{ind} is the induced Lagrangian.
The action of the latter Lagrangian can be written:

$$\begin{aligned} S_{ind.}\left[v_{\mu}, A_{\pm}\right] \ &= \ \int d^4x \mathrm{tr} \left[\left(W_{+}\left[v(x)\right] - A_{+}(x) \right) j_{-}^{reg} \right] \\ &+ \int d^4x \mathrm{tr} \left[\left(W_{-}\left[v(x)\right] - A_{-}(x) \right) j_{+}^{reg} \right] \ , \end{aligned} \tag{2.14}$$

where $j_{\pm}^{reg} = j_{\pm}^{reg}(A_{\pm})$ are Reggeon currents satisfying the kinematical constraints $\partial_{\mp} j_{\pm}^{reg} = 0$ (see Eq. 2.12) which are important for the gauge invariant of action (2.14). The two functionals $W_{\pm}[v]$ are defined through the following operator

$$W_{\pm}[v] = v_{\pm} \frac{1}{D_{\pm}} \partial_{\pm} \quad \text{where} \quad D_{\pm} = \partial_{\pm} + g v_{\pm} \, . \tag{2.15}$$

The effective action (2.14) describes the coupling of the Reggeized gluon field $A_{\pm}(x)$ to the gluonic field $v_{\mu}(x)$, local in rapidity. In terms of the amplitude (Fig.1.2) locality in rapidity means that the interactions between particles and Reggeized gluons is always restricted to a single rapidity cluster, whereas the interaction between clusters is mediated by Reggeized gluons alone.

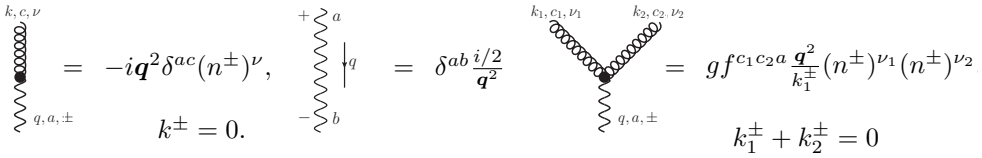

(a) (b) (c)

Figure 2.1: The direct transition vertex (a), the Reggeized gluon propagator (b) and the order g induced vertex (c)

2.1.2 Feynman rules of the effective action

Feynman rules of the high-energy effective have been determined in [80] and they are given by the conventional QCD Feynman rules and an infinity number of induced vertices.
In the following we state them explicitly up to $\mathcal{O}(g)$, which covers all induced vertices that will need in this thesis. We show them using curly lines for the conventional QCD gluon field and wavy (photon-like) lines for the Reggeized gluon field.

- Induced vertex of the zero order, which describes the direct transition of a QCD-gluon into a Reggeized gluon (Fig. 2.1 (a)).
- From the effective action we also obtain a new element: the propagator of the bare Reggeized gluon (Fig. 2.1 (b)).
- For the induced vertex of the first order (Fig. 2.1 (c)).

Here $\mathbf{q}^2 = -q_\perp^2$ denotes the Euclidean, two-dimensional squared momentum of the Reggeized gluon and ν the polarization of the gluon.
An explicit expression for the $\mathcal{O}(g^2)$ induced vertex can be found in [80].
All of these vertices obey Bose-symmetry, i.e. symmetry under simultaneous exchange of color, polarization and momenta of the external gluons of the order g^n vertex.

2.2 Summary

The effective action[81] can be used to determine tree amplitudes with Quasi-Multi-Regge-Kinematics to arbitrary accuracy. In particular the production vertices needed for the derivation of the BFKL-equation at NNLA have been derived in [80] and they have been used for the construction of real corrections in [82].
This action is a powerful tool that allows also for the determination of the virtual corrections in the Regge-limit. In particular it enables us to determine loop corrections to the Regge-trajectory and to the vertices describing coupling of the Reggeized gluons to QCD-particles, which are required for the determination of high-order corrections to the BFKL equation.
Using the Feynman rules [80] of the effective action, a number of complications is introduced. In particular the evaluation of loop diagrams within the effective action approach leads to a new type of longitudinal divergences, which are not present in conventional quantum corrections to QCD amplitudes. As it was demonstrated in [83, 84], a convenient way to regularize these divergencies is to introduce a parameter ρ which deforms the light-like four vectors of the effective action (the Sudakov projections) in the form [83]

$$\begin{aligned} n^- &\to n_a = e^{-\rho} n^+ + n^- \\ n^+ &\to n_b = n^+ + e^{-\rho} n^- . \end{aligned} \tag{2.16}$$

The deformation of the original reference momenta is considered to be asymptotically small ($\rho \to \infty$) and ρ can be given the interpretation of a logarithm of the center-of-mass energy.

Mueller-Tang impact factor The effective action can be used to calculate next-to-leading order (NLO) corrections to cross-sections in the high-energy limit. In particular we calculated [85, 86] NLO corrections for the forward jet impact factor from the effective action and real NLO corrections to the Mueller-Tang [87] impact factor.
The determination of the Mueller-Tang impact factor requires to consider diagrams where two Reggeized gluons couple to the quark induced jet, see Fig. 2.2

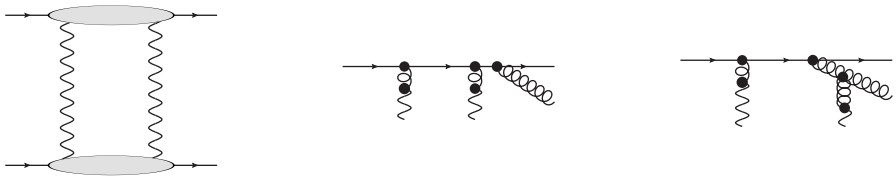

(a) (b) (c)

Figure 2.2

(a). With the virtual NLO corrections already known [60], we focus on the real NLO corrections. The relevant diagrams split into two groups: the two Reggeized gluon state couples either to a single parton (Fig. 2.2 (b)) or to two different partons (Fig. 2.2 (c)).
The calculation is still in progress, but we will get it as soon as.

Chapter 3

The NLO jet vertex for Mueller-Navelet and forward jets

3.1 Introduction

The large center of mass energy of hadron colliders like the Tevatron and the Large Hadron Collider (LHC) is not only useful for the production of possible new heavy particles, but also allows to investigate the high-energy regime of Quantum Chromodynamics (QCD). An especially interesting situation is the production of Mueller-Navelet jets.

Jet Mueller-Navelet The Mueller-Navelet jet production process [88] was suggested as an ideal tool to study the Regge limit of perturbative QCD in proton-proton (or proton-antiproton) collisions. It is an inclusive process

$$p(p_1) + p(p_2) \to J_1(k_{J,1}) + J_2(k_{J,2}) + X\,, \tag{3.1}$$

where two hard jets J_1 and J_2 are produced. Their transverse momenta are much large than the QCD scale, $\vec{k}_{J,1}^{\,2} \sim \vec{k}_{J,2}^{\,2} \gg \Lambda^2_{\rm QCD}$, so that it is possible to use perturbative QCD. Moreover, they are separated by a large interval of rapidity, $\Delta y \gg 1$, which means large center of mass energy $\sqrt{s}$ of the proton collisions, $s = 2p_1 \cdot p_2 \gg \vec{k}_{J\,1,2}^{\,2}$, since $\Delta y \sim \ln s/\vec{k}_{J\,1,2}^{\,2}$.
Since large logarithms of the energy compensate the small QCD coupling, they must be resummed to all orders of perturbative theory.

The BFKL approach (see Chapter 1) is the most suitable framework for the theoretical description of the high-energy limit of hard or semi-hard processes. It provides a systematic way to perform the resummation in the leading logarithmic approximation (LLA), which means resummation of all terms $(\alpha_s \ln(s))^n$, and in the next-to-leading logarithmic approximation (NLA), which means resummation of all terms $\alpha_s(\alpha_s \ln(s))^n$.
The only ingredient for the complete description of a process in the BFKL approach (see Chapter 1) is the impact factors of the colliding particle.

We recalculate, within the BFKL approach and at the next-to-leading order, the jet vertex relevant for the production of Mueller-Navelet jets in proton collisions and of forward jets in DIS.
Even if recently the results of a complete NLA analysis of the process (3.1) were reported [89], which incorporates NLO corrections to both the BFKL Green's function and the jets impact factors, calculated earlier in [72, 73], in our opinion, it would be important to have an independent calculation of Mueller-Navelet jet observables in NLA. The aim of this work [74] is the calculation of NLO correction to the jet impact factor in order to have an independent check of the results of [72, 73].
In many technical steps we follow closely the method used in [72, 73], but we will take advantage of starting from the general definition for the impact factors at NLO Eq. (1.14), see Ref. [43], which allows us to come to the results more shortly.

3.2 General framework

It is possible to describe a state of jets by their rapidities, y_1 and y_2, their transverse momenta, $\vec{k}_{J,1}$ and $\vec{k}_{J,2}$, and their azimuthal angles of the produced jets ϕ_1 and ϕ_2. It is convenient to define the Sudakov decomposition for the jets momenta. For a jet in the fragmentation region of the proton with momentum p_1, one has

$$k_{J,1} = x_{J,1} p_1 + \frac{\vec{k}^2_{J,1}}{x_{J,1} s} p_2 + k_{J,1\perp} \ , \qquad k^2_{J,1\perp} = -\vec{k}^2_{J,1} \ , \tag{3.2}$$

where we assume $p_1^2 = p_2^2 = 0$ neglecting the proton mass and the longitudinal fraction $x_{J,1} = \mathcal{O}(1)$ is related to the jet rapidity in the center of mass system by

$$y_1 = \frac{1}{2} \ln \frac{x_{J,1}^2 s}{\vec{k}_{J,1}^2}, \qquad dy_1 = \frac{dx_{J,1}}{x_{J,1}}.$$

In QCD collinear factorization the cross section of the process reads

$$\frac{d\sigma}{dx_{J,1} dx_{J,2} d^2\vec{k}_{J,1} d^2\vec{k}_{J,2}} \tag{3.3}$$
$$= \sum_{i,j=q,\bar{q},g} \int_0^1 \int_0^1 dx_1 dx_2 f_i(x_1,\mu) f_j(x_2,\mu) \frac{d\hat{\sigma}_{i,j}(x_1 x_2 s, \mu)}{dx_{J,1} dx_{J,2} d^2\vec{k}_{J,1} d^2\vec{k}_{J,2}},$$

where the i, j indices specify parton types (quarks $q = u, d, s$; antiquarks $\bar{q} = \bar{u}, \bar{d}, \bar{s}$; or gluon g), $f_i(x, \mu)$ denotes the initial proton parton density function (PDF), the longitudinal fractions of the partons involved in the hard subprocess are $x_{1,2}$, μ is the factorization scale and $d\hat{\sigma}_{i,j}(x_1 x_2 s, \mu)$ is the partonic cross section for the production of jets, and $\hat{s} = x_1 x_2 s$ is the energy of parton-parton collision.

At lowest order each jet is represented by a single parton having high transverse momentum, and the partonic subprocess is given by an elementary two-to-two scattering. In the discussed Mueller-Navelet kinematics the higher-order contributions to the partonic cross section have to be resummed using BFKL approach. Such resummation at NLA accuracy depends on the details of jet definition (jet algorithm) and will be specified later.

3.2.1 Parton impact factors

We can write the LO impact factor for the quark case as

$$\Phi_q^{(0)}(\vec{q}) = \sum_{\{a\}} \int \frac{dM_a^2}{2\pi} \Gamma_{aq}^{(0)}(\vec{q}) \left[\Gamma_{aq}^{(0)}(\vec{q})\right]^* d\rho_a, \tag{3.4}$$

where $\vec{q}$ is the Reggeon transverse momentum, and $\Gamma_{aq}^{(0)}$ denotes the Reggeon-quark vertices in the LO or Born approximation. The sum $\{a\}$ is over all intermediate states a which contribute to the $q \to q$ transition. The phase

space element $d\rho_a$ of a state a, consisting of particles with momenta ℓ_n, is (p_q is initial quark momentum)

$$d\rho_a \;=\; (2\pi)^D\,\delta^{(D)}\left(p_q+q-\sum_{n\in a}\ell_n\right)\prod_{n\in a}\frac{d^{D-1}\ell_n}{(2\pi)^{D-1}2E_n}\,, \tag{3.5}$$

while the remaining integration in (3.4) is over the squared invariant mass of the state a,

$$M_a^2 \;=\; (p_q+q)^2\,.$$

In the LO the only intermediate state which contributes is a one-quark state, $\{a\}=q$. The integration in Eq. (3.4) with the known Reggeon-quark vertices $\Gamma_{qq}^{(0)}$ is trivial and the quark impact factor reads [60]

$$\Phi_q^{(0)}(\vec{q}\,) \;= g^2\frac{\sqrt{N_c^2-1}}{2N_c}\,, \tag{3.6}$$

where g is QCD coupling, $\alpha_s=g^2/(4\pi)$, $N_c=3$ is the number of QCD colors.

In the NLO the expression (3.4) for the quark impact factor has to be changed in two ways. First one has to take into account the radiative corrections to the vertices,

$$\Gamma_{qq}^{(0)}\to\Gamma_{qq}=\Gamma_{qq}^{(0)}+\Gamma_{qq}^{(1)}\,. \tag{3.7}$$

Second, in the sum over $\{a\}$ in (3.4), we have to include more complicated states which appear in the next order of perturbative theory. For the quark impact factor this is a state with an additional gluon, $a=qg$. However, the integral over M_a^2 becomes divergent when an extra-gluon appears in the final state. The divergence arises because the gluon may be emitted not only in the fragmentation region of initial quark, but also in the central rapidity region. The contribution of the central region must be subtracted from the impact factor, since it is to be assigned in the BFKL approach to the Green's function. Therefore the result for the forward quark impact factor, see Ref. [60] and Fig. 3.1, reads [60]

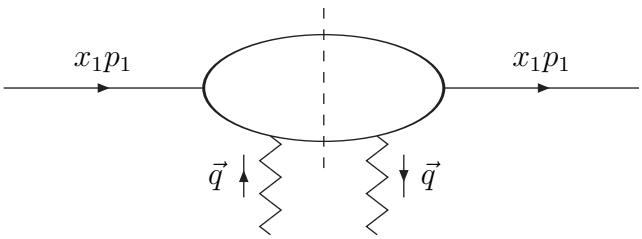

Figure 3.1: Schematic representation of the forward parton impact factor. Here p_1 is the proton momentum, x_1 is the fraction of proton momentum carried by the parton and $\vec{q}$ is the transverse momentum of the incoming Reggeized gluon.

$$\Phi_q(\vec{q}, s_0) = \left(\frac{s_0}{\vec{q}^{\,2}}\right)^{\omega(-\vec{q}^{\,2})} \sum_{\{a\}} \int \frac{dM_a^2}{2\pi} \Gamma_{aq}(\vec{q}) \left[\Gamma_{aq}(\vec{q})\right]^* d\rho_a \, \theta(s_\Lambda - M_a^2)$$
$$-\frac{1}{2} \int d^{D-2}k \frac{\vec{q}^{\,2}}{\vec{k}^{\,2}} \Phi_q^{(0)}(\vec{k}) \mathcal{K}_r^{(0)}(\vec{k}, \vec{q}) \ln\left(\frac{s_\Lambda^2}{(\vec{k}-\vec{q})^2 s_0}\right) . \quad (3.8)$$

For the description of the object in the R.H.S. of Eq. (3.8), see the discussion after Eq. (1.14).

The gluon impact factor $\Phi_g(\vec{q})$ is defined similarly. In the gluon case only the single-gluon intermediate state contributes in the LO, $a = g$, wich result in [59]

$$\Phi_g^{(0)}(\vec{q}) = \frac{C_A}{C_F} \Phi_q^{(0)}(\vec{q}) , \quad (3.9)$$

with $C_A = N_c$ and $C_F = (N_c^2 - 1)/(2N_c)$. Whereas in NLO additional two-gluon, $a = gg$, and quark-antiquark, $a = q\bar{q}$, intermediate states have to be taken into account in the calculation of the gluon impact factor.

3.3 Jet impact factor

In the BFKL approach the resummed cross section of the hard subprocess is represented as the convolution of the jet impact factors of the colliding particles with the Green's function G_ω, see Eq. (1.22),

$$\frac{d\hat{\sigma}}{dJ_1 dJ_2} = \frac{1}{(2\pi)^{D-2}} \int \frac{d^{D-2}q_1}{\vec{q}_1^{\,2}} \frac{d\Phi_{J,1}(\vec{q}_1, s_0)}{dJ_1} \int \frac{d^{D-2}q_2}{\vec{q}_2^{\,2}} \frac{d\Phi_{J,2}(-\vec{q}_2, s_0)}{dJ_2} \times \int_{\delta-i\infty}^{\delta+i\infty} \frac{d\omega}{2\pi i} \left(\frac{\hat{s}}{s_0}\right)^{\omega} G_\omega(\vec{q}_1, \vec{q}_2)\,. \tag{3.10}$$

where we introduce jet impact factors $\frac{d\Phi_{J,i}(\vec{q}_i, s_0)}{dJ_i}$ differential with respect to the variables parameterizing the jet phase space,

$$dJ_1 \equiv dx_{J,1} d^{D-2}k_{J,1}\,, \qquad dJ_2 \equiv dx_{J,2} d^{D-2}k_{J,2}\,. \tag{3.11}$$

Here $\vec{q}_1$, $\vec{q}_2$ are the transverse momenta of the Reggeized gluons and the energy scale parameter s_0 is arbitrary, since the amplitude does not depend on its choice within NLA accuracy.

Following [72] we consider our process in the frame of a generic and infrared-safe jet algorithm. In practice, this is done by introducing into the integration over the partonic phase space a suitably defined function which identifies the jet momentum with the momentum of one parton or with the sum of the two or more parton momenta when the jet is originated from the a multi-parton intermediate state.
In our accuracy the jet can be formed by one parton in LO and by one (virtual corrections) or two (real corrections) partons when the process is considered in NLO.

Jet Function In the simplest case, the jet momentum is identified with the momentum of the parton in the intermediate state k by the following jet function [90, 91]:

$$S_J^{(2)}(\vec{k}; x) = \delta(x - x_J)\delta^{(D-2)}(\vec{k} - \vec{k}_J)\,. \tag{3.12}$$

In this way, having the results for the lowest order parton impact factors Eqs. (3.6) and (3.9), the **jet impact factor at the LO** is given as the sum of the gluon and all possible quark and antiquark PDFs contributions:

$$\frac{d\Phi_J^{(0)}(\vec{q})}{dJ} = g^2 \frac{\sqrt{N_c^2 - 1}}{2N_c} \int_0^1 dx \left(\frac{C_A}{C_F} f_g(x) + \sum_{a=q,\bar{q}} f_a(x)\right) S_J^{(2)}(\vec{q}; x)\,. \tag{3.13}$$

In the more complicated case when the jet originates from a state of two partons with momenta k_1 and k_2, we need another function $S_J^{(3)}$, whose explicit form is specific for the chosen jet algorithm. An example of jet selection function in the case of the *cone algorithm* is the following [90, 91]:

$$S_J^{(3,\mathrm{cone})}(\vec{k}_2, \vec{k}_1, x\beta_1; x) \tag{3.14}$$

$$\begin{aligned}
&= S_J^{(2)}(\vec{k}_2; x(1-\beta_1))\Theta\left(\left[\Delta y^2 + \Delta\phi^2\right] - \left[\frac{|\vec{k}_1| + |\vec{k}_2|}{\max(|\vec{k}_1|, |\vec{k}_2|)} R_{\mathrm{cone}}\right]^2\right) \\
&+ S_J^{(2)}(\vec{k}_1; x\beta_1)\Theta\left(\left[\Delta y^2 + \Delta\phi^2\right] - \left[\frac{|\vec{k}_1| + |\vec{k}_2|}{\max(|\vec{k}_1|, |\vec{k}_2|)} R_{\mathrm{cone}}\right]^2\right) \\
&+ S_J^{(2)}(\vec{k}_1 + \vec{k}_2; x)\Theta\left(\left[\frac{|\vec{k}_1| + |\vec{k}_2|}{\max(|\vec{k}_1|, |\vec{k}_2|)} R_{\mathrm{cone}}\right]^2 - \left[\Delta y^2 + \Delta\phi^2\right]\right),
\end{aligned}$$

where the Sudakov decomposition of the parton momenta

$$k_1 = x\beta_1 p_1 + \frac{\vec{k}_1^{\,2}}{x\beta_1 s} p_2 + k_{1_\perp}, \qquad k_1^2 = 0, \tag{3.15}$$

$$k_2 = x\beta_2 p_1 + \frac{\vec{k}_2^{\,2}}{x\beta_2 s} p_2 + k_{2_\perp}, \qquad k_2^2 = 0, \tag{3.16}$$

is used, with $\beta_1 + \beta_2 = 1$ and $\vec{k}_1 + \vec{k}_2 = \vec{q}$, owing to momentum conservation in the partonic subprocess. R_{cone} in (3.14) is the cone-size parameter, Δy and $\Delta\phi$ are the difference of rapidity and azimuthal angle in the two parton state, respectively:

$$\Delta y = \ln\left(\frac{1-\beta_1}{\beta_1}\frac{|\vec{k}_1|}{|\vec{k}_2|}\right), \qquad \Delta\phi = \arccos\frac{\vec{k}_1 \cdot \vec{k}_2}{\sqrt{\vec{k}_1^{\,2}\vec{k}_2^{\,2}}}. \tag{3.17}$$

The three terms in $S_J^{(3,\mathrm{cone})}$ represent the case in which the jet is formed by the parton k_2 or the parton k_1 or both, respectively.
In the generic case, the following relations for the jet function must be fulfilled in order the jet algorithm be infrared safe:

$$S_J^{(3)}(\vec{k}_2,\vec{k}_1,x\beta_1;x) \longrightarrow S_J^{(2)}(\vec{k}_2;x)\,, \qquad \vec{k}_1\to 0\,, \quad \beta_1\to 0\,, \tag{3.18}$$

$$S_J^{(3)}(\vec{k}_2,\vec{k}_1,x\beta_1;x) \longrightarrow S_J^{(2)}(\vec{k}_1+\vec{k}_2;x)\,, \qquad \vec{k}_1\beta_2\to \vec{k}_2\beta_1\,, \tag{3.19}$$

$$S_J^{(3)}(\vec{k}_2,\vec{k}_1,x\beta_1;x) \longrightarrow S_J^{(2)}(\vec{k}_2;x(1-\beta_1))\,, \quad \vec{k}_1\to 0\,, \tag{3.20}$$

$$S_J^{(3)}(\vec{k}_2,\vec{k}_1,x\beta_1;x) \longrightarrow S_J^{(2)}(\vec{k}_1;x\beta_1)\,, \qquad \vec{k}_2\to 0\,. \tag{3.21}$$

Such reduction of $S_J^{(3)} \to S_J^{(2)}$ is required in order that the singular contributions generated by the real emission be proportional to the lowest order cross section. These contributions are canceled with the soft and collinear singularities arising from the virtual corrections and the collinear counterterms coming from the PDFs renormalization.

Besides, we assume that the jet selection function $S_J^{(3)}$ is symmetric under the exchange of the final state parton kinematic variables, $\beta_1 \leftrightarrow \beta_2$ and $\vec{k}_1 \leftrightarrow \vec{k}_2$,

$$S_J^{(3)}(\vec{k}_2,\vec{k}_1,x\beta_1;x) = S_J^{(3)}(\vec{k}_1,\vec{k}_2,x\beta_2;x)\,. \tag{3.22}$$

3.3.1 Counterterms

The collinear counterterms appear due to the replacement of the bare PDFs by the renormalized physical quantities which obey DGLAP evolution equations, in the $\overline{\rm MS}$ factorization scheme:

$$f_q(x) = f_q(x,\mu_F) \tag{3.23}$$

$$- \frac{\alpha_s}{2\pi}\left(\frac{1}{\hat{\varepsilon}} + \ln\frac{\mu_F^2}{\mu^2}\right)\int_x^1 \frac{dz}{z}\left[P_{qq}(z) f_q(\frac{x}{z},\mu_F) + P_{qg}(z) f_g(\frac{x}{z},\mu_F)\right]\,,$$

$$f_g(x) = f_g(x,\mu_F) \tag{3.24}$$

$$- \frac{\alpha_s}{2\pi}\left(\frac{1}{\hat{\varepsilon}} + \ln\frac{\mu_F^2}{\mu^2}\right)\int_x^1 \frac{dz}{z}\left[P_{gq}(z) f_q(\frac{x}{z},\mu_F) + P_{gg}(z) f_g(\frac{x}{z},\mu_F)\right]\,,$$

(3.25)

where $\frac{1}{\hat{\varepsilon}} = \frac{1}{\varepsilon} + \gamma_E - \ln(4\pi) \approx \frac{\Gamma(1-\varepsilon)}{\varepsilon(4\pi)^\varepsilon}$ and the DGLAP splitting functions are (see, for instance, Ref. [92]):

$$
\begin{aligned}
P_{qq}(\beta) &= C_F \left(\frac{1+\beta^2}{1-\beta} \right)_+ = C_F \left[\frac{1+\beta^2}{(1-\beta)_+} + \frac{3}{2}\delta(1-\beta) \right] , && (3.26)\\
P_{qg}(\beta) &= T_R \left[\beta^2 + (1-\beta)^2 \right] , \quad \text{with } T_R = \frac{1}{2} , && (3.27)\\
P_{gg}(\beta) &= 2C_A \left(\frac{\beta}{(1-\beta)_+} + \frac{(1-\beta)}{\beta} + \beta(1-\beta) \right) && (3.28)\\
&+ \frac{(11C_A - 4N_F T_R)}{6} \delta(1-\beta) , \\
P_{gq}(\beta) &= C_F \frac{[1+(1-\beta)^2]}{\beta} ; && (3.29)
\end{aligned}
$$

here the plus-prescription is defined by

$$
\int_a^1 dx \frac{F(x)}{(1-x)_+} = \int_a^1 dx \frac{F(x) - F(1)}{1-x} - \int_0^a dx \frac{F(1)}{1-x} . \qquad (3.30)
$$

The other counterterm is related with QCD charge renormalization, in the $\overline{\text{MS}}$ scheme:

$$
\alpha_s = \alpha_s(\mu_R) \left[1 + \frac{\alpha_s(\mu_R)}{4\pi} \left(\frac{11C_A}{3} - \frac{2N_F}{3} \right) \left(\frac{1}{\hat{\varepsilon}} + \ln \frac{\mu_R^2}{\mu^2} \right) \right] . \qquad (3.31)
$$

Substituting in the LO jet impact factor the bare QCD coupling and bare PDFs by the renormalized ones, we obtain the following expressions for the counterterms:

$$
\begin{aligned}
\frac{d\Phi_J(\vec{q})|_{\text{charge c.t.}}}{dJ} &= \frac{\alpha_s}{2\pi} \left(\frac{1}{\hat{\varepsilon}} + \ln \frac{\mu_R^2}{\mu^2} \right) \left(\frac{11C_A}{6} - \frac{N_F}{3} \right) \Phi_q^{(0)} \\
&\times \int_0^1 dx \left(\frac{C_A}{C_F} f_g(x) + \sum_{a=q,\bar{q}} f_a(x) \right) S_J^{(2)}(\vec{q}; x) \qquad (3.32)
\end{aligned}
$$

for the charge renormalization, and

$$
\begin{aligned}
\frac{d\Phi_J(\vec{q})|_{\text{collinear c.t.}}}{dJ} &= -\frac{\alpha_s}{2\pi} \left(\frac{1}{\hat{\varepsilon}} + \ln \frac{\mu_F^2}{\mu^2} \right) \Phi_q^{(0)} \int_0^1 dx\, S_J^{(2)}(\vec{q}; x) \qquad (3.33)\\
&\times \int_x^1 \frac{d\beta}{\beta} \left[\sum_{a=q,\bar{q}} \left(P_{qq}(\beta) f_a \left(\frac{x}{\beta} \right) + P_{qg}(\beta) f_g \left(\frac{x}{\beta} \right) \right) \right. \\
&\left. + \frac{C_A}{C_F} \left(P_{gg}(\beta) f_g \left(\frac{x}{\beta} \right) + P_{gq}(\beta) \sum_{a=q,\bar{q}} f_a \left(\frac{x}{\beta} \right) \right) \right]
\end{aligned}
$$

for the collinear counterterm. The latter can be rewritten in the form

$$\frac{d\Phi_J(\vec{q})|_{\text{collinear c.t.}}}{dJ} = -\frac{\alpha_s}{2\pi}\left(\frac{1}{\hat{\varepsilon}} + \ln\frac{\mu_F^2}{\mu^2}\right)\Phi_q^{(0)}\int\limits_0^1 d\beta \int\limits_0^1 dx\, S_J^{(2)}(\vec{q};\beta x)$$

$$\times\left[\sum_{a=q,\bar{q}}\left(P_{qq}(\beta)f_a(x) + P_{qg}(\beta)f_g(x)\right) + \frac{C_A}{C_F}\left(P_{gg}(\beta)f_g(x) + P_{gq}(\beta)\sum_{a=q,\bar{q}} f_a(x)\right)\right]. \tag{3.34}$$

Finally, we present the expression for the BFKL counterterm which, in accordance to the second line of Eq. (3.8), provides the subtraction of the gluon radiation in the central rapidity region:

$$\begin{aligned}\frac{d\Phi_J(\vec{q})|_{\text{BFKL c.t.}}}{dJ} &= -\Phi_q^{(0)}\frac{C_A\, g^2}{(2\pi)^{D-1}}\int_0^1 dx\left(\frac{C_A}{C_F}f_g(x) + \sum_{a=q,\bar{q}} f_a(x)\right)\\ &\times \int d^{D-2}k\,\frac{\vec{q}^{\,2}}{\vec{k}^{\,2}(\vec{k}-\vec{q})^2}\ln\left(\frac{s_\Lambda^2}{s_0\,\vec{k}^2}\right) S_J^{(2)}(\vec{q}-\vec{k};x)\,.\end{aligned} \tag{3.35}$$

Now we have all the necessary ingredients to perform our calculation of the NLO corrections to the jet impact factor. As a starting point for our consideration we will use the results of [59, 60] for the partonic amplitudes obtained in the calculation of partonic impact factors, introducing there the appropriate jet functions: $S_J^{(2)}$ for the amplitudes with one-parton state in the case of one-loop virtual corrections and $S_J^{(3)}$ for the cases with two partons in the final state (real emission), in order to define the corresponding contribution to jet cross sections.

For shortness we will present intermediate results for V structures defined always as

$$\frac{d\Phi_J^{(1)}(\vec{q})}{dJ} \equiv \frac{\alpha_s}{2\pi}\,\Phi_q^{(0)}\,V(\vec{q})\,. \tag{3.36}$$

We will consider separately the subprocesses initiated by the quark and the gluon PDFs and denote

$$V = V_q + V_g\,. \tag{3.37}$$

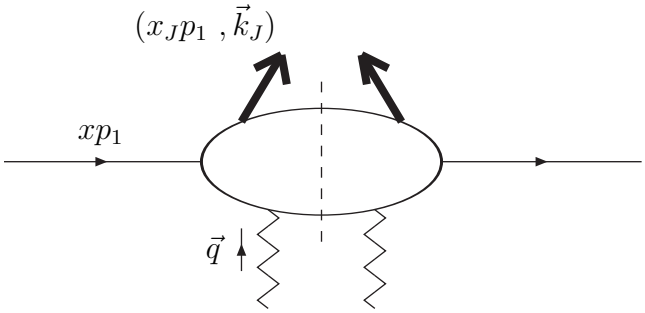

Figure 3.2: Schematic representation of the jet vertex for the case of quark in the initial state. Here p_1 is the proton momentum, x is the fraction of proton momentum carried by the quark, $x_J p_1$ is the longitudinal jet momentum, $\vec{k}_J$ is the transverse jet momentum and $\vec{q}$ is the transverse momentum of the incoming Reggeized gluon.

3.4 NLA jet impact factor: the quark contribution

We start with the case of incoming quark (see Fig. 3.2).

3.4.1 Virtual correction

Virtual corrections are the same as in the case of the inclusive quark impact factor [60, 61]:

$$V_q^{(V)}(\vec{q}) = -\frac{\Gamma[1-\varepsilon]}{\varepsilon\,(4\pi)^\varepsilon}\frac{\Gamma^2(1+\varepsilon)}{\Gamma(1+2\varepsilon)}\left(\vec{q}^{\,2}\right)^\varepsilon \int_0^1 dx \sum_{a=q,\bar{q}} f_a(x)\, S_J^{(2)}(\vec{q};x)$$

$$\times\left\{C_F\left(\frac{2}{\varepsilon}-\frac{4}{1+2\varepsilon}+1\right)-N_F\frac{1+\varepsilon}{(1+2\varepsilon)(3+2\varepsilon)}+C_A\left(\ln\frac{s_0}{\vec{q}^{\,2}}+\psi(1-\varepsilon)\right.\right.$$

$$\left.\left.-2\psi(\varepsilon)+\psi(1)+\frac{1}{4(1+2\varepsilon)(3+2\varepsilon)}-\frac{2}{\varepsilon(1+2\varepsilon)}-\frac{7}{4(1+2\varepsilon)}-\frac{1}{2}\right)\right\}. \quad (3.38)$$

Here and in what follows we put the arbitrary scale of dimensional regularization equal to unity, $\mu = 1$. We expand (3.38) in ε and get

$$V_q^{(V)}(\vec{q}) = -\frac{\Gamma[1-\varepsilon]}{\varepsilon\,(4\pi)^\varepsilon}\frac{\Gamma^2(1+\varepsilon)}{\Gamma(1+2\varepsilon)}\left(\vec{q}^{\,2}\right)^\varepsilon \int_0^1 dx \sum_{a=q,\bar{q}} f_a(x)\, S_J^{(2)}(\vec{q};x)$$

$$\times\left[C_F\left(\frac{2}{\varepsilon}-3\right)-\frac{N_F}{3}+C_A\left(\ln\frac{s_0}{\vec{q}^{\,2}}+\frac{11}{6}\right)\right.$$

$$+\varepsilon\left\{8\,C_F+\frac{5N_F}{9}-C_A\left(\frac{85}{18}+\frac{\pi^2}{2}\right)\right\}\Bigg]+\mathcal{O}(\varepsilon)\,. \tag{3.39}$$

3.4.2 Real corrections

For the incoming quark case, real corrections originate from the quark-gluon intermediate state. We denote the momentum of the gluon by k, then the momentum of the quark is $q-k$; the longitudinal fraction of the gluon momentum is denoted by βx. Thus, the real contribution has the form [60, 61, 93]

$$\begin{aligned} V_q^{(R)}(\vec{q}) &= \frac{1}{(4\pi)^\varepsilon}\int_0^1 dx\sum_{a=q,\bar{q}} f_a(x)\int\frac{d^{D-2}k}{\pi^{1+\varepsilon}}\int_{\beta_0}^1 d\beta\,\mathcal{P}_{gq}(\varepsilon,\beta) \\ &\times \frac{\vec{q}^{\,2}}{\vec{k}^{\,2}(\vec{q}-\vec{k})^2(\vec{k}-\beta\vec{q})^2}\left\{C_F\beta^2(\vec{q}-\vec{k})^2+C_A(1-\beta)\vec{k}\cdot(\vec{k}-\beta\vec{q})\right\} \\ &\times S_J^{(3)}\left(\vec{q}-\vec{k},\vec{k},x\beta;x\right), \end{aligned} \tag{3.40}$$

where

$$\beta_0=\frac{\vec{k}^{\,2}}{s_\Lambda}\,,\qquad \mathcal{P}_{gq}(\varepsilon,\beta)=\frac{1+(1-\beta)^2+\varepsilon\beta^2}{\beta}\,.$$

The low limit in the β-integration appears due to the restriction on the invariant mass of intermediate state, which enters the definition (3.8) of NLO impact factor. Since

$$M_{qg}^2=\frac{\vec{k}^2}{\beta}+\frac{(\vec{q}-\vec{k})^2}{1-\beta}-\vec{q}^{\,2}\,,\quad M_{qg}^2\le s_\Lambda\,,$$

and assuming $s_\Lambda\to\infty$, we obtain that $\beta\ge\beta_0$.
We consider separately the term proportional to C_F and to C_A.

The C_F-term is not singular for $\beta\to 0$, therefore the limit $s_\Lambda\to\infty$, or $\beta_0\to 0$, can be safely taken. We get

$$\begin{aligned} V_q^{(R)(C_F)}(\vec{q}) &= \frac{C_F}{(4\pi)^\varepsilon}\int_0^1 dx\sum_{a=q,\bar{q}} f_a(x)\int\frac{d^{D-2}k}{\pi^{1+\varepsilon}}\int_0^1 d\beta\,\mathcal{P}_{gq}(\varepsilon,\beta) \\ &\times \frac{\vec{q}^{\,2}\beta^2}{\vec{k}^{\,2}(\vec{k}-\beta\vec{q})^2}S_J^{(3)}\left(\vec{q}-\vec{k},\vec{k},x\beta;x\right). \end{aligned} \tag{3.41}$$

In order to isolate all divergences, it is convenient to perform the change of variable $\vec{k}=\beta\vec{l}$ and to present the integral in the form

$$V_q^{(R)(C_F)}(\vec{q}) = \frac{C_F}{(4\pi)^\varepsilon}\int_0^1 dx \sum_{a=q,\bar{q}} f_a(x) \int_0^1 d\beta\, \mathcal{P}_{gq}(\varepsilon,\beta)\beta^{2\varepsilon} \tag{3.42}$$
$$\times \int \frac{d^{D-2}l}{\pi^{1+\varepsilon}} \frac{\vec{q}^{\,2}}{\vec{l}^{\,2}+(\vec{l}-\vec{q})^2}\left[\frac{1}{(\vec{l}-\vec{q})^2}+\frac{1}{\vec{l}^{\,2}}\right] S_J^{(3)}\left(\vec{q}-\beta\vec{l},\beta\vec{l},x\beta;x\right) .$$

The soft divergence appears for $\beta \to 0$; in this region we can introduce the counterterm

$$V_q^{(R)(C_F,\mathrm{soft})}(\vec{q}) = \frac{C_F}{(4\pi)^\varepsilon}\int_0^1 dx \sum_{a=q,\bar{q}} f_a(x) \int_0^1 d\beta\, \frac{2}{\beta^{1-2\varepsilon}} \tag{3.43}$$
$$\times \int \frac{d^{D-2}l}{\pi^{1+\varepsilon}} \frac{\vec{q}^{\,2}}{\vec{l}^{\,2}+(\vec{l}-\vec{q})^2}\left[\frac{1}{(\vec{l}-\vec{q})^2}+\frac{1}{\vec{l}^{\,2}}\right] S_J^{(2)}\left(\vec{q};x\right) ,$$

which equals (see Eq. (A.1))

$$V_q^{(R)(C_F,\mathrm{soft})}(\vec{q}) = \frac{2C_F}{\varepsilon}\frac{\Gamma[1-\varepsilon]}{\varepsilon\,(4\pi)^\varepsilon}\frac{\Gamma^2(1+\varepsilon)}{\Gamma(1+2\varepsilon)}\left(\vec{q}^{\,2}\right)^\varepsilon \int_0^1 dx \sum_{a=q,\bar{q}} f_a(x)\, S_J^{(2)}(\vec{q};x) . \tag{3.44}$$

Collinear divergences arise for $\vec{l}-\vec{q}=0$ and for $\vec{l}=0$; in these regions we can isolate the two following counterterms:

$$V_q^{(R)(C_F,\mathrm{coll}_1)}(\vec{q}) = \frac{C_F}{(4\pi)^\varepsilon}\int \frac{d^{D-2}l}{\pi^{1+\varepsilon}(\vec{l}-\vec{q})^2}\Theta(\Lambda^2-(\vec{l}-\vec{q})^2) \tag{3.45}$$
$$\times \int_0^1 d\beta\beta^{2\varepsilon}\left[\mathcal{P}_{gq}(\varepsilon,\beta)-\frac{2}{\beta}\right]\int_0^1 dx \sum_{a=q,\bar{q}} f_a(x) S_J^{(2)}(\vec{q};x) ,$$

$$V_q^{(R)(C_F,\mathrm{coll}_2)}(\vec{q}) = \frac{C_F}{(4\pi)^\varepsilon}\int \frac{d^{D-2}l}{\pi^{1+\varepsilon}\vec{l}^{\,2}}\Theta(\Lambda^2-\vec{l}^{\,2})\int_0^1 dx \sum_{a=q,\bar{q}} f_a(x) \tag{3.46}$$
$$\times \int_0^1 d\beta\ \beta^{2\varepsilon}\left[S_J^{(2)}(\vec{q};x(1-\beta))\mathcal{P}_{gq}(\varepsilon,\beta)-\frac{2}{\beta}S_J^{(2)}(\vec{q};x)\right] ,$$

where we made use of the Eq. (3.19) for the Eq. (3.45) and Eq. (3.20) for (3.46). In both these expressions we have introduced an arbitrary cutoff parameter Λ and subtracted the soft divergence. After a simple calculation we obtain (see Eq. (A.2))

$$V_q^{(R)(C_F,\mathrm{coll}_1)}(\vec{q}) = \frac{\Gamma[1-\varepsilon]}{\varepsilon\,(4\pi)^\varepsilon}\frac{\Gamma^2(1+\varepsilon)}{\Gamma(1+2\varepsilon)}\left(\Lambda^2\right)^\varepsilon \int_0^1 dx \sum_{a=q,\bar{q}} f_a(x) S_J^{(2)}(\vec{q};x) \times C_F\left[-\frac{3}{2}+4\varepsilon\right]+\mathcal{O}(\varepsilon)\,. \tag{3.47}$$

The term $V_q^{(R)(C_F,\mathrm{coll}_2)}$ can be rewritten in the following form:

$$V^{(R)(C_F,\mathrm{coll}_2)}(\vec{q}) = \tag{3.48}$$

$$\frac{\Gamma[1-\varepsilon]}{\varepsilon\,(4\pi)^\varepsilon}\frac{\Gamma^2(1+\varepsilon)}{\Gamma(1+2\varepsilon)}\left(\Lambda^2\right)^\varepsilon \int_0^1 dx \sum_{a=q,\bar{q}} f_a(x)\left\{-\frac{3}{2}C_F S_J^{(2)}(\vec{q};x) + \int_0^1 d\beta\left[P_{qq}(\beta)+\,2\varepsilon(1+\beta^2)\left(\frac{\ln(1-\beta)}{1-\beta}\right)_+ C_F+\varepsilon\,C_F(1-\beta)\right] \times S_J^{(2)}(\vec{q};x\beta)\right\}+\mathcal{O}(\varepsilon)\,, \tag{3.49}$$

where we performed the change of variable $\beta \to 1-\beta$, used the plus-prescription (3.30) and the expansion

$$(1-\beta)^{2\varepsilon-1} = \frac{1}{2\varepsilon}\delta(1-\beta)+\frac{1}{(1-\beta)_+}+2\varepsilon\left(\frac{\ln(1-\beta)}{1-\beta}\right)_+ +\mathcal{O}(\varepsilon^2)\,.$$

Finally, we can define the term

$$V_q^{(R)(C_F,\mathrm{finite})} = V_q^{(R)(C_F)} - V_q^{(R)(C_F,\mathrm{soft})} - V_q^{(R)(C_F,\mathrm{coll}_1)} - V_q^{(R)(C_F,\mathrm{coll}_2)}\,, \tag{3.50}$$

which can be calculated at $\varepsilon = 0$. We remark that $V_q^{(R)(C_F,\mathrm{finite})}$ and $V_q^{(R)(C_F,\mathrm{cool}_{1,2})}$ depend on the cutoff Λ, but in the total expression $V_q^{(R)(C_F)}$ this dependence disappears.

The part proportional to C_A in the r.h.s. of Eq. (3.40) reads

$$V_q^{(R)(C_A)}(\vec{q}) = \frac{1}{(4\pi)^\varepsilon}\int_0^1 dx \sum_{a=q,\bar{q}} f_a(x)\int \frac{d^{D-2}k}{\pi^{1+\varepsilon}}\int_{\beta_0}^1 d\beta\,\mathcal{P}_{gq}(\varepsilon,\beta) \times \vec{q}^{\,2} C_A\,\frac{(1-\beta)\vec{k}\cdot(\vec{k}-\beta\vec{q})}{\vec{k}^{\,2}(\vec{q}-\vec{k})^2(\vec{k}-\beta\vec{q})^2} S_J^{(3)}\left(\vec{q}-\vec{k},\vec{k},x\beta;x\right)\,. \tag{3.51}$$

The collinear singularity appears at $\vec{k}-\vec{q}\to 0$; in this region we can introduce the counterterm and making use of Eq. (3.21) we have

$$V_q^{(R)(C_A,\mathrm{coll})}(\vec{q}) = \frac{C_A}{(4\pi)^\varepsilon}\int\frac{d^{D-2}k}{\pi^{1+\varepsilon}(\vec{q}-\vec{k})^2}\Theta\left(\Lambda^2-(\vec{k}-\vec{q})^2\right) \times \int_0^1 dx\sum_{a=q,\bar{q}} f_a(x)\int_0^1 d\beta\,\mathcal{P}_{gq}(\varepsilon,\beta)\,S_J^{(2)}(\vec{q};x\beta)\,, \tag{3.52}$$

where β_0 has been set equal to zero since the expression is finite in the $\beta\to 0$ limit and, again, the cutoff Λ was introduced.
Making use of Eq. (A.2) we found

$$V_q^{(R)(C_A,\mathrm{coll})}(\vec{q}) = \frac{\Gamma[1-\varepsilon]}{\varepsilon\,(4\pi)^\varepsilon}\frac{\Gamma^2(1+\varepsilon)}{\Gamma(1+2\varepsilon)}\left(\Lambda^2\right)^\varepsilon\int_0^1 dx\sum_{a=q,\bar{q}} f_a(x) \times \int_0^1 d\beta\,\left[\frac{C_A}{C_F}P_{gq}(\beta)+\varepsilon\,C_A\,\beta\right]\,S_J^{(2)}(\vec{q};x\beta)+\mathcal{O}(\varepsilon)\,. \tag{3.53}$$

Another singularity appears when $\beta\to 0$, actually at any value of gluon transverse momentum $\vec{k}$. In this region $S_J^{(3)}\left(\vec{q}-\vec{k},\vec{k},x\beta;x\right)\to S_J^{(2)}\left(\vec{q}-\vec{k};x\right)$ and it is convenient to introduce the counterterm

$$\begin{aligned} V_q^{(R)(C_A,\mathrm{soft})}(\vec{q}) &= \frac{C_A}{(4\pi)^\varepsilon}\int_0^1 dx\sum_{a=q,\bar{q}} f_a(x)\int\frac{d^{D-2}k}{\pi^{1+\varepsilon}}\int_{\beta_0}^1 d\beta\,\frac{2}{\beta} \\ &\times \vec{q}^{\,2}\,\frac{(1-\beta)\vec{k}\cdot(\vec{k}-\beta\vec{q})}{\vec{k}^{\,2}(\vec{q}-\vec{k})^2(\vec{k}-\beta\vec{q})^2}S_J^{(2)}\left(\vec{q}-\vec{k};x\right) \\ &= \frac{C_A}{(4\pi)^\varepsilon}\int_0^1 dx\sum_{a=q,\bar{q}} f_a(x)\int\frac{d^{D-2}k}{\pi^{1+\varepsilon}}\int_{\beta_0}^1 d\beta\,\frac{2}{\beta} \\ &\times \frac{\vec{q}^{\,2}\Theta[(1-\beta)|\vec{k}|-\beta|\vec{q}-\vec{k}|]}{\vec{k}^2(\vec{q}-\vec{k})^2}S_J^{(2)}\left(\vec{q}-\vec{k};x\right)\,, \end{aligned} \tag{3.54}$$

where the averaging over the relative angle between the vectors $\vec{k}$ and $\vec{q}-\vec{k}$ has been performed (see Eq. (A.3)). The integration over β gives the following result for the counterterm:

$$V_q^{(R)(C_A,\mathrm{soft})}(\vec{q}) = \frac{C_A}{(4\pi)^\varepsilon}\int_0^1 dx\sum_{a=q,\bar{q}} f_a(x)\int\frac{d^{D-2}k}{\pi^{1+\varepsilon}}\,\frac{\vec{q}^{\,2}}{\vec{k}^2(\vec{q}-\vec{k})^2} \times \ln\frac{s_\Lambda^2}{\vec{k}^2(|\vec{k}|+|\vec{q}-\vec{k}|)^2}\;S_J^{(2)}\left(\vec{q}-\vec{k};x\right)\,. \tag{3.55}$$

The finite part of the real corrections proportional to C_A is therefore defined by

$$V_q^{(R)(C_A,\text{finite})} = V_q^{(R)(C_A)} - V_q^{(R)(C_A,\text{coll})} - V_q^{(R)(C_A,\text{soft})}\,. \tag{3.56}$$

When the quark part of BFKL counterterm, given in (3.35),

$$\begin{aligned} V_q^{(C)}(\vec{q}) \;&=\; -\frac{C_A}{(4\pi)^\varepsilon}\int_0^1 dx \sum_{a=q,\bar{q}} f_a(x) \int \frac{d^{D-2}k}{\pi^{1+\varepsilon}} \ln\left(\frac{s_\Lambda^2}{s_0 \vec{k}^2}\right) \\ &\quad \times \frac{\vec{q}^{\,2}}{\vec{k}^{\,2}(\vec{q}-\vec{k})^2} S_J^{(2)}\left(\vec{q}-\vec{k}\,;\, x\right)\,, \end{aligned} \tag{3.57}$$

is combined with $V_q^{(R)(C_A,\text{soft})}$ given in (3.55), we see that the dependence on s_Λ disappears, as expected, and we get

$$\begin{aligned} &V_q^{(R)(C_A,\text{soft})}(\vec{q}) + V_q^{(C)}(\vec{q}) = \frac{C_A}{(4\pi)^\varepsilon}\int_0^1 dx \sum_{a=q,\bar{q}} f_a(x) \\ &\times \int \frac{d^{D-2}k}{\pi^{1+\varepsilon}} \frac{\vec{q}^{\,2}}{\vec{k}^{\,2}(\vec{k}-\vec{q})^2} \ln\left(\frac{s_0}{(|\vec{k}|+|\vec{q}-\vec{k}|)^2}\right)\; S_J^{(2)}(\vec{q}-\vec{k};x)\,. \end{aligned} \tag{3.58}$$

3.4.3 Final result for the quark in the initial state

We collect first the contributions given in (3.39), (3.44), (3.47), (3.48) and (3.53):

$$\begin{aligned} V_q^{(1)}(\vec{q}) &\equiv \left(V_q^{(V)} + V_q^{(R)(C_F,\text{soft})} + V_q^{(R)(C_F,\text{coll}_1)} + V_q^{(R)(C_F,\text{coll}_2)} + V_q^{(R)(C_A,\text{coll})}\right)(\vec{q}) \\ &= \frac{\Gamma[1-\varepsilon]}{\varepsilon\,(4\pi)^\varepsilon}\frac{\Gamma^2(1+\varepsilon)}{\Gamma(1+2\varepsilon)}\int_0^1 dx \sum_{a=q,\bar{q}} f_a(x) \\ &\times \left\{\left[(\vec{q}^{\,2})^\varepsilon\left(\frac{N_F}{3} - C_A\ln\left(\frac{s_0}{\vec{q}^{\,2}}\right) - \frac{11C_A}{6}\right) + \varepsilon\left(C_A\left(\frac{85}{18}+\frac{\pi^2}{2}\right)\right.\right.\right. \\ &- \left.\left.\left.\frac{5}{9}N_F + C_F\left(3\ln\frac{\vec{q}^{\,2}}{\Lambda^2} - 4\right)\right)\right]\; S_J^{(2)}(\vec{q};x) \\ &+ (\Lambda^2)^\varepsilon\int_0^1 d\beta\left[P_{qq}(\beta) + \frac{C_A}{C_F}P_{gq}(\beta)\right]\; S_J^{(2)}(\vec{q};x\beta) + \varepsilon\int_0^1 d\beta\left[2(1+\beta^2)\right. \\ &\times \left.\left(\frac{\ln(1-\beta)}{1-\beta}\right)_+ C_F + C_F(1-\beta) + C_A\beta\right]\; S_J^{(2)}(\vec{q};x\beta)\Bigg\} + \mathcal{O}(\varepsilon)\,. \end{aligned} \tag{3.59}$$

Then, we collect the finite contributions, given in Eqs. (3.50) and (3.56), transforming them to the form used in [72]:

$$
\begin{aligned}
V_q^{(2)}(\vec{q}) &\equiv \left(V_q^{(R)(C_F,\text{finite})} + V_q^{(R)(C_A,\text{finite})}\right)(\vec{q}) \\
&= \int_0^1 dx \sum_{a=q,\bar{q}} f_a(x) \left[C_F \int_0^1 d\beta \frac{1}{(1-\beta)_+}(1+\beta^2) \int \frac{d^2l}{\pi\,\vec{l}^{\,2}} \left[\frac{\vec{q}^{\,2}}{\vec{l}^2 + (\vec{q}-\vec{l})^2} \right.\right. \\
&\quad \times \Big\{ S_J^{(3)}(\vec{q} - (1-\beta)\vec{l}, (1-\beta)\vec{l}, x(1-\beta); x) \\
&\quad + S_J^{(3)}(\vec{q}\beta + (1-\beta)\vec{l}, (1-\beta)(\vec{q}-\vec{l}), x(1-\beta); x) \Big\} \\
&\quad \left.\left. - \Theta(\Lambda^2 - \vec{l}^{\,2}) \left\{ S_J^{(2)}(\vec{q}; x\beta) + S_J^{(2)}(\vec{q}; x) \right\} \right] \right. \\
&\quad + C_A \int \frac{d^2k}{\pi\vec{k}^2} \int_0^1 d\beta \left\{ \frac{1+(1-\beta)^2}{\beta} \right. \\
&\quad \times \left[\frac{\vec{q}^{\,2}(1-\beta)(\vec{q}-\vec{k})\cdot(\vec{q}(1-\beta)-\vec{k})}{(\vec{q}-\vec{k})^2(\vec{q}(1-\beta)-\vec{k})^2} S_J^{(3)}(\vec{k}, \vec{q}-\vec{k}, x\beta; x) \right. \\
&\left. \left. - \Theta(\Lambda^2 - \vec{k}^2) S_J^{(2)}(\vec{q}; x\beta) \right] - \frac{2\,\vec{q}^{\,2}\Theta[(1-\beta)|\vec{q}-\vec{k}| - \beta|\vec{k}|]}{\beta(\vec{q}-\vec{k})^2} S_J^{(2)}(\vec{k}; x) \right\} \Bigg] + \mathcal{O}(\varepsilon)\,.
\end{aligned}
\tag{3.60}
$$

Besides, we define

$$
V_q^{(3)}(\vec{q}) \equiv \left(V_q^{(R)(C_A,\text{soft})} + V_q^{(C)}\right)(\vec{q})\,,
$$

given in Eq. (3.58).

Another contribution originates from the collinear and charge renormalization counterterms, see Eqs. (3.32) and (3.34),

$$
\begin{aligned}
V_q^{(4)}(\vec{q}) = \frac{\Gamma[1-\varepsilon]}{\varepsilon\,(4\pi)^\varepsilon} \int_0^1 dx \sum_{a=q,\bar{q}} f_a(x) \Bigg[\left(\mu_R^2\right)^\varepsilon \left(\frac{11 C_A}{6} - \frac{N_F}{3} \right) S_J^{(2)}(\vec{q}; x) \\
- \left(\mu_F^2\right)^\varepsilon \int_0^1 d\beta \left[P_{qq}(\beta) + \frac{C_A}{C_F} P_{gq}(\beta) \right] S_J^{(2)}(\vec{q}; x\beta) \Bigg]\,.
\end{aligned}
\tag{3.61}
$$

Finally, the quark part of the jet impact factor is given by the sum of the above four contributions and can be presented as the sum of two terms:

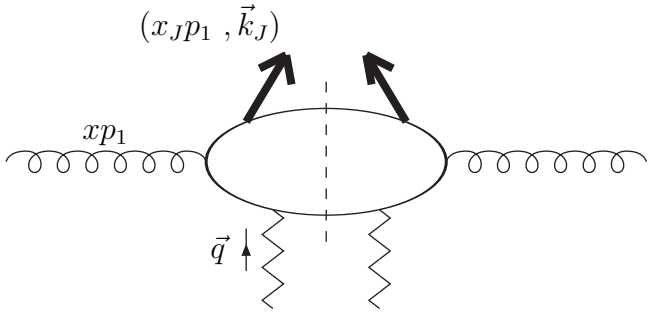

Figure 3.3: Schematic representation of the jet vertex for the case of gluon in the initial state. Here p_1 is the proton momentum, x is the fraction of proton momentum carried by the gluon, $x_J p_1$ is the longitudinal jet momentum, $\vec{k}_J$ is the transverse jet momentum and $\vec{q}$ is the transverse momentum of the incoming Reggeized gluon.

$$V_q^{(I)}(\vec{q}) = \int_0^1 dx \sum_{a=q,\bar{q}} f_a(x) \left[\frac{C_A}{(4\pi)^\varepsilon} \int \frac{d^{D-2}k}{\pi^{1+\varepsilon}} \frac{\vec{q}^{\,2}}{\vec{k}^{\,2}(\vec{k}-\vec{q})^2} \ln \frac{s_0}{(|\vec{k}|+|\vec{q}-\vec{k}|)^2} \right.$$

$$\left. \times S_J^{(2)}(\vec{k};x) - C_A \ln\left(\frac{s_0}{\vec{q}^{\,2}}\right) \left(\vec{q}^{\,2}\right)^\varepsilon \frac{\Gamma[1-\varepsilon]}{\varepsilon\,(4\pi)^\varepsilon} \frac{\Gamma^2(1+\varepsilon)}{\Gamma(1+2\varepsilon)} S_J^{(2)}(\vec{q};x) \right] \tag{3.62}$$

and

$$V_q^{(II)}(\vec{q}) = V_q^{(2)}(\vec{q}) + \int_0^1 dx \sum_{a=q,\bar{q}} f_a(x) \tag{3.63}$$

$$\times \left\{ \left[\left(\frac{N_F}{3} - \frac{11 C_A}{6} \right) \ln \frac{\vec{q}^{\,2}}{\mu_R^2} + C_A \left(\frac{85}{18} + \frac{\pi^2}{2} \right) - \frac{5}{9} N_F + C_F \left(3 \ln \frac{\vec{q}^{\,2}}{\Lambda^2} - 4 \right) \right] \right.$$

$$\times S_J^{(2)}(\vec{q};x) + \int_0^1 d\beta \left[P_{qq}(\beta) + \frac{C_A}{C_F} P_{gq}(\beta) \right] \ln \frac{\Lambda^2}{\mu_F^2}\ S_J^{(2)}(\vec{q};x\beta)$$

$$\left. + \int_0^1 d\beta \left[2 \left(\frac{\ln(1-\beta)}{1-\beta} \right)_+ (1+\beta^2)\, C_F + C_F(1-\beta) + C_A \beta \right]\ S_J^{(2)}(\vec{q};x\beta) \right\} .$$

3.5 NLA jet impact factor: the gluon contribution

We consider now the case of incoming gluon (see Fig. 3.3).

3.5.1 Virtual corrections

Virtual corrections are the same as in the case of the inclusive gluon impact factor [59, 93]:

$$
\begin{aligned}
V_g^{(V)}(\vec{q}) &= -\frac{\Gamma[1-\varepsilon]}{\varepsilon\,(4\pi)^\varepsilon}\frac{\Gamma^2(1+\varepsilon)}{\Gamma(1+2\varepsilon)}\left(\vec{q}^{\,2}\right)^\varepsilon \int_0^1 dx\,\frac{C_A}{C_F}\,f_g(x)\,S_J^{(2)}(\vec{q};x) \qquad (3.64)\\
&\times \left[C_A \ln\left(\frac{s_0}{\vec{q}^{\,2}}\right) + C_A\left(\frac{2}{\varepsilon} - \frac{11+9\varepsilon}{2(1+2\varepsilon)(3+2\varepsilon)}\right.\right.\\
&+ \left.\left.\frac{N_F}{C_A}\frac{(1+\varepsilon)(2+\varepsilon)-1}{(1+\varepsilon)(1+2\varepsilon)(3+2\varepsilon)} + \psi(1) + \psi(1-\varepsilon) - 2\psi(1+\varepsilon)\right)\right.\\
&+ \left. C_A\frac{\varepsilon}{(1+\varepsilon)(1+2\varepsilon)(3+2\varepsilon)}\left(1+\varepsilon-\frac{N_F}{C_A}\right)\frac{1}{(1+\varepsilon)}\right].
\end{aligned}
$$

The ε-expansion has the form

$$
\begin{aligned}
V_g^{(V)}(\vec{q}) &= -\frac{\Gamma[1-\varepsilon]}{\varepsilon\,(4\pi)^\varepsilon}\frac{\Gamma^2(1+\varepsilon)}{\Gamma(1+2\varepsilon)}\left(\vec{q}^{\,2}\right)^\varepsilon \int_0^1 dx\,\frac{C_A}{C_F}\,f_g(x)\,S_J^{(2)}(\vec{q};x)\\
&\times \left[C_A\left(\ln\left(\frac{s_0}{\vec{q}^{\,2}}\right) + \frac{2}{\varepsilon} - \frac{11}{6}\right) + \frac{N_F}{3}\right.\\
&+ \left.\varepsilon\left\{C_A\left(\frac{67}{18} - \frac{\pi^2}{2}\right) - \frac{5}{9}N_F\right\}\right] + \mathcal{O}(\varepsilon)\,. \qquad (3.65)
\end{aligned}
$$

3.5.2 Real corrections: $q\bar{q}$ intermediate state

In the NLO gluon impact factor real corrections come from intermediate states of two particles, which can be quark-antiquark or gluon-gluon.
The real contribution from the quark-antiquark case is [59, 61, 93]:

$$
\begin{aligned}
V_g^{(R_{q\bar{q}})}(\vec{q}) &= \frac{N_F}{(4\pi)^\varepsilon}\int_0^1 dx\,\frac{C_A}{C_F}\,f_g(x)\int_0^1 d\beta\int\frac{d^{D-2}k}{\pi^{1+\varepsilon}}\,\frac{\vec{q}^{\,2}}{\vec{k}^{\,2}(\vec{k}-\vec{q})^2} \qquad (3.66)\\
&\times\; T_R\,\mathcal{P}_{qg}(\varepsilon,\beta)\left[\frac{C_F}{C_A} + \frac{\beta(1-\beta)\vec{k}\cdot(\vec{q}-\vec{k})}{(\vec{k}-\beta\vec{q})^2}\right] S_J^{(3)}(\vec{q}-\vec{k},\vec{k},x\beta;x)\,,
\end{aligned}
$$

with

$$
\mathcal{P}_{qg}(\varepsilon,\beta) = 1 - \frac{2\beta(1-\beta)}{1+\varepsilon}\,. \qquad (3.67)
$$

Below we discuss separately the first and the second contributions in the r.h.s. of Eq. (3.66), which we denote $V_g^{(R_{q\bar{q}})(C_F)}$ and $V_g^{(R_{q\bar{q}})(C_A)}$.
The first contribution is

$$
\begin{aligned}
V_g^{(R_{q\bar{q}})(C_F)}(\vec{q}) &= \frac{N_F}{(4\pi)^\varepsilon}\int_0^1 dx\,\frac{C_A}{C_F}\,f_g(x)\int_0^1 d\beta\int\frac{d^{D-2}k}{\pi^{1+\varepsilon}}\frac{\vec{q}^{\,2}}{\vec{k}^{\,2}(\vec{k}-\vec{q})^2}\\
&\times\; T_R\,\mathcal{P}_{qg}(\varepsilon,\beta)\,\frac{C_F}{C_A}\,S_J^{(3)}(\vec{q}-\vec{k},\vec{k},x\beta;x) \qquad (3.68)\\
&= \frac{N_F}{(4\pi)^\varepsilon}\int_0^1 dx\,f_g(x)\int_0^1 d\beta\,T_R\,\mathcal{P}_{qg}(\varepsilon,\beta)\int\frac{d^{D-2}k}{\pi^{1+\varepsilon}}\\
&\times\; \frac{\vec{q}^{\,2}}{\vec{k}^2+(\vec{q}-\vec{k})^2}\left[\frac{1}{\vec{k}^2}+\frac{1}{(\vec{q}-\vec{k})^2}\right]S_J^{(3)}(\vec{q}-\vec{k},\vec{k},x\beta;x)\,.
\end{aligned}
$$

Here we have collinear divergences for $\vec{k}=0$ and $\vec{q}-\vec{k}=0$. The contribution in these kinematical regions is the same, as can be easily seen after the changes of variables $\vec{k}\to\vec{q}-\vec{k}$ and $\beta\to 1-\beta$, since $\mathcal{P}_{qg}(\varepsilon,\beta)=\mathcal{P}_{qg}(\varepsilon,1-\beta)$ and taking into account the property (3.22) that the $S_J^{(3)}$ jet selection function has to possess. Therefore we can write

$$
\begin{aligned}
V_g^{(R_{q\bar{q}})(C_F)}(\vec{q}) &= \frac{2N_F}{(4\pi)^\varepsilon}\int_0^1 dx\,f_g(x)\int_0^1 d\beta\,T_R\,\mathcal{P}_{qg}(\varepsilon,\beta)\\
&\times\; \int\frac{d^{D-2}k}{\pi^{1+\varepsilon}\,\vec{k}^2}\;\frac{\vec{q}^{\,2}}{\vec{k}^2+(\vec{q}-\vec{k})^2}\;S_J^{(3)}(\vec{k},\vec{q}-\vec{k},x\beta;x) \qquad (3.69)
\end{aligned}
$$

and isolate the collinearly divergent part given by

$$
\begin{aligned}
V_g^{(R_{q\bar{q}})(C_F,\mathrm{coll})}(\vec{q}) &= \frac{2N_F}{(4\pi)^\varepsilon}\int_0^1 dx\,f_g(x)\int_0^1 d\beta\,T_R\,\mathcal{P}_{qg}(\varepsilon,\beta) \qquad (3.70)\\
&\times\; \int\frac{d^{D-2}k}{\pi^{1+\varepsilon}\,\vec{k}^2}\;\Theta(\Lambda^2-\vec{k}^2)\;S_J^{(2)}(\vec{q};x\beta) \qquad (3.71)
\end{aligned}
$$

where we have introduced, as before, the cutoff parameter Λ and we made use of Eq. (3.21). After a simple calculation we obtain (see Eq. (A.2))

$$
\begin{aligned}
V_g^{(R_{q\bar{q}})(C_F,\mathrm{coll})}(\vec{q}) &= 2N_F\,\frac{\Gamma[1-\varepsilon]}{\varepsilon\,(4\pi)^\varepsilon}\frac{\Gamma^2(1+\varepsilon)}{\Gamma(1+2\varepsilon)}\left(\Lambda^2\right)^\varepsilon\int_0^1 dx\,f_g(x) \qquad (3.72)\\
&\times\; \int_0^1 d\beta\;\left[P_{qg}(\beta)+\varepsilon\beta(1-\beta)\right]\;S_J^{(2)}(\vec{q};x\beta)+\mathcal{O}(\varepsilon)\,,
\end{aligned}
$$

The finite part is therefore defined by

$$
V_g^{(R_{q\bar{q}})(C_F,\mathrm{finite})}=V_g^{(R_{q\bar{q}})(C_F)}-V_g^{(R_{q\bar{q}})(C_F,\mathrm{coll})}\,, \qquad (3.73)
$$

where one can take $\varepsilon \to 0$ limit and get

$$V_g^{(R_{q\bar{q}})(C_F,\text{finite})} = 2N_F \int_0^1 dx\, f_g(x) \int_0^1 d\beta\, P_{qg}(\beta) \tag{3.74}$$

$$\times \int \frac{d^2\vec{k}}{\pi\,\vec{k}^2} \left[\frac{\vec{q}^{\,2}}{\vec{k}^2 + (\vec{q}-\vec{k})^2} S_J^{(3)}(\vec{k}, \vec{q}-\vec{k}, x\beta; x) - \Theta(\Lambda^2 - \vec{k}^2)\; S_J^{(2)}(\vec{q}; x\beta) \right] + \mathcal{O}(\varepsilon)\,.$$

The second contribution in (3.66) is

$$V_g^{(R_{q\bar{q}})(C_A)}(\vec{q}) = \frac{N_F}{(4\pi)^\varepsilon} \int_0^1 dx\, \frac{C_A}{C_F}\, f_g(x) \int_0^1 d\beta \int \frac{d^{D-2}k}{\pi^{1+\varepsilon}} \frac{\vec{q}^{\,2}}{\vec{k}^{\,2}(\vec{q}-\vec{k})^2}$$

$$\times\, T_R\, \mathcal{P}_{qg}(\varepsilon,\beta) \frac{\beta(1-\beta)\vec{k}\cdot(\vec{q}-\vec{k})}{(\vec{k}-\beta\vec{q})^2} S_J^{(3)}(\vec{q}-\vec{k}, \vec{k}, x\beta; x)\,. \tag{3.75}$$

Here the collinear divergence appears for $\vec{k} - \beta\vec{q} = 0$ and the integral in this region, using the Eq. (3.19), can be identified with (see Eq. (A.2))

$$\begin{aligned} V_g^{(R_{q\bar{q}})(C_A,\text{coll})}(\vec{q}) \;&=\; \frac{N_F}{(4\pi)^\varepsilon} \int_0^1 dx\, \frac{C_A}{C_F}\, f_g(x) \int_0^1 d\beta\, T_R\, \mathcal{P}_{qg}(\varepsilon,\beta) \\ &\times\; \int \frac{d^{D-2}k}{\pi^{1+\varepsilon}(\vec{k}-\beta\vec{q})^2} \Theta(\Lambda^2 - (\vec{k}-\beta\vec{q})^2) S_J^{(2)}(\vec{q}; x) \\ &=\; N_F\, \frac{\Gamma[1-\varepsilon]}{\varepsilon\,(4\pi)^\varepsilon} \frac{\Gamma^2(1+\varepsilon)}{\Gamma(1+2\varepsilon)} \left(\Lambda^2\right)^\varepsilon \left(\frac{1}{3} + \frac{\varepsilon}{6}\right) \\ &\times\; \int_0^1 dx\, \frac{C_A}{C_F}\, f_g(x) S_J^{(2)}(\vec{q}; x) + \mathcal{O}(\varepsilon)\,. \end{aligned} \tag{3.76}$$

Then, the finite part can be written as

$$V_g^{(R_{q\bar{q}})(C_A,\text{finite})} = V_g^{(R_{q\bar{q}})(C_A)} - V_g^{(R_{q\bar{q}})(C_A,\text{coll})}\,. \tag{3.77}$$

After the change of variable $\vec{k} \to \vec{q} - \vec{k}$ in (3.75) and (3.76) we have

$$V_g^{(R_{q\bar{q}})(C_A,\text{finite})}(\vec{q}) \;=\; N_F \int_0^1 dx\, \frac{C_A}{C_F}\, f_g(x) \int_0^1 d\beta\, P_{qg}(\beta) \tag{3.78}$$

$$\times \int \frac{d^2\vec{k}}{\pi\,(\vec{k}-(1-\beta)\vec{q})^2} \left[\frac{\vec{q}^{\,2}\beta(1-\beta)\vec{k}\cdot(\vec{q}-\vec{k})}{\vec{k}^{\,2}(\vec{k}-\vec{q})^2} S_J^{(3)}(\vec{k}, \vec{q}-\vec{k}, x\beta; x) \right.$$

$$\left. -\Theta(\Lambda^2 - (\vec{k}-(1-\beta)\vec{q})^2) S_J^{(2)}(\vec{q}; x) \right] + \mathcal{O}(\varepsilon)\,.$$

3.5.3 Real corrections: gg intermediate state

The real contribution from the gluon-gluon case is [59, 61, 93]:

$$\begin{aligned} V_g^{(R_{gg})}(\vec{q}) &= \frac{C_A}{(4\pi)^\varepsilon}\int_0^1 dx\,\frac{C_A}{C_F}\,f_g(x)\int\frac{d^{D-2}k}{\pi^{1+\varepsilon}}\int_{\beta_0}^{1-\beta_0}d\beta\frac{\vec{q}^{\,2}\;\mathcal{P}_{gg}(\beta)}{(\vec{k}-\beta\vec{q})^2\vec{k}^2(\vec{k}-\vec{q})^2} \\ &\times \Big\{\beta^2(\vec{k}-\vec{q})^2+(1-\beta)^2\vec{k}^2-\beta(1-\beta)\vec{k}\cdot(\vec{q}-\vec{k})\Big\} \\ &\times S_J^{(3)}(\vec{q}-\vec{k},\vec{k},x\beta;x)\,. \end{aligned} \tag{3.79}$$

where

$$\mathcal{P}_{gg}(\beta)=P(\beta)+P(1-\beta)\,,\qquad\text{with}\qquad P(\beta)=\left(\frac{1}{\beta}+\frac{\beta}{2}\right)(1-\beta)\,.$$

We note that here the lower integration limit in β is $\beta_0=\vec{k}^{\,2}/s_\Lambda$, whereas the upper limit is $1-\beta_0$. This comes from the Θ function in the impact factor definition (3.8), which restricts the radiation of either of the two gluons into the central region of rapidity.
Using the symmetry of the integrand under the change of variables describing the two gluons, $\beta\to 1-\beta$ and $\vec{k}\to\vec{q}-\vec{k}$ (thanks to the symmetry property (3.22) of the jet function), we get

$$\begin{aligned} V_g^{(R_{gg})}(\vec{q}) &= 2\,\frac{C_A}{(4\pi)^\varepsilon}\int_0^1 dx\,\frac{C_A}{C_F}\,f_g(x)\int\frac{d^{D-2}k}{\pi^{1+\varepsilon}}\int_{\beta_0}^{1-\beta_0}d\beta\,P(\beta) \\ &\times \frac{\vec{q}^{\,2}}{(\vec{k}-\beta\vec{q})^2\vec{k}^2(\vec{k}-\vec{q})^2}\Big\{\beta^2(\vec{k}-\vec{q})^2+(1-\beta)\vec{k}\cdot(\vec{k}-\beta\vec{q})\Big\} \\ &\times S_J^{(3)}(\vec{q}-\vec{k},\vec{k},x\beta;x)\equiv V_g^{(R_{gg})(A)}(\vec{q})+V_g^{(R_{gg})(B)}(\vec{q})\,. \end{aligned} \tag{3.80}$$

In this form the upper limit of β integration can be put to unity.

In $V_g^{(R_{gg})(A)}$ the lower integration limit β_0 can be put equal to zero. Then, after the change of variable $\vec{k}=\beta\vec{l}$, we obtain

$$\begin{aligned} V_g^{(R_{gg})(A)}(\vec{q}) &= 2\,\frac{C_A}{(4\pi)^\varepsilon}\int_0^1 dx\,\frac{C_A}{C_F}\,f_g(x)\int_0^1 d\beta P(\beta)\beta^{2\varepsilon}\int\frac{d^{D-2}l}{\pi^{1+\varepsilon}} \\ &\times \frac{\vec{q}^{\,2}}{\vec{l}^{\,2}(\vec{l}-\vec{q})^2}S_J^{(3)}(\vec{q}-\beta\vec{l},\beta\vec{l},x\beta;x) \end{aligned} \tag{3.81}$$

$$
\begin{aligned}
&= 2\,\frac{C_A}{(4\pi)^\varepsilon}\int_0^1 dx\,\frac{C_A}{C_F}\,f_g(x)\int_0^1 d\beta P(\beta)\beta^{2\varepsilon}\int\frac{d^{D-2}l}{\pi^{1+\varepsilon}}\\
&\times\ \frac{\vec{q}^{\,2}}{\vec{l}^{\,2}+(\vec{l}-\vec{q})^2}\left[\frac{1}{\vec{l}^{\,2}}+\frac{1}{(\vec{l}-\vec{q})^2}\right]S_J^{(3)}(\vec{q}-\beta\vec{l},\beta\vec{l},x\beta;x)\,.
\end{aligned}
$$

In this expression one has both soft and collinear divergences. The soft divergence can be isolated in the counterterm

$$
\begin{aligned}
V_g^{(R_{gg})(A,\mathrm{soft})}(\vec{q}) &= 2\,\frac{C_A}{(4\pi)^\varepsilon}\int_0^1 dx\,\frac{C_A}{C_F}\,f_g(x)\int_0^1\frac{d\beta}{\beta^{1-2\varepsilon}}\int\frac{d^{D-2}l}{\pi^{1+\varepsilon}}\frac{\vec{q}^{\,2}}{\vec{l}^{\,2}+(\vec{l}-\vec{q})^2}\\
&\times\ \left[\frac{1}{(\vec{l}-\vec{q})^2}+\frac{1}{\vec{l}^{\,2}}\right]S_J^{(2)}(\vec{q};x)\,, \qquad (3.82)
\end{aligned}
$$

which equals (see Eq. (A.1))

$$
V_g^{(R_{gg})(A,\mathrm{soft})}(\vec{q}) = \frac{\Gamma[1-\varepsilon]}{\varepsilon\,(4\pi)^\varepsilon}\frac{\Gamma^2(1+\varepsilon)}{\Gamma(1+2\varepsilon)}\left(\vec{q}^{\,2}\right)^\varepsilon\,\frac{2\,C_A}{\varepsilon}\int_0^1 dx\,\frac{C_A}{C_F}\,f_g(x)\,S_J^{(2)}(\vec{q};x)\,. \qquad (3.83)
$$

After the subtraction of the soft divergence, collinear divergences still appear for $\vec{l}-\vec{q}=0$ and $\vec{l}=0$ and can be isolated by the following two counterterms:

$$
\begin{aligned}
V_g^{(R_{gg})(A,\mathrm{coll}_1)}(\vec{q}) &= 2\,\frac{C_A}{(4\pi)^\varepsilon}\int_0^1 dx\,\frac{C_A}{C_F}\,f_g(x)\int\frac{d^{D-2}l}{\pi^{1+\varepsilon}(\vec{q}-\vec{l})^2}\,\Theta\left(\Lambda^2-(\vec{q}-\vec{l})^2\right)\\
&\times\ \int_0^1 d\beta\beta^{2\varepsilon}\left(P(\beta)-\frac{1}{\beta}\right)S_J^{(2)}(\vec{q};x) \qquad (3.84)
\end{aligned}
$$

and

$$
\begin{aligned}
V_g^{(R_{gg})(A,\mathrm{coll}_2)}(\vec{q}) &= 2\,\frac{C_A}{(4\pi)^\varepsilon}\int_0^1 dx\,\frac{C_A}{C_F}\,f_g(x)\int\frac{d^{D-2}l}{\pi^{1+\varepsilon}\vec{l}^{\,2}}\,\Theta\left(\Lambda^2-\vec{l}^{\,2}\right) \qquad (3.85)\\
&\times\ \int_0^1 d\beta\,\beta^{2\varepsilon}\left(P(\beta)S_J^{(2)}(\vec{q};x(1-\beta))-\frac{1}{\beta}S_J^{(2)}(\vec{q};x)\right)\,,
\end{aligned}
$$

where we made use of Eq. (3.19) for the first case and Eq. (3.20) for the second case. These counterterms equal (see Eq. (A.2))

$$
\begin{aligned}
V_g^{(R_{gg})(A,\mathrm{coll}_1)}(\vec{q}) &= \frac{\Gamma[1-\varepsilon]}{\varepsilon\,(4\pi)^\varepsilon}\frac{\Gamma^2(1+\varepsilon)}{\Gamma(1+2\varepsilon)}\left(\Lambda^2\right)^\varepsilon\int_0^1 dx\,\frac{C_A}{C_F}\,f_g(x)\,S_J^{(2)}(\vec{q};x)\\
&\times\ C_A\left(-\frac{11}{6}+\varepsilon\,\frac{67}{18}\right)+\mathcal{O}(\varepsilon)\,, \qquad (3.86)
\end{aligned}
$$

$$
\begin{aligned}
V_g^{(R_{gg})(A,\mathrm{coll}_2)}(\vec{q}) &= \frac{\Gamma[1-\varepsilon]}{\varepsilon\,(4\pi)^{\varepsilon}}\frac{\Gamma^2(1+\varepsilon)}{\Gamma(1+2\varepsilon)}\left(\Lambda^2\right)^{\varepsilon}\int_0^1 dx\,\frac{C_A}{C_F}\,f_g(x) \\
&\times \int_0^1 d\beta(1-\beta)P(1-\beta)2\,C_A\left[\frac{1}{(1-\beta)_+}\right. \\
&+ \left. 2\varepsilon\left(\frac{\ln(1-\beta)}{1-\beta}\right)_+\right] S_J^{(2)}(\vec{q};x\beta)+\mathcal{O}(\varepsilon)\,, \qquad (3.87)
\end{aligned}
$$

where to obtain the last equation we made the change of variable $\beta \to 1-\beta$ and expanded the term $(1-\beta)^{2\varepsilon-1}$. The finite part is therefore defined by

$$
V_g^{(R_{gg})(A,\mathrm{finite})} = V_g^{(R_{gg})(A)} - V_g^{(R_{gg})(A,\mathrm{soft})} - V_g^{(R_{gg})(A,\mathrm{coll}_1)} - V_g^{(R_{gg})(A,\mathrm{coll}_2)}\,. \quad (3.88)
$$

The $V_g^{(R_{gg})(B)}$ term, defined in (3.80), has a collinear divergence for $\vec{k}-\vec{q}=0$. It can be isolated in the following integral:

$$
\begin{aligned}
V_g^{(R_{gg})(B,\mathrm{coll})}(\vec{q}) &= 2\,\frac{C_A}{(4\pi)^{\varepsilon}}\int_0^1 dx\,\frac{C_A}{C_F}\,f_g(x)\int_0^1 d\beta P(\beta) \qquad (3.89)\\
&\times \int\frac{d^{D-2}k}{\pi^{1+\varepsilon}(\vec{k}-\vec{q})^2}\Theta\left(\Lambda^2-(\vec{k}-\vec{q})^2\right)S_J^{(2)}(\vec{q};x\beta)\,, \\
&= \frac{\Gamma[1-\varepsilon]}{\varepsilon\,(4\pi)^{\varepsilon}}\frac{\Gamma^2(1+\varepsilon)}{\Gamma(1+2\varepsilon)}\left(\Lambda^2\right)^{\varepsilon}\int_0^1 dx\,\frac{C_A}{C_F}\,f_g(x) \\
&\times \int_0^1 d\beta\,2\,C_A\,P(\beta)\,S_J^{(2)}(\vec{q};x\beta)+\mathcal{O}(\varepsilon)\,,
\end{aligned}
$$

where β_0 has been put equal to zero thanks to the property of lowest order jet function (3.12) and the Eq. (3.21) and (A.2) are used.

Another singularity appears when $\beta \to 0$; in this region we can isolate the term

$$
V_g^{(R_{gg})(B,\mathrm{soft})}(\vec{q}) \qquad (3.90)
$$

$$
= 2\frac{C_A}{(4\pi)^{\varepsilon}}\int_0^1 dx\,\frac{C_A}{C_F}\,f_g(x)\int\frac{d^{D-2}k}{\pi^{1+\varepsilon}}\int_{\beta_0}^1\frac{d\beta}{\beta}\,\frac{\vec{q}^{\,2}\,(1-\beta)\vec{k}\cdot(\vec{k}-\beta\vec{q})}{\vec{k}^{\,2}(\vec{q}-\vec{k})^2(\vec{k}-\beta\vec{q})^2}\;S_J^{(2)}(\vec{q}-\vec{k};x)
$$

$$
\begin{aligned}
&= 2\frac{C_A}{(4\pi)^\varepsilon}\int_0^1 dx\,\frac{C_A}{C_F}\,f_g(x)\int\frac{d^{D-2}k}{\pi^{1+\varepsilon}}\int_{\beta_0}^1\frac{d\beta}{\beta}\frac{\vec{q}^{\,2}\Theta[(1-\beta)|\vec{k}|-\beta|\vec{q}-\vec{k}|]}{\vec{k}^2(\vec{k}-\vec{q})^2}\\
&\times\ S_J^{(2)}(\vec{q}-\vec{k};x)\\
&= 2\,\frac{C_A}{(4\pi)^\varepsilon}\int_0^1 dx\,\frac{C_A}{C_F}\,f_g(x)\int\frac{d^{D-2}k}{\pi^{1+\varepsilon}}\int_{\beta_0}^1\frac{d\beta}{\beta}\frac{\vec{q}^{\,2}\Theta[(1-\beta)|\vec{k}|-\beta|\vec{q}-\vec{k}|]}{\vec{k}^2(\vec{k}-\vec{q})^2}\\
&\times\ S_J^{(2)}(\vec{q}-\vec{k};x)\\
&= \frac{C_A}{(4\pi)^\varepsilon}\int_0^1 dx\,\frac{C_A}{C_F}\,f_g(x)\int\frac{d^{D-2}k}{\pi^{1+\varepsilon}}\frac{\vec{q}^{\,2}}{\vec{k}^2(\vec{k}-\vec{q})^2}\ln\frac{s_\Lambda^2}{\vec{k}^2(|\vec{k}|+|\vec{q}-\vec{k}|)^2}\\
&\times\ S_J^{(2)}(\vec{q}-\vec{k};x)\,,
\end{aligned}
$$

where we made use of (A.3).
The finite part of $V_g^{(R_{gg})(B)}$ is therefore defined by

$$
V_g^{(R_{gg})(B,\mathrm{finite})} = V_g^{(R_{gg})(B)} - V_g^{(R_{gg})(B,\mathrm{coll})} - V_g^{(R_{gg})(B,\mathrm{soft})}\,. \tag{3.91}
$$

When the gluon part of BFKL counterterm, given in (3.35), is combined with $V_q^{(R_{gg})(B,\mathrm{soft})}$, given in (3.90), we see that the dependence on s_Λ disappears and we obtain

$$
\begin{aligned}
V_g^{(R_{gg})(B,\mathrm{soft})}(\vec{q}) + V_g^{(C)}(\vec{q}) \;&=\; \frac{C_A}{(4\pi)^\varepsilon}\int_0^1 dx\,\frac{C_A}{C_F}\,f_g(x) \\
&\times\int\frac{d^{D-2}k}{\pi^{1+\varepsilon}}\frac{\vec{q}^{\,2}}{\vec{k}^2(\vec{k}-\vec{q})^2}\ln\frac{s_0}{(|\vec{k}|+|\vec{q}-\vec{k}|)^2}\;\; S_J^{(2)}(\vec{q}-\vec{k};x)\,.
\end{aligned} \tag{3.92}
$$

3.5.4 Final result for the gluon in the initial state

We collect first the contributions which contain singularities given in (3.65), (3.70), (3.76), (3.83), (3.86), (3.87) and (3.89) and get

$$
\begin{aligned}
V_g^{(1)}(\vec{q}) \;&\equiv\; \big(V_g^{(V)} + V_g^{(R_{q\bar{q}})(C_F,\mathrm{coll})} + V_g^{(R_{q\bar{q}})(C_A,\mathrm{coll})} + V_g^{(R_{gg})(A,\mathrm{soft})} \\
&+\; V_g^{(R_{gg})(A,\mathrm{coll}_1)} + V_g^{(R_{gg})(A,\mathrm{coll}_2)} + V_g^{(R_{gg})(B,\mathrm{coll})}\big)\,(\vec{q})
\end{aligned} \tag{3.93}
$$

$$
\begin{aligned}
&= \frac{\Gamma[1-\varepsilon]}{\varepsilon\,(4\pi)^{\varepsilon}}\frac{\Gamma^2(1+\varepsilon)}{\Gamma(1+2\varepsilon)}\int_0^1 dx\,\frac{C_A}{C_F}\,f_g(x)\left\{\left[(\vec{q}^{\,2})^{\varepsilon}\left(\frac{11C_A}{6}-\frac{N_F}{3}\right.\right.\right.\\
&- \left.\left.\left. C_A\ln\left(\frac{s_0}{\vec{q}^{\,2}}\right)\right)-2\left(\Lambda^2\right)^{\varepsilon}\left(\frac{11C_A}{6}-\frac{N_F}{3}\right)+\varepsilon\left(\frac{\pi^2 C_A}{2}+\frac{13N_F}{18}\right)\right]\right.\\
&\times\; S_J^{(2)}(\vec{q};x)+\left(\Lambda^2\right)^{\varepsilon}\int_0^1 d\beta\left(P_{gg}(\beta)+2N_F\frac{C_F}{C_A}P_{qg}(\beta)\right)S_J^{(2)}(\vec{q};x\beta)\\
&+\; 2\varepsilon\int_0^1 d\beta\left[N_F\frac{C_F}{C_A}(1-\beta)\beta+\,2\,C_A\left(\frac{\ln(1-\beta)}{1-\beta}\right)_+(1-\beta)P(1-\beta)\right]\\
&\times\; \left.S_J^{(2)}(\vec{q};x\beta)\right\}+\mathcal{O}(\varepsilon)\,.
\end{aligned}
$$

Then, we collect the contributions given in (3.74), (3.78), (3.88), (3.91), and get (transforming to the form used in [73])

$$
\begin{aligned}
&V_g^{(2)}(\vec{q})\equiv\left(V_g^{(R_{q\bar{q}})(C_F,\text{finite})}+V_g^{(R_{q\bar{q}})(C_A,\text{finite})}+V_g^{(R_{gg})(A,\text{finite})}\right.\\
&\left.+\,V_g^{(R_{gg})(B,\text{finite})}\right)(\vec{q})\\
&=\int_0^1 dx f_g(x)\int_0^1 d\beta\left[2\,N_F\,P_{qg}(\beta)\int\frac{d^2k}{\pi\vec{k}^2}\left\{\frac{\vec{q}^{\,2}}{\vec{k}^2+(\vec{q}-\vec{k})^2}\right.\right.\\
&\left.\left.\times S_J^{(3)}(\vec{k},\vec{q}-\vec{k},x\beta;x)-\Theta(\Lambda^2-\vec{k}^2)S_J^{(2)}(\vec{q};x\beta)\right\}+\,N_F\frac{C_A}{C_F}\,P_{qg}(\beta)\right.\\
&\times\int\frac{d^2k}{\pi(\vec{k}-(1-\beta)\vec{q})^2}\left\{\frac{\vec{q}^{\,2}\beta(1-\beta)\vec{k}\cdot(\vec{q}-\vec{k})}{\vec{k}^2(\vec{k}-\vec{q})^2}\,S_J^{(3)}(\vec{k},\vec{q}-\vec{k},x\beta;x)\right.\\
&\left.\left.-\Theta(\Lambda^2-(\vec{k}-(1-\beta)\vec{q})^2)S_J^{(2)}(\vec{q};x)\right\}\right]+\int_0^1 dx\,2\,C_A\frac{C_A}{C_F}\,f_g(x)\\
&\times\left[\int_0^1\frac{d\beta}{(1-\beta)_+}[(1-\beta)P(1-\beta)]\int\frac{d^2l}{\pi\vec{l}^2}\right.\\
&\times\left\{\frac{\vec{q}^{\,2}}{\vec{l}^2+(\vec{l}-\vec{q})^2}\right.\Big(\,S_J^{(3)}(\vec{q}-(1-\beta)\vec{l},(1-\beta)\vec{l},x(1-\beta);x)\\
&+S_J^{(3)}(\beta\vec{q}+(1-\beta)\vec{l},(1-\beta)(\vec{q}-\vec{l}),x(1-\beta);x)\Big)\\
&\left.-\Theta\left(\Lambda^2-\vec{l}^{\,2}\right)\left(S_J^{(2)}(\vec{q};x\beta)+S_J^{(2)}(\vec{q};x)\right)\right\}+\int_0^1 d\beta\int\frac{d^2k}{\pi}\\
&\times\left\{P(\beta)\left(\frac{\vec{q}^{\,2}(1-\beta)\vec{k}\cdot(\vec{k}-\beta\vec{q})}{(\vec{k}-\beta\vec{q})^2(\vec{k}-\vec{q})^2\vec{k}^{\,2}}\,S_J^{(3)}(\vec{q}-\vec{k},\vec{k},x\beta;x)\right.\right.
\end{aligned}
\tag{3.94}
$$

$$
-\frac{1}{(\vec{k}-\vec{q})^2}\Theta\left(\Lambda^2-(\vec{k}-\vec{q})^2\right) S_J^{(2)}(\vec{q};x\beta)\Bigg)
$$
$$
-\frac{1}{\beta}\,\frac{\vec{q}^{\,2}\Theta[(1-\beta)|\vec{q}-\vec{k}|-\beta|\vec{k}|]}{\vec{k}^2(\vec{q}-\vec{k})^2}\,S_J^{(2)}(\vec{k};x)\Bigg\}\Bigg]\,.
$$

Besides, we define

$$
V_g^{(3)}(\vec{q}) \equiv \left(V_g^{(R_{gg})(B,\mathrm{soft})}+V_g^{(C)}\right)(\vec{q}) = \frac{C_A}{(4\pi)^\varepsilon}\int_0^1 dx\,\frac{C_A}{C_F}\,f_g(x)
$$
$$
\int\frac{d^{D-2}k}{\pi^{1+\varepsilon}}\frac{\vec{q}^{\,2}}{\vec{k}^2(\vec{k}-\vec{q})^2}\ln\frac{s_0}{(|\vec{k}|+|\vec{q}-\vec{k}|)^2}\;S_J^{(2)}(\vec{q}-\vec{k};x)\,, \tag{3.95}
$$

given in Eq. (3.92).

Another contribution originates from the collinear and charge renormalization counterterms, see Eqs. (3.32) and (3.34),

$$
V_g^{(4)}(\vec{q}) = \frac{\Gamma[1-\varepsilon]}{\varepsilon\,(4\pi)^\varepsilon}\int_0^1 dx\,f_g(x)\left[\left(\mu_R^2\right)^\varepsilon\left(\frac{11C_A}{6}-\frac{N_F}{3}\right)\frac{C_A}{C_F}\,S_J^{(2)}\,(\vec{q};x)\right.
$$
$$
\left.-\left(\mu_F^2\right)^\varepsilon\int_0^1 d\beta\left[2N_F P_{qg}(\beta)+\frac{C_A}{C_F}P_{gg}(\beta)\right]\;S_J^{(2)}(\vec{q};x\beta)\right]\,. \tag{3.96}
$$

Finally, the gluon part of the jet impact factor is given by the sum of the above four contributions and can be presented as a sum of two terms:

$$
\begin{aligned}
V_g^{(I)}(\vec{q}) \;&=\; \int_0^1 dx\,\frac{C_A}{C_F}\,f_g(x)\left[\frac{C_A}{(4\pi)^\varepsilon}\int\frac{d^{D-2}k}{\pi^{1+\varepsilon}}\frac{\vec{q}^{\,2}}{\vec{k}^{\,2}(\vec{k}-\vec{q})^2}\ln\frac{s_0}{(|\vec{k}|+|\vec{q}-\vec{k}|)^2}\right.\\
&\times\;\left. S_J^{(2)}(\vec{k};x)-C_A\ln\left(\frac{s_0}{\vec{q}^{\,2}}\right)\left(\vec{q}^{\,2}\right)^\varepsilon\frac{\Gamma[1-\varepsilon]}{\varepsilon\,(4\pi)^\varepsilon}\frac{\Gamma^2(1+\varepsilon)}{\Gamma(1+2\varepsilon)}S_J^{(2)}(\vec{q};x)\right]
\end{aligned} \tag{3.97}
$$

and

$$
\begin{aligned}
V_g^{(II)}(\vec{q}) \;&=\; V_g^{(2)}(\vec{q})+\int_0^1 dx\,\frac{C_A}{C_F}\,f_g(x)\left\{\left[\left(\frac{11C_A}{6}-\frac{N_F}{3}\right)\ln\frac{\vec{q}^{\,2}\mu_R^2}{\Lambda^4}\right.\right. \qquad (3.98)\\
&+\;\left.\left. C_A\frac{\pi^2}{2}+\frac{13}{18}N_F\right]\;S_J^{(2)}(\vec{q};x)+\int_0^1 d\beta\left[P_{gg}(\beta)+\,2\,N_F\,\frac{C_F}{C_A}P_{qg}(\beta)\right]
\end{aligned}
$$

$$\times \quad \ln\frac{\Lambda^2}{\mu_F^2}\; S_J^{(2)}(\vec{q};x\beta) + \int_0^1 d\beta \left[4\left(\frac{\ln(1-\beta)}{1-\beta}\right)_+ [(1-\beta)P(1-\beta)]\, C_A \right.$$
$$\left. + \quad 2\, N_F\, \frac{C_F}{C_A}\beta(1-\beta)\right] \Big\}\, S_J^{(2)}(\vec{q};x\beta)\,.$$

3.6 Summary

We have recalculated the jet vertices for the cases of quark and gluon in the initial state, first found in the papers by Bartels *et al.* [72, 73]. Our approach is different since the starting point of our calculation is the known general expression for NLO BFKL impact factors, given in Ref. [43], applied to the special case of partons in the initial state. Nevertheless, in many technical steps we followed closely the derivation of Refs. [72, 73].
We checked our result by replacing everywhere the jet selection functions $S_J^{(2)}$ and $S_J^{(3)}$ by 1 and performing all integrations: we got back to known results for the NLO quark and gluon impact factors [59, 60].

Let us discuss now the infrared finiteness of the obtained result for the jet impact factor. The NLO correction to the jet vertex (impact factor) has the form

$$\frac{d\Phi_J^{(1)}(\vec{q})}{dJ} \;=\; \frac{\alpha_s}{2\pi}\,\Phi_q^{(0)}\,V(\vec{q})\;, \qquad V(\vec{q}) = V^{(I)}(\vec{q}) + V^{(II)}(\vec{q})\,, \tag{3.99}$$

where each part is the sum of the quark and gluon contributions,

$$V^{(I)}(\vec{q}) = V_q^{(I)}(\vec{q}) + V_g^{(I)}(\vec{q})\,, \quad V^{(II)}(\vec{q}) = V_q^{(II)}(\vec{q}) + V_g^{(II)}(\vec{q})$$

given in Eqs. (3.62), (3.63) and in Eqs. (3.97), (3.98), respectively. $V_q^{(II)}(\vec{q})$ and $V_g^{(II)}(\vec{q})$ are manifestly finite. For $V^{(I)}(\vec{q})$ we have

$$V^{(I)}(\vec{q}) = \int_0^1 dx\, \left(\sum_{a=q,\bar{q}} f_a(x) + \frac{C_A}{C_F}\, f_g(x)\right) \tag{3.100}$$

$$\times \left[\frac{C_A}{(4\pi)^\varepsilon}\int \frac{d^{D-2}k}{\pi^{1+\varepsilon}}\frac{\vec{q}^{\,2}}{\vec{k}^{\,2}(\vec{k}-\vec{q})^2}\ln\frac{s_0}{(|\vec{k}|+|\vec{q}-\vec{k}|)^2}\; S_J^{(2)}(\vec{k};x)\right.$$

$$-C_A \ln\left(\frac{s_0}{\vec{q}^{\,2}}\right)\left(\vec{q}^{\,2}\right)^{\varepsilon}\frac{\Gamma[1-\varepsilon]}{\varepsilon\,(4\pi)^{\varepsilon}}\frac{\Gamma^2(1+\varepsilon)}{\Gamma(1+2\varepsilon)}S_J^{(2)}(\vec{q};x)\Bigg]\ .$$

Having the explicit form of the lowest order jet function (3.12), it is easy to see that the integration of $V^{(I)}(\vec{q})$ over $\vec{q}$ with any function, regular at $\vec{q}=\vec{k}_J$, will give some finite result. In particular, the finite result will be obtained after the convolution of $V^{(I)}(\vec{q})$ with BFKL Green's function, see Eq. (3.10), which is required for the calculation of the jet cross section.

This may look somewhat surprising, but, in fact, it is not so since the impact factor is not, strictly speaking, a physical observable. The divergence in (3.100) arises from virtual corrections and, precisely, from the factor $(s_0/\vec{q}^{\,2})^{\omega(\vec{q}^{\,2})}$ entering the definition of the impact factor. In the computation of physical impact factors this divergence is cancelled by the one arising from the integration in the first term of Eq. (3.100), which is related with real emission. In the calculation of the jet vertex the $\vec{q}$ integration is "opened" and, therefore, there is no way to get the divergence needed to balance the one arising from virtual corrections. However, in the construction of any physical cross section, the jet vertex is to be convoluted with the BFKL Green's function, which implies the integration over the Reggeon transverse momentum $\vec{q}$.

Another difference from Refs. [72, 73] is that in our approach the energy scale s_0 remains untouched and need not be fixed at any definite scale. The dependence on s_0 will disappear in the next-to-leading logarithmic approximation in any physical cross section in which jet vertices are used. However, the dependence on this energy scale will survive in terms beyond this approximation and will provide a parameter to be optimized with the method adopted in Refs. [94, 95, 96, 97].

In order to compare our results with the ones of Refs. [72, 73], we need to perform the transition from the standard BFKL scheme with arbitrary energy scale s_0 to the one used in Refs. [72, 73], where the scale of energy depends on the Reggeon momentum. The change to the scheme where the energy scale s_0 is replaced to any factorizable scale $\sqrt{f_1(\vec{q}_1^{\,2})f_2(\vec{q}_2^{\,2})}$ leads to the following modification of each impact factor ($i=1,2$), see Ref. [98],

$$\Phi_i(\vec{q}; f_i(\vec{q}^{\,2})) = \Phi_i(\vec{q}; s_0) + \frac{1}{2}\int d^{D-2}k\ \Phi_i^{(0)}(\vec{k})\ \ln\left(\frac{f_i(\vec{k}^2)}{s_0}\right) K^{(0)}(\vec{k},\vec{q})\ \frac{\vec{q}^{\,2}}{\vec{k}^{\,2}}\,, \tag{3.101}$$

where $\Phi_i^{(0)}$ and $K^{(0)}$ are the lowest order impact factor and BFKL kernel. Therefore changing from s_0 to $s_0 = \sqrt{\vec{q}_1^{\,2}\vec{q}_2^{\,2}}$ we obtain the following replacement in our result for the jet impact factor:

$$V^{(I)}(\vec{q}) \to \bar{V}^{(I)}(\vec{q}) = \int_0^1 dx\ \left(\sum_{a=q,\bar{q}} f_a(x) + \frac{C_A}{C_F}\, f_g(x)\right) \tag{3.102}$$

$$\times\left[\frac{C_A}{(4\pi)^\varepsilon}\int \frac{d^{D-2}k}{\pi^{1+\varepsilon}}\frac{\vec{q}^{\,2}}{\vec{k}^{\,2}(\vec{k}-\vec{q})^2}\ln\frac{\vec{k}^2}{(|\vec{k}|+|\vec{q}-\vec{k}|)^2}\ S_J^{(2)}(\vec{k};x)\right].$$

Note that $\bar{V}^{(I)}(\vec{q})$ is not singular at $\vec{q}\to\vec{k}$ and, therefore, it can be calculated at $D=4$. Such contribution to the jet impact factors, $\bar{V}^{(I)}(\vec{q})$, in the considered scheme with $s_0 = \sqrt{\vec{q}_1^{\,2}\vec{q}_2^{\,2}}$ produces a completely equivalent effect on the physical jet cross section as the factors H_L and H_R which enter Eq. (76) of Ref. [73] (see Eqs. (101), (102) in Ref. [72] for the definition of H_L, H_R).

Therefore, for the final comparison one needs to consider our results for $V_q^{(II)}(\vec{q})$ and $V_g^{(II)}(\vec{q})$ (modulo the appropriate normalization factor) with the ones given in Eq. (105) of Ref. [72] and Eq. (67) of Ref. [73] for the quark and gluon contributions, respectively. For this purpose we identify, following Refs. [72, 73], the Λ parameter with the collinear factorization scale μ_F. We found a complete agreement taking into account the misprints in the Eq. (105) of Ref. [72] and subsequently pointed out in Ref. [89]. In that paper the results for the quark and gluon contributions to the jet vertices are presented in a form different from the one used in the original calculation of Refs. [72, 73]. However, one can see after some analysis, that these two forms turn to be completely equivalent.

Recently another work devoted to the calculation of the jet impact factor appeared [83]. It is an interesting application of the Lipatov's effective action method [9] to the problem in question. Within this method, a particular regularization of the longitudinal divergences has been proposed. In the traditional approach, these divergences are regularized by the account of the BFKL counterterm, see Eq. (3.35).

Chapter 4

Mueller-Navelet jets at LHC in next-to-leading BFKL

The results of Chapter 3 could be used for a numerical estimation in the NLA of the cross section for Mueller-Navelet jets at LHC and for the analysis of the azimuthal correlation of the produced jets. They are given by a complicated expression of the transverse momenta, which, for reasons that will be clarified later on, must be transferred numerically to the (ν, n)-representation (see Section 4.2). A complete NLA analysis of the process proton(p_1) + proton$(p_2) \to$ jet(k_{J_1}) + jet(k_{J_2}) + X was reported in Ref. [89] (see also Ref. [99]) using the jet vertices calculated in Refs. [72, 73] that are equivalent to the results of the Chapter 3 (Ref. [74]). This numerical study followed previous ones [100, 101, 102] based on the inclusion of NLA effects only in the Green's functions.
We studied [103, 104] the production of two Mueller-Navelet jets in proton-proton collision in the full NLA BFKL approach, taking the convolution of the BFKL Green's function with the jet vertices calculated in the "Small Cone Approximation" (SCA) [75], i.e. for small jet cone aperture in the rapidity-azimuthal angle plane [105, 106, 107]. The use of the SCA allows to get a simple analytical result for the jet vertices, easily implementable in numerical calculations and therefore particularly suitable for a semi-analytical cross-check of the numerical approaches which treat the cone size exactly.

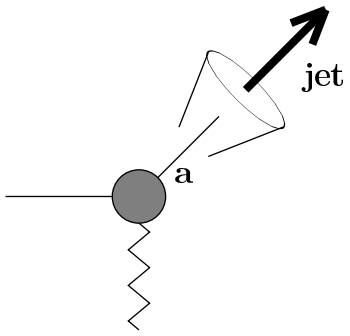

Figure 4.1: Parton-Reggeon collision, the jet is formed by a single parton [75].

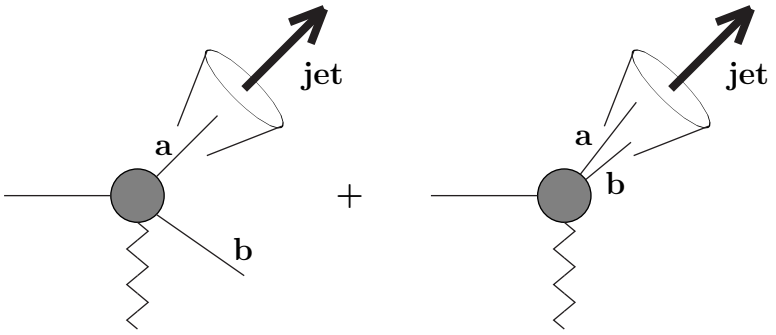

Figure 4.2: Parton-Reggeon collision, two partons are produced and the jet is formed either by one of the partons or by both partons [75].

4.1 Small Cone Approximation

At LO [75] only one parton is produced in the collision between the incoming parton and the Reggeon. This parton, as shown in the Fig. 4.1, will form the jet and its kinematics is totally fixed by the jet kinematics.

At NLO there are two contributions: the virtual corrections with the kinematical structure shown in Fig. 4.1 and the real corrections with two-particle production in the parton-Reggeon collisions. In the latter case the jet can be produced by one of the two partons or by both together.

Calling the produced partons a and b, there are three different possibilities, as shown in Fig. 4.2 (see, for instance, Ref. [75] or [108]):

- the parton a generates the jet, while the parton b can have arbitrary

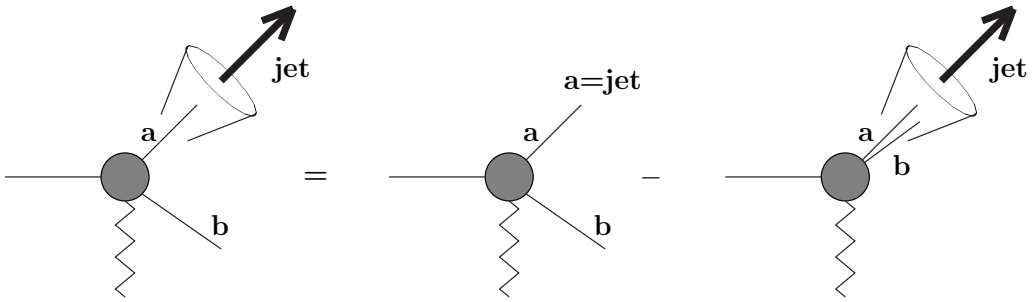

Figure 4.3: The production of the jet by one parton when the second one is outside the cone cam be seen as the "inclusive" production minus the contribution when the second parton is inside the cone [75].

kinematics (provided that it lies outside the jet cone). It can be seen as the "inclusive" production minus the contribution when the second parton is inside the cone (see Fig. 4.3).

- similarly with $a \leftrightarrow b$;
- the two partons a and b both generate the jet.

For two partons, one with transverse momentum $\vec{k}$ and longitudinal fraction β and the other with transverse momenta $\vec{q}-\vec{k}$ and longitudinal fraction $1-\beta$, the relative rapidity and the azimuthal angle are

$$\Delta y = \ln \frac{\beta^2 \left(\vec{k}-\vec{q}\right)^2}{(1-\beta)^2 \vec{k}^{\,2}}\,, \qquad \Delta\phi = \arccos \frac{\vec{q}\cdot\vec{k}-\vec{k}^{\,2}}{|\vec{k}||\vec{q}-\vec{k}|}\,. \tag{4.1}$$

- If the parton with momentum $\vec{k}$ generates the jet, while the other parton is a spectator, it is possible to introduce a vector $\vec{\Delta}$ (see Ref. [75]) such that

$$\vec{q} = \frac{\vec{k}}{\beta} + \vec{\Delta}\,. \tag{4.2}$$

For $\vec{\Delta} \to 0$ the condition of cone with aperture smaller than R in the rapidity-azimuthal angle plane becomes

$$\Delta\phi^2 + \Delta y^2 \;=\; \frac{\beta^2 \vec{\Delta}^2}{(1-\beta)^2 \vec{k}^{\,2}} \leq R^2 \tag{4.3}$$

and therefore

$$|\vec{\Delta}| \leq \frac{1-\beta}{\beta}\,|\vec{k}|\,R\,. \tag{4.4}$$

- If both partons form a jet, the jet momentum becomes $\vec{k} = \vec{k}_1 + \vec{k}_2$ and the jet fraction is $1 = \beta + (1-\beta)$.
  The relative rapidity and the azimuthal angle between the jet and the first (second) parton are

$$\Delta y_1 \;=\; \frac{1}{2}\ln\frac{\vec{k}_1^{\,2}}{\beta^2\vec{k}^{\,2}}\,, \qquad \Delta\phi_1 \;=\; \arccos\frac{\vec{k}\cdot\vec{k}_1}{|\vec{k}||\vec{k}_1|}\,, \tag{4.5}$$

  and

$$\Delta y_2 \;=\; \frac{1}{2}\ln\frac{\left(\vec{k}_1-\vec{k}\right)^2}{(1-\beta)^2\,\vec{k}^{\,2}}\,, \qquad \Delta\phi_2 \;=\; \arccos\frac{\vec{k}\cdot\left(\vec{k}-\vec{k}_1\right)}{|\vec{k}||\vec{k}-\vec{k}_1|}\,. \tag{4.6}$$

  Here one can introduce the vector $\vec{\Delta}$ (see Ref. [75]) as

$$\vec{k}_1 \;=\; \beta\vec{k} + \vec{\Delta}\,, \tag{4.7}$$

  and find

$$\Delta y_1^2 + \Delta\phi_1^2 \;=\; \frac{\vec{\Delta}^{\,2}}{\beta^2\vec{k}^{\,2}}\,, \qquad \Delta y_2^2 + \Delta\phi_2^2 \;=\; \frac{\vec{\Delta}^{\,2}}{(1-\beta)^2\,\vec{k}^{\,2}}\,. \tag{4.8}$$

  The condition that both partons form the jet is

$$|\vec{\Delta}| \leq R\,|\vec{k}|\,\min\left(\beta,(1-\beta)\right)\,. \tag{4.9}$$

4.2 BFKL cross section

In QCD collinear factorization the cross section reads (see Eq. (3.3))

$$\frac{d\sigma}{dx_{J_1}dx_{J_2}d^2k_{J_1}d^2k_{J_2}} = \sum_{i,j=q,\bar{q},g}\int_0^1 dx_1\int_0^1 dx_2\, f_i(x_1,\mu_F)f_j(x_2,\mu_F)\frac{d\hat{\sigma}_{i,j}(x_1x_2s,\mu_F)}{dx_{J_1}dx_{J_2}d^2k_{J_1}d^2k_{J_2}}\,. \tag{4.10}$$

The partonic cross section $d\hat{\sigma}_{i,j}\left(x_1 x_2 s, \mu\right)$ for the production of jets in the BFKL approach (Chapter 1) is

$$\frac{d\hat{\sigma}_{i,j}(x_1 x_2 s, \mu)}{dx_{J_1} dx_{J_2} d^2 k_{J_1} d^2 k_{J_2}} = \frac{s}{(2\pi)^2} \int \frac{d^2 q_1}{\vec{q}_1^{\,2}} V_i(\vec{q}_1, s_0, x_1; \vec{k}_{J_1}, x_{J_1}) \tag{4.11}$$

$$\times \int \frac{d^2 q_2}{\vec{q}_2^{\,2}} V_j(-\vec{q}_2, s_0, x_2; \vec{k}_{J_2}, x_{J_2}) \int\limits_{\delta - i\infty}^{\delta + i\infty} \frac{d\omega}{2\pi i} \left(\frac{x_1 x_2 s}{s_0}\right)^{\omega} G_\omega(\vec{q}_1, \vec{q}_2)\,,$$

where $V_i(\vec{q}_1, s_0, x_1; \vec{k}_{J_1}, x_{J_1})$ and $V_j(-\vec{q}_2, s_0, x_2; \vec{k}_{J_2}, x_{J_2})$ are the jet vertices (impact factors) describing the transitions parton i $(x_1 p_1) \to$ jet (k_{J_1}) and parton j $(x_2 p_2) \to$ jet (k_{J_2}), in the scattering off a Reggeized gluon with transverse momentum $\vec{q}_1$ and $\vec{q}_2$, respectively. The artificial scale s_0 is introduced in the BFKL approach to perform the Mellin transform from the s-space to the complex angular momentum plane and cancels in the full expression for the cross section with the NLA accuracy.

The Green's function in (4.11) obeys the BFKL equation[1]

$$\delta^2(\vec{q}_1 - \vec{q}_2) = \omega\, G_\omega(\vec{q}_1, \vec{q}_2) - \int d^2\vec{q}\, K(\vec{q}_1, \vec{q})\, G_\omega(\vec{q}, \vec{q}_2)\,, \tag{4.12}$$

where $K(\vec{q}_1, \vec{q}_2)$ is the BFKL kernel.

In what follows we proceed along the lines similar to ones used in Ref. [94, 95, 96]. It is convenient to work in the transverse momentum representation, defined by

$$\hat{\vec{q}}\,|\vec{q}_i\rangle = \vec{q}_i |\vec{q}_i\rangle\,, \tag{4.13}$$

$$\langle \vec{q}_1 | \vec{q}_2 \rangle = \delta^{(2)}(\vec{q}_1 - \vec{q}_2)\,, \qquad \langle A | B \rangle = \langle A | \vec{k} \rangle \langle \vec{k} | B \rangle = \int d^2 k A(\vec{k}) B(\vec{k})\,; \tag{4.14}$$

the kernel of the operator $\hat{K}$ is

$$K(\vec{q}_2, \vec{q}_1) = \langle \vec{q}_2 | \hat{K} | \vec{q}_1 \rangle \tag{4.15}$$

and the equation for the Green's function reads

$$\hat{1} = (\omega - \hat{K})\hat{G}_\omega\,, \tag{4.16}$$

[1] We notice that this form of the BFKL differs from the one gives in Eq. (1.15) because here a different normalization of the kernel is used; moreover here we consider only the forward case.

its solution being

$$\hat{G}_\omega = (\omega - \hat{K})^{-1} \,. \tag{4.17}$$

The kernel is given as an expansion in the strong coupling,

$$\hat{K} = \bar{\alpha}_s \hat{K}^0 + \bar{\alpha}_s^2 \hat{K}^1 \,, \tag{4.18}$$

where

$$\bar{\alpha}_s = \frac{\alpha_s N_c}{\pi} \tag{4.19}$$

and N_c is the number of colors. In Eq. (4.18) $\hat{K}^0$ is the BFKL kernel in the LLA, $\hat{K}^1$ represents the NLA correction.

To determine the partonic cross section with NLA accuracy we need an approximate solution of Eq. (4.17). With the required accuracy this solution is

$$\hat{G}_\omega = (\omega - \bar{\alpha}_s \hat{K}^0)^{-1} + (\omega - \bar{\alpha}_s \hat{K}^0)^{-1} \left(\bar{\alpha}_s^2 \hat{K}^1\right) (\omega - \bar{\alpha}_s \hat{K}^0)^{-1} + \mathcal{O}\left[\left(\bar{\alpha}_s^2 \hat{K}^1\right)^2\right] . \tag{4.20}$$

The basis of eigenfunctions of the LLA kernel,

$$\hat{K}^0 |n,\nu\rangle = \chi(n,\nu) |n,\nu\rangle \,,$$

$$\chi(n,\nu) = 2\psi(1) - \psi\left(\frac{n}{2} + \frac{1}{2} + i\nu\right) - \psi\left(\frac{n}{2} + \frac{1}{2} - i\nu\right) \,, \tag{4.21}$$

is given by the following set of functions:

$$\langle \vec{q} | n,\nu\rangle = \frac{1}{\pi\sqrt{2}} \left(\vec{q}^{\,2}\right)^{i\nu - \frac{1}{2}} e^{in\phi} \,, \tag{4.22}$$

here ϕ is the azimuthal angle of the vector $\vec{q}$ counted from some fixed direction in the transverse space, $\cos\phi \equiv q_x/|\vec{q}|$. Then, the orthonormality condition takes the form

$$\langle n',\nu' | n,\nu\rangle = \int \frac{d^2q}{2\pi^2} \left(\vec{q}^{\,2}\right)^{i\nu - i\nu' - 1} e^{i(n-n')\phi} = \delta(\nu - \nu')\, \delta_{nn'} \,. \tag{4.23}$$

The action of the full NLA BFKL kernel on these functions may be expressed as follows:

$$\begin{aligned} \hat{K}|n,\nu\rangle &= \bar{\alpha}_s(\mu_R)\chi(n,\nu)|n,\nu\rangle + \bar{\alpha}_s^2(\mu_R) \left(\frac{\beta_0}{4N_c}\chi(n,\nu)\ln(\mu_R^2)\right. \\ &+ \left.\chi^{(1)}(n,\nu)\right)|n,\nu\rangle + \bar{\alpha}_s^2(\mu_R)\frac{\beta_0}{4N_c}\chi(n,\nu)\left(i\frac{\partial}{\partial\nu}\right)|n,\nu\rangle \,, \end{aligned} \tag{4.24}$$

where μ_R is the renormalization scale of the QCD coupling, the first term represents the action of LLA kernel, while the second and the third ones stand for the diagonal and the non-diagonal parts of the NLA kernel and we have used

$$\beta_0 = \frac{11N_c}{3} - \frac{2n_f}{3}\,, \tag{4.25}$$

where n_f is the number of active quark flavors.
The function $\chi^{(1)}(n,\nu)$, calculated in [109] (see also [110]), is conveniently represented in the form

$$\chi^{(1)}(n,\nu) = -\frac{\beta_0}{8\,N_c}\left(\chi^2(n,\nu) - \frac{10}{3}\chi(n,\nu) - i\chi'(n,\nu)\right) + \bar{\chi}(n,\nu)\,, \tag{4.26}$$

where

$$\begin{aligned}\bar{\chi}(n,\nu) \;=\; -\frac{1}{4}\Bigg[&\frac{\pi^2-4}{3}\chi(n,\nu) - 6\zeta(3) - \chi''(n,\nu) + 2\,\phi(n,\nu) + 2\,\phi(n,-\nu)\\ &+\frac{\pi^2\sinh(\pi\nu)}{2\,\nu\,\cosh^2(\pi\nu)}\left(\left(3+\left(1+\frac{n_f}{N_c^3}\right)\frac{11+12\nu^2}{16(1+\nu^2)}\right)\delta_{n0}\right.\\ &\left.-\left(1+\frac{n_f}{N_c^3}\right)\frac{1+4\nu^2}{32(1+\nu^2)}\delta_{n2}\right)\Bigg]\,,\end{aligned} \tag{4.27}$$

$$\begin{aligned}\phi(n,\nu) \;=\; -\int_0^1 dx\,\frac{x^{-1/2+i\nu+n/2}}{1+x}\Bigg[&\frac{1}{2}\left(\psi'\left(\frac{n+1}{2}\right) - \zeta(2)\right) + \mathrm{Li}_2(x) + \mathrm{Li}_2(-x)\\ &+\ln x\left(\psi(n+1) - \psi(1) + \ln(1+x) + \sum_{k=1}^{\infty}\frac{(-x)^k}{k+n}\right) + \sum_{k=1}^{\infty}\frac{x^k}{(k+n)^2}(1-(-1)^k)\Bigg]\\ =\sum_{k=0}^{\infty}\frac{(-1)^{k+1}}{k+(n+1)/2+i\nu}\Big[&\psi'(k+n+1) - \psi'(k+1) + (-1)^{k+1}\left(\beta'(k+n+1)\right.\\ &\left.+\beta'(k+1)\right) - \frac{1}{k+(n+1)/2+i\nu}(\psi(k+n+1) - \psi(k+1))\Big]\,,\end{aligned} \tag{4.28}$$

$$\beta'(z) = \frac{1}{4}\left[\psi'\left(\frac{z+1}{2}\right) - \psi'\left(\frac{z}{2}\right)\right]\,, \qquad \mathrm{Li}_2(x) = -\int_0^x dt\,\frac{\ln(1-t)}{t}\,.$$

Here and below $\chi'(n,\nu) = d\chi(n,\nu)/d\nu$ and $\chi''(n,\nu) = d^2\chi(n,\nu)/d^2\nu$.
For the quark and the gluon jet vertices in (4.11) the projection onto the eigenfunctions of LO BFKL kernel, *i.e.* the transfer to the (ν, n)-representation, is done as follows:

$$\begin{aligned}
\frac{V(\vec{q}_1)}{\vec{q}_1^{\,2}} &= \sum_{n=-\infty}^{+\infty} \int_{-\infty}^{+\infty} d\nu \, \Phi_1(\nu, n) \langle n, \nu | \vec{q}_1 \rangle \,, \\
\frac{V(-\vec{q}_2)}{\vec{q}_2^{\,2}} &= \sum_{n=-\infty}^{+\infty} \int_{-\infty}^{+\infty} d\nu \, \Phi_2(\nu, n) \langle \vec{q}_2 | n, \nu \rangle \,, \\
\Phi_1(\nu, n) &= \int d^2 q_1 \, \frac{V(\vec{q}_1)}{\vec{q}_1^{\,2}} \frac{1}{\pi\sqrt{2}} \left(\vec{q}_1^{\,2}\right)^{i\nu - \frac{1}{2}} e^{in\phi_1} \,, \\
\Phi_2(\nu, n) &= \int d^2 q_2 \, \frac{V(-\vec{q}_2)}{\vec{q}_2^{\,2}} \frac{1}{\pi\sqrt{2}} \left(\vec{q}_2^{\,2}\right)^{-i\nu - \frac{1}{2}} e^{-in\phi_2} \,.
\end{aligned} \tag{4.29}$$

The vertices can be represented as an expansion in α_s,

$$\Phi_{1,2}(n, \nu) = \alpha_s(\mu_R) v_{1,2}(n, \nu) + \alpha_s^2(\mu_R) v_{1,2}^{(1)}(n, \nu) \,. \tag{4.30}$$

In Eqs. (4.29) and (4.30) we suppressed for brevity the partonic indices i, j and the other arguments in $v_{1,2}$. The explicit forms of LLA and NLA jet vertices in the (ν, n)-representation both for the quark and gluon cases can be found in [75]. In particular for the LLA quark vertices one has

$$\begin{aligned}
v_1^q(n, \nu) &= 2\sqrt{\frac{C_F}{C_A}} (\vec{k}_{J_1}^{\,2})^{i\nu - 3/2} \, e^{in\phi_{J_1}} \delta(x_{J_1} - x_1) \,, \\
v_2^q(n, \nu) &= 2\sqrt{\frac{C_F}{C_A}} (\vec{k}_{J_2}^{\,2})^{-i\nu - 3/2} \, e^{-in(\phi_{J_2} + \pi)} \delta(x_{J_2} - x_2) \,,
\end{aligned} \tag{4.31}$$

where $C_A = N_c$, $C_F = (N_c^2 - 1)/2N_c$, the angle $\phi_{J_2} + \pi$ in the last equation appears due to the fact that the Reggeon momentum which enters the second vertex is $-\vec{q}_2$. Note that in LLA vertices the partonic and the jet longitudinal momentum fractions coincide.
The partonic cross section can be written with NLA accuracy as follows

$$\frac{d\hat{\sigma}(x_1x_2s)}{dx_{J_1}dx_{J_2}d^2k_{J_1}d^2k_{J_2}} = \frac{1}{(2\pi)^2}\sum_{n=-\infty}^{+\infty}\int_{-\infty}^{+\infty} d\nu \left(\frac{x_1x_2s}{s_0}\right)^{\bar{\alpha}_s(\mu_R)\chi(n,\nu)}$$
$$\times\alpha_s^2(\mu_R)v_1(n,\nu)v_2(n,\nu)\left[1+\alpha_s(\mu_R)\left(\frac{v_1^{(1)}(n,\nu)}{v_1(n,\nu)}+\frac{v_2^{(1)}(n,\nu)}{v_2(n,\nu)}\right)\right.$$
$$+\bar{\alpha}_s^2(\mu_R)\ln\left(\frac{x_1x_2s}{s_0}\right)\left(\bar{\chi}(n,\nu)+\frac{\beta_0}{8N_c}\chi(n,\nu)\left[-\chi(n,\nu)+\frac{10}{3}\right.\right.$$
$$\left.\left.\left.+i\frac{d\ln\left(\frac{v_1(n,\nu)}{v_2(n,\nu)}\right)}{d\nu}+2\ln\mu_R^2\right]\right)\right] . \tag{4.32}$$

For the subsequent calculation it is convenient to make the substitution

$$\left(\frac{x_1x_2s}{s_0}\right)^{\bar{\alpha}_s(\mu_R)\chi(n,\nu)} = \left(\frac{x_{J_1}x_{J_2}s}{s_0}\right)^{\bar{\alpha}_s(\mu_R)\chi(n,\nu)}\left(\frac{x_1}{x_{J_1}}\right)^{\bar{\alpha}_s(\mu_R)\chi(n,\nu)} \times \left(\frac{x_2}{x_{J_2}}\right)^{\bar{\alpha}_s(\mu_R)\chi(n,\nu)} , \tag{4.33}$$

and to assign the last two factors in the r.h.s. to the corresponding jet vertices. This procedure affects only the NLA parts of the jet vertices, since for the LLA vertices $x_i = x_{J_i}$. Also with NLA accuracy, one can make in (4.32) the replacement

$$\ln\left(\frac{x_1x_2s}{s_0}\right) \to \ln\left(\frac{x_{J_1}x_{J_2}s}{s_0}\right) . \tag{4.34}$$

This procedure allows to perform in the MN-jet cross section first the integration over partonic momentum fractions, before taking the sum over n and the integration over ν; it allows also to consider together the contributions of quarks and gluons to the jet vertices.

The differential cross section has the form

$$\frac{d\sigma}{dy_{J_1}dy_{J_2}\,d|\vec{k}_{J_1}|\,d|\vec{k}_{J_2}|d\phi_{J_1}d\phi_{J_2}} = \frac{1}{(2\pi)^2}\left[\mathcal{C}_0+\sum_{n=1}^{\infty}2\cos(n\phi)\,\mathcal{C}_n\right] , \tag{4.35}$$

where $\phi = \phi_{J_1} - \phi_{J_2} - \pi$, and

$$\mathcal{C}_m = \int_0^{2\pi}d\phi_{J_1}\int_0^{2\pi}d\phi_{J_2}\,\cos[m(\phi_{J_1}-\phi_{J_2}-\pi)]\,\frac{d\sigma}{dy_{J_1}dy_{J_2}\,d|\vec{k}_{J_1}|\,d|\vec{k}_{J_2}|d\phi_{J_1}d\phi_{J_2}} . \tag{4.36}$$

In particular, taking into account the Jacobian of the transformation from the variables $\vec{k}_{J_i}$, x_{J_i} to the variables $|\vec{k}_{J_i}|$, y_{J_i}, and the ν-dependence of LLA jet vertices, see (4.31), we get

$$\mathcal{C}_n = \frac{x_{J_1}x_{J_2}}{|\vec{k}_{J_1}||\vec{k}_{J_2}|}\int_{-\infty}^{+\infty} d\nu \left(\frac{x_{J_1}x_{J_2}s}{s_0}\right)^{\bar{\alpha}_s(\mu_R)\chi(n,\nu)} \tag{4.37}$$

$$\times\alpha_s^2(\mu_R)c_1(n,\nu,|\vec{k}_{J_1}|,x_{J_1})c_2(n,\nu,|\vec{k}_{J_2}|,x_{J_2})$$

$$\times\left[1+\alpha_s(\mu_R)\left(\frac{c_1^{(1)}(n,\nu,|\vec{k}_{J_1}|,x_{J_1})}{c_1(n,\nu,|\vec{k}_{J_1}|,x_{J_1})}+\frac{c_2^{(1)}(n,\nu,|\vec{k}_{J_2}|,x_{J_2})}{c_2(n,\nu,|\vec{k}_{J_2}|,x_{J_2})}\right)\right.$$

$$\left.+\bar{\alpha}_s^2(\mu_R)\ln\left(\frac{x_{J_1}x_{J_2}s}{s_0}\right)\left(\bar{\chi}(n,\nu)+\frac{\beta_0}{8C_A}\chi(n,\nu)\left(-\chi(n,\nu)+\frac{10}{3}+\ln\frac{\mu_R^4}{\vec{k}_{J_1}^2\vec{k}_{J_2}^2}\right)\right)\right],$$

where

$$c_1(n,\nu,|\vec{k}|,x) = 2\sqrt{\frac{C_F}{C_A}}(\vec{k}^{\,2})^{i\nu-1/2}\left(\frac{C_A}{C_F}f_g(x,\mu_F)+\sum_{a=q,\bar{q}}f_q(x,\mu_F)\right), \tag{4.38}$$

$$c_2(n,\nu,|\vec{k}|,x) = \left[c_1(n,\nu,|\vec{k}|,x)\right]^*, \tag{4.39}$$

$$c_1^{(1)}(n,\nu,|\vec{k}|,x) = \frac{1}{\pi}\sqrt{\frac{C_F}{C_A}}\left(\vec{k}^{\,2}\right)^{i\nu-1/2}\int_x^1\frac{d\zeta}{\zeta}\zeta^{-\bar{\alpha}_s(\mu_R)\chi(n,\nu)}\left\{\sum_{a=q,\bar{q}}f_a\left(\frac{x}{\zeta}\right)\right. \tag{4.40}$$

$$\times\left[\left(P_{qq}(\zeta)+\frac{C_A}{C_F}P_{gq}(\zeta)\right)\ln\frac{\vec{k}^{\,2}}{\mu_F^2}-2\zeta^{-2\gamma}\ln R\,\{P_{qq}(\zeta)+P_{gq}(\zeta)\}\right.$$

$$-\frac{\beta_0}{2}\ln\frac{\vec{k}^{\,2}}{\mu_R^2}\delta(1-\zeta)+C_A\delta(1-\zeta)\left(\chi(n,\gamma)\ln\frac{s_0}{\vec{k}^{\,2}}+\frac{85}{18}+\frac{\pi^2}{2}\right.$$

$$\left.+\frac{1}{2}\left(\psi'\left(1+\gamma+\frac{n}{2}\right)-\psi'\left(\frac{n}{2}-\gamma\right)-\chi^2(n,\gamma)\right)\right)$$

$$+(1+\zeta^2)\left\{C_A\left(\frac{(1+\zeta^{-2\gamma})\,\chi(n,\gamma)}{2(1-\zeta)_+}-\zeta^{-2\gamma}\left(\frac{\ln(1-\zeta)}{1-\zeta}\right)_+\right)\right.$$

$$\left.+\left(C_F-\frac{C_A}{2}\right)\left[\frac{\bar{\zeta}}{\zeta^2}I_2-\frac{2\ln\zeta}{1-\zeta}+2\left(\frac{\ln(1-\zeta)}{1-\zeta}\right)_+\right]\right\}$$

$$\left.+\delta(1-\zeta)\left(C_F\left(3\ln 2-\frac{\pi^2}{3}-\frac{9}{2}\right)-\frac{5n_f}{9}\right)\right.$$

$$+C_A\zeta + C_F\bar{\zeta} + \frac{1+\bar{\zeta}^2}{\zeta}\left(C_A\frac{\bar{\zeta}}{\zeta}I_1 + 2C_A\ln\frac{\bar{\zeta}}{\zeta} + C_F\zeta^{-2\gamma}(\chi(n,\gamma) - 2\ln\bar{\zeta})\right)\Bigg]$$

$$+f_g\left(\frac{x}{\zeta}\right)\frac{C_A}{C_F}$$

$$\times\left[\left(P_{gg}(\zeta) + 2\,n_f\frac{C_F}{C_A}P_{qg}(\zeta)\right)\ln\frac{\vec{k}^{\,2}}{\mu_F^2} - 2\zeta^{-2\gamma}\ln R\,(P_{gg}(\zeta) + 2\,n_f P_{qg}(\zeta))\right.$$

$$-\frac{\beta_0}{2}\ln\frac{\vec{k}^{\,2}}{4\mu_R^2}\delta(1-\zeta) + C_A\delta(1-\zeta)\left(\chi(n,\gamma)\ln\frac{s_0}{\vec{k}^{\,2}} + \frac{1}{12} + \frac{\pi^2}{6}\right.$$

$$\left.+\frac{1}{2}\left(\psi'\left(1+\gamma+\frac{n}{2}\right) - \psi'\left(\frac{n}{2}-\gamma\right) - \chi^2(n,\gamma)\right)\right)$$

$$+2C_A(1-\zeta^{-2\gamma})\left(\left(\frac{1}{\zeta} - 2 + \zeta\bar{\zeta}\right)\ln\bar{\zeta} + \frac{\ln(1-\zeta)}{1-\zeta}\right)$$

$$+C_A\left[\frac{1}{\zeta} + \frac{1}{(1-\zeta)_+} - 2 + \zeta\bar{\zeta}\right]\left((1+\zeta^{-2\gamma})\chi(n,\gamma) - 2\ln\zeta + \frac{\bar{\zeta}^2}{\zeta^2}I_2\right)$$

$$\left.+n_f\left[2\zeta\bar{\zeta}\,\frac{C_F}{C_A} + (\zeta^2+\bar{\zeta}^2)\left(\frac{C_F}{C_A}\chi(n,\gamma) + \frac{\bar{\zeta}}{\zeta}I_3\right) - \frac{1}{12}\delta(1-\zeta)\right]\right]\Bigg\}\ ,$$

$$c_2^{(1)}(n,\nu,|\vec{k}|,x) = \left[c_1^{(1)}(n,\nu,|\vec{k}|,x)\right]^*. \tag{4.41}$$

Here $\bar{\zeta} = 1-\zeta$, $\gamma = i\nu - 1/2$, $P_{ij}(\zeta)$ are leading order DGLAP kernels. For the $I_{1,2,3}$ functions we have the results:

$$I_2 = \frac{\zeta^2}{\bar{\zeta}^2}\left[\zeta\left(\frac{{}_2F_1(1,1+\gamma-\frac{n}{2},2+\gamma-\frac{n}{2},\zeta)}{\frac{n}{2}-\gamma-1} - \frac{{}_2F_1(1,1+\gamma+\frac{n}{2},2+\gamma+\frac{n}{2},\zeta)}{\frac{n}{2}+\gamma+1}\right)\right.$$

$$+\zeta^{-2\gamma}\left(\frac{{}_2F_1(1,-\gamma-\frac{n}{2},1-\gamma-\frac{n}{2},\zeta)}{\frac{n}{2}+\gamma} - \frac{{}_2F_1(1,-\gamma+\frac{n}{2},1-\gamma+\frac{n}{2},\zeta)}{\frac{n}{2}-\gamma}\right)$$

$$\left.+\left(1+\zeta^{-2\gamma}\right)\left(\chi(n,\gamma) - 2\ln\bar{\zeta}\right) + 2\ln\zeta\right]\ , \tag{4.42}$$

$$I_1 = \frac{\bar{\zeta}}{2\zeta}I_2 + \frac{\zeta}{\bar{\zeta}}\left[\ln\zeta + \frac{1-\zeta^{-2\gamma}}{2}\left(\chi(n,\gamma) - 2\ln\bar{\zeta}\right)\right]\ , \tag{4.43}$$

$$I_3 = \frac{\bar{\zeta}}{2\zeta}I_2 - \frac{\zeta}{\bar{\zeta}}\left[\ln\zeta + \frac{1-\zeta^{-2\gamma}}{2}\left(\chi(n,\gamma) - 2\ln\bar{\zeta}\right)\right]\ . \tag{4.44}$$

The factor $\zeta^{-\bar{\alpha}_s(\mu_R)\chi(n,\nu)}$ appears in (4.40) due to extra-contributions attributed to the jet vertices, as discussed after Eq. (4.33). Note that the $\mathcal{C}_n$ coefficients do not depend on the azimuthal angles of the jets, ϕ_{J_1} and ϕ_{J_2},

$$\mathcal{C}_n = \mathcal{C}_n\left(y_{J_1}, y_{J_2}, \vec{k}_{J_1}, \vec{k}_{J_2}, \mu_R, \mu_F, s_0\right) \ , \tag{4.45}$$

they depend instead on the jet rapidities, the transverse momenta and on the factorization, renormalization and energy scale parameters.

Exponentiated form An alternative way to present the differential cross section of the hard process, equivalent to the formula (4.37) in the NLA, is the so-called exponentiated form (see Refs. [94, 95, 96]),

$$\mathcal{C}_n^{\rm exp} = \frac{x_{J_1} x_{J_2}}{|\vec{k}_{J_1}||\vec{k}_{J_2}|} \int_{-\infty}^{+\infty} d\nu \, \exp\Bigg[(Y - Y_0)\Bigg(\bar{\alpha}_s(\mu_R)\chi(n,\nu) \tag{4.46}$$

$$+\bar{\alpha}_s^2(\mu_R)\left(\bar{\chi}(n,\nu) + \frac{\beta_0}{8C_A}\chi(n,\nu)\left(-\chi(n,\nu) + \frac{10}{3} + \ln\frac{\mu_R^4}{\vec{k}_{J_1}^2\vec{k}_{J_2}^2}\right)\right)\Bigg)\Bigg]$$

$$\times\alpha_s^2(\mu_R) c_1(n,\nu,|\vec{k}_{J_1}|,x_{J_1},\mu_F) c_2(n,\nu,|\vec{k}_{J_2}|,x_{J_2},\mu_F)$$

$$\times\left[1 + \alpha_s(\mu_R)\left(\frac{c_1^{(1)}(n,\nu,|\vec{k}_{J_1}|,x_{J_1},\mu_F)}{c_1(n,\nu,|\vec{k}_{J_1}|,x_{J_1},\mu_F)} + \frac{c_2^{(1)}(n,\nu,|\vec{k}_{J_2}|,x_{J_2},\mu_F)}{c_2(n,\nu,|\vec{k}_{J_2}|,x_{J_2},\mu_F)}\right)\right] \ .$$

Here we set $\ln\left(\frac{x_{J_1}x_{J_2}s}{s_0}\right) = Y - Y_0$, where $\Delta y \equiv Y = \ln\frac{x_{J_1}x_{J_2}s}{|\vec{k}_{J_1}||\vec{k}_{J_2}|}$ is the rapidity gap between the two jets and $Y_0 = \ln\frac{s_0}{|\vec{k}_{J_1}||\vec{k}_{J_2}|}$.

Below we will discuss the differential cross section integrated over the jet azimuthal angles

$$\mathcal{C}_0 = \int d\phi_{J_1} d\phi_{J_2} d\sigma \ ,$$

the coefficients $\mathcal{C}_n$ and the moments of the azimuthal decorrelations, which are defined as

$$\langle\cos(n\phi)\rangle = \frac{\int d\phi_{J_1} d\phi_{J_2} \cos[n(\phi_{J_1} - \phi_{J_2} - \pi)] d\sigma}{\int d\phi_{J_1} d\phi_{J_2} d\sigma} = \frac{\mathcal{C}_n}{\mathcal{C}_0} \ . \tag{4.47}$$

4.3 Results

In this section we present our results for the dependence on Y of the functions $\mathcal{C}_n$. In what follows we take the factorization and renormalization scales equal to each other, $\mu_F = \mu_R$. We perform our calculation both in the LLA and in the NLA. In the former case, the expression for $\mathcal{C}_n$ reads

$$\mathcal{C}_n^{\rm LLA} = \frac{d\sigma_{\rm LLA}}{dy_{J_1} dy_{J_2} d|\vec{k}_{J_1}|\, d|\vec{k}_{J_2}|} = \frac{x_{J_1} x_{J_2}}{|\vec{k}_{J_1}||\vec{k}_{J_2}|} \int_{-\infty}^{+\infty} d\nu \, \exp\Big[(Y - Y_0)\bar{\alpha}_s(\mu_R)\chi(n,\nu)\Big] \times \alpha_s^2(\mu_R) c_1(n,\nu,|\vec{k}_{J_1}|, x_{J_1}) c_2(n,\nu,|\vec{k}_{J_2}|, x_{J_2}) \; . \tag{4.48}$$

For our NLA analysis we use the exponentiated representation given in Eq. (4.46).

For the center-of-mass energy $\sqrt{s}$ we take the LHC design value 14 TeV. We fix the jet cone size at the value $R = 0.5$, in order to compare our predictions with the forthcoming LHC data. We study Mueller-Navelet jets with symmetric and asymmetric values of the transverse momenta, in particular, consider the choices: $|\vec{k}_{J_1}| = |\vec{k}_{J_2}| = 35$ GeV, $|\vec{k}_{J_1}| = |\vec{k}_{J_2}| = 20$ GeV for the symmetric cases and $|\vec{k}_{J_1}| = 20$ GeV, $|\vec{k}_{J_2}| = 35$ GeV for asymmetric case.
Moreover, to make possible the comparison with the experiments at present LHC energy, we perform calculations for $\sqrt{s} = 7$ TeV, where we consider the $|\vec{k}_{J_1}| = |\vec{k}_{J_2}| = 35$ GeV case.

Following a quite recent CMS study [111], we restrict the rapidities of the Mueller-Navelet jets to the region $3 \leq |y_J| \leq 5$. We will present our results for $\mathcal{C}_0$, *i.e.* the differential cross section integrated over the jet azimuthal angles, the coefficients $\mathcal{C}_n$ for $n \neq 0$, and $\langle \cos(n\phi) \rangle$ versus the relative rapidity, $Y = y_{J_1} - y_{J_2}$. For our choice of forward jets rapidities, Y takes values between 6 and 10. Our approach is similar to the one used in [89], we introduce rapidity bins with step Δy_J equal to 0.5, so the considered values for jet rapidities and rapidity difference are

$$\begin{aligned} \{(y_{J_1})_i\} &= \{3.0, 3.5, 4.0, 4.5, 5.0\} \\ \{(y_{J_2})_i\} &= \{-3.0, -3.5, -4.0, -4.5, -5.0\} \end{aligned}$$

and $\{Y_i\} = \{6.0, 6.5, 7.0, 7.5, 8.0, 8.5, 9.0, 9.5, 10.0\}$. Then we evaluate the following sum

$$C_n(Y_i) = \sum 0.5\ \mathcal{C}_n\left((y_{J_1})_j, (y_{J_1})_j - Y_i\right)$$

where the sum runs over the possible values of $(y_{J_1})_j$ for a given Y_i.

In our analysis we use the PDF set MSTW2008nnlo [112] and the two-loop running coupling with $\alpha_s(M_Z) = 0.11707$.

Our predictions depend on the values of energy and renormalization scales, s_0 and μ_R. For the analysis in the LLA we fixed the values of these scales, μ_R and s_0, as suggested by the kinematics of the process, *i.e.* $\mu_R^2 = s_0 = |\vec{k}_{J_1}||\vec{k}_{J_2}|$. In general LLA results depend very strongly on s_0 and μ_R, and one really needs to come to the NLA analysis in order to reduce this scale dependence and to have some reliable predictions for observables. One should stress that the dependence of the correlations C_n on the scales μ_R and s_0 cancels with NLA accuracy; nevertheless in both representations (4.37) and (4.46) there unavoidably exist contributions subleading to NLA, depending on μ_R and s_0, whose numerical impact is important for the considered kinematics, therefore we need some prescription for the choice of these scales.

Following Ref. [94, 95, 96], we use here an adaptation of the *principle of minimal sensitivity* (PMS) [113, 114], which consists in taking as optimal choices for μ_R and s_0 those values for which the physical observable under examination exhibits the minimal sensitivity to changes of both of these scales. The motivation of this procedure is that the complete resummation of the perturbative series would not depend on the scales μ_R and s_0, so the optimization method is supposed to mimic the effect of the most relevant unknown subleading terms.

In our search for optimal values, we took integer values for Y_0 in the range 0 – 5 and values for μ_R given as integer multiples of $\sqrt{|\vec{k}_{J_1}||\vec{k}_{J_2}|}$,

$$\mu_R = n_R \sqrt{|\vec{k}_{J_1}||\vec{k}_{J_2}|}\,, \tag{4.49}$$

taking the integer n_R in the range 1 – 15. The systematic uncertainty of the optimization procedure in the determination of observables, which will be discussed below, originates from the resolution of the grid in the n_R – Y_0 plane. This uncertainty has been estimated as the standard deviation of the optimal value from the determinations in the nearest neighbors of the grid. The error bars around the NLA data points presented in the figures below represent this uncertainty. We did not evaluate the impact on our predictions of the PDF uncertainties, since we expect it to be of the same size as determined in Ref. [89], where the same PDF set adopted here is used.

Cross section integrated over the jet azimuthal angles, $\mathbf{C_0}$ Let us start with the cross section integrated over the jet azimuthal angles, C_0. We found that for this observable a stationary point in the n_R – Y_0 plane could always be singled out, typically a local maximum. For $\sqrt{s} = 14$ TeV our results, in $\left[\frac{\text{nb}}{\text{GeV}^2}\right]$ units, are presented in Figs. 4.4–4.6 and in Tables 4.1–4.3; results for $\sqrt{s} = 7$ TeV are given in Fig. 4.7 and Table 4.4. The optimal values of Y_0 and $n_R = \mu_R/\sqrt{|\vec{k}_{J_1}||\vec{k}_{J_2}|}$ are also reported in the tables. As in previous works [94, 95, 96], the optimal values of the energy scales turn to be far from the kinematic scale. On the other hand, the uncertainty related of our optimization procedure, described above, turns out to be small, therefore our NLA results for the cross section integrated over jet azimuthal angles, presented in Figs. 4.4–4.7 have relatively small "error bars".

Moments of the azimuthal decorrelations $\mathbf{C_1/C_0}$ and $\mathbf{C_2/C_0}$ The other issue we addressed in a similar manner is the analysis of the observables C_1/C_0 and C_2/C_0, which encode the first two nontrivial angular decorrelations: $\langle\cos\phi\rangle$ and $\langle\cos(2\phi)\rangle$. For $|\vec{k}_{J_1}| = |\vec{k}_{J_2}| = 35$ GeV at $\sqrt{s} = 14$ TeV our results are presented in Figs. 4.8, 4.9 and Tables 4.5 and 4.6. For the smaller values of jet transverse momenta, $|\vec{k}_{J_1}| = |\vec{k}_{J_2}| = 20$ GeV, they are given in Figs. 4.10, 4.11 and Tables 4.7 and 4.8. Finally, for the asymmetric case, $|\vec{k}_{J_1}| = 20$ GeV and $|\vec{k}_{J_2}| = 35$ GeV, we present our results for $\langle\cos\phi\rangle$ and $\langle\cos(2\phi)\rangle$ in Figs. 4.12, 4.13 and Tables 4.9, 4.10.

In our search for optimal scale values we found that these observables, angular decorrelations, are less stable than C_0, thus making our analysis more complicated. Indeed, only for a few values of Y_i we could find a stationary point. In other cases we found a local maximum only in the direction of one of the two parameters. When this happened, we took as "optimal" value the one exhibiting the least standard deviation from neighboring points in the adopted grid. As a result the uncertainties related with our optimization procedure are larger for the angular decorrelations than for the integrated cross sections discussed above, therefore Figs. 4.8–4.13 show larger "error bars" in comparison to the NLA results presented in Figs. 4.4–4.7. Note that for the asymmetric case, $|\vec{k}_{J_1}| = 20$ GeV and $|\vec{k}_{J_2}| = 35$ GeV, the search for optimal scale values was more problematic for the observable $\langle\cos(2\phi)\rangle$, which is affected by uncertainties larger than those of the correlation $\langle\cos\phi\rangle$.

Even if in general the energy dependence of the cross section and the azimuthal decorrelations is driven mainly by the kernel, in considered kinematics the contribution of the NLO corrections to impact factors happened to be important. In order to show this, in the analysis at $|\vec{k}_{J_1}| = |\vec{k}_{J_2}| = 35$ GeV and $\sqrt{s} = 14$ TeV we calculated the coefficient C_0 and the correlations C_1/C_0 and C_2/C_0 using the NLA BFKL kernel together with the LO impact factors (properly modified to take into account the NLO dependence on the scales μ_R and s_0). We find that the NLO corrections to impact factors are relevant especially at large values of Y, as shown in Figs. 4.4, 4.8 and 4.9 and in the corresponding Tables 4.1, 4.5 and 4.6.

In the following Section we discuss the results presented here, make some comparison with Refs. [89, 99].

4.4 Discussion

We considered in NLA BFKL approach the Mueller-Navelet jet production in proton-proton collisions, using the results for NLA jet vertices obtained recently in the "small-cone" approximation. Having a simple analytic result

for the jet vertices, projected on the eigenfunction of LLA BFKL equation ((ν, n)-representation), one can implement them easily in the calculation of the Mueller-Navelet jet cross section. All necessary formulae are presented in Section 4.2.
We confirm the observation found earlier in the works devoted to forward electroproduction of a pair of vector mesons [94, 95, 96], and to Mueller-Navelet jets production [89], that NLA corrections to the impact factors (jet vertices) are very important and can not be ignored in a consistent NLA BFKL analysis.

Our numerical results, presented in Section 4.3, depend on the energy and renormalization scales, s_0 and μ_R. The dependence of the coefficients C_n on these scales cancels with NLA accuracy after the inclusion of NLA corrections to jet vertices. Nevertheless, due to next-to-NLA contributions depending on μ_R and s_0, the observables we calculated are sensitive to the choice of these scales. Here, following Ref. [94, 95, 96], we used an optimization procedure, based on the *principle of minimal sensitivity* [113, 114], which consists in taking as optimal choices for μ_R and s_0 those values for which the physical observable exhibits the minimal sensitivity to changes of both these scales.

The small-cone approximation, which we adopted here, is expected to be an adequate tool. Indeed, it is known that in the general case the dependence of the cross section on the jet cone parameter has, in the limit $R \to 0$, the form $d\sigma \sim A \ln R + B + \mathcal{O}(R^2)$ (see, for instance, [105] and Appendix C there). Indeed, in SCA the coefficients A and B are evaluated exactly. The neglected pieces $\mathcal{O}(R^2)$ for typical R values are presumably less important than the other uncertainties of our NLA BFKL calculation, in particular those related with the choice of the scales μ_R and s_0, which mimic in our method the effect of the most relevant unknown next-to-NLA BFKL terms.

To support this statement it seems natural to make a comparison between our results obtained in SCA and the numerical results presented in [89, 99], where the jet cone size was treated exactly. We can make such comparison for $|\vec{k}_{J_1}| = |\vec{k}_{J_2}| = 35$ GeV and $\sqrt{s} = 7$ and 14 TeV.

For this purpose we present in Tables 4.11, 4.12 and 4.13 our NLA results obtained with the above-discussed optimal scales setting (presented in the third column) and compare them with those for C_0, $\langle \cos\phi \rangle$ and $\langle \cos 2\phi \rangle$ taken from Table 1, 5 and 9 of [89] and reported in the second column of our Tables 4.11, 4.12 and 4.13. Moreover we show our NLA results in the case when kinematic values of the scales were used, $\mu_R^2 = s_0 = |\vec{k}_{J_1}| = |\vec{k}_{J_2|}$ (the fourth column).

Let us discuss the numbers presented in Tables 4.11, 4.12 and 4.13. Firstly one needs to say that NLA results obtained with our formulae at kinematic scale setting, $\mu_R^2 = s_0 = |\vec{k}_{J_1}||\vec{k}_{J_2}|$, can not be regarded as acceptable predictions. Indeed we got in this case results for $\langle \cos\phi \rangle$ (fourth column of Table 4.12) which are away from the kinematic range of the cosine function and for the integrated cross section C_0 (fourth column of Table 4.11) we obtained negative value in the case of the largest value of rapidity difference, $Y = 10$. This is related to the fact that NLO corrections to the jet vertices are negative and very large in the absolute value when the kinematic scale setting is used. A similar observation was done in [94, 95, 96], where the electroproduction of pair of vector meson was considered. In such situation we actually need PMS procedure in order to make reliable predictions.

Returning to the comparison with the results of [89], we observe that our results when the kinematic scales were used (forth column of Tables 4.11, 4.12 and 4.13) are quite different from those of Ref. [89] (second column of Tables 4.11, 4.12 and 4.13), where the same scales were used. As discussed above, in our opinion such big difference cannot be attributed only to the SCA. Most probably the real source of discrepancy is in the actually different representations of the NLA BFKL cross sections adopted in the two calculations, which are equivalent with NLA accuracy. Though being nontrivial, this issue definitely deserves a further study. At this stage we can only compare our results obtained with PMS procedure with those of [89].

For the integrated cross section, C_0,[2] the results presented in the second and in the third columns of Table 4.11 are rather close each other. Let us discuss now the observable $\langle \cos\phi \rangle$. Our predictions for it in the case of $|\vec{k}_{J_1}| = |\vec{k}_{J_2}| = 35$ GeV and $\sqrt{s} = 14$ TeV are shown in Fig. 4.8. In Table 4.12 we compare them (the second and the third columns) with those obtained in Ref. [89]. In this case we see more difference between two approaches, in particular our results show clear tendency for $\langle \cos\phi \rangle$ to decrease with Y, whereas [89] predicts flat Y dependence of $\langle \cos\phi \rangle$. Instead, for the observable $\langle \cos(2\phi) \rangle$ the agreement between two approaches turns to be rather good, see in Table 4.13 in the second and in the third columns.

Similarly, we compared our predictions for C_0 at present LHC energy $\sqrt{s} = 7$ TeV with those of Ref. [99]. The agreement is fair, except for the case $Y = 10$, as shown in Table 4.14.

Traditionally the BFKL predictions are assumed to be compared with the fixed order DGLAP ones, trying to find a kinematic range where possible experiment can discriminate between these two approaches. For Mueller-Navelet process the relevant parameter which can describe the separation of these two regimes is $\eta = \bar{\alpha}_s(|\vec{k}_J|)Y$, which has the meaning of the mean number of hard undetected partons inclusively produced in the process. For $|\vec{k}_J| = 35$ GeV and $Y = 6 \div 10$ this parameter takes the values $\eta = 0.82 \div 1.37$. In Section 4.3 we presented also our predictions for smaller jets transverse momenta, $|\vec{k}_J| = 20$ GeV, where $\eta = 0.92 \div 1.53$ for $Y = 6 \div 10$. In this case the BFKL description is expected to give results more different with respect to the NLO DGLAP ones. We hope that experiments with such Mueller-Navelet jet transverse momenta will be possible in the future at LHC.

[2]Our LLA results coincide with those of [89] with high accuracy. We note, in passing, that the results quoted in Tables 15, 19, 35, 38, 53 and 56 of Ref. [89], giving the coefficients C_1 and C_2 for several values of the jet kinematics, should be multiplied by a factor two to correctly reproduce the values of the ratios C_1/C_0 and C_2/C_0 quoted in other tables of that paper. We stress that this normalization problem does not affect any of the comparisons presented in this work between our results and those of Ref. [89].

Our PMS optimization procedure for the kinematics considered gives us optimal energy and factorization scales values which are substantially larger than the scale given by the kinematics, $\mu_R^2 = |\vec{k}_{J_1}||\vec{k}_{J_2}|$. This fact indicates the presence of important contributions subleading to the NLA. Therefore the estimates of the uncertainties in our predictions should be taken with care. Nevertheless they reflect the reliability of PMS method in the considered kinematics. Note that despite very large negative contribution to the MN- jets cross section coming both from the NLA corrections to the BFKL kernel and NLA corrections to the jet vertices with respect to LLA MN- jets cross section we got with our PMS procedure rather precise results in all cases except for the $\langle \cos(2\phi) \rangle$ observable at $|\vec{k}_{J_1}| = 20$ GeV and $|\vec{k}_{J_2}| = 35$ GeV and $\sqrt{s} = 14$ TeV. It would be very interesting to confront our predictions with experiment.

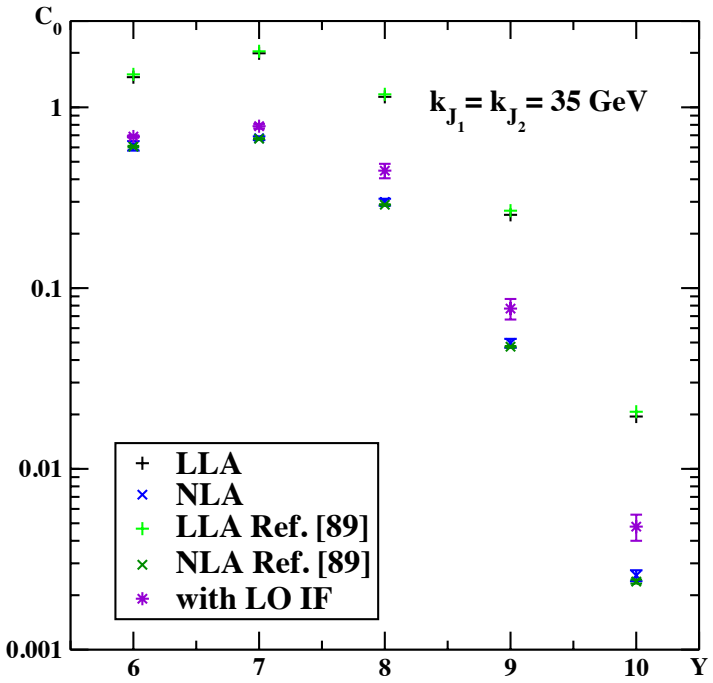

Figure 4.4: Y dependence of C_0 for $|\vec{k}_{J_1}| = |\vec{k}_{J_2}| = 35$ GeV at $\sqrt{s} = 14$ TeV.

Y	$C_0^{(\mathrm{LLA})}$	$C_0^{(\mathrm{NLA})}$	Y_0	n_R	$C_0^{(\mathrm{NLA/LO\ IF})}$	Y_0	n_R
6	1.468	0.613(37)	1	6	0.689(11)	1	12
7	1.990	0.675(16)	1	4	0.786(23)	1	6
8	1.142	0.299(13)	2	3	0.446(41)	1	2
9	0.2542	0.0496(28)	3	3	0.077(10)	1	2
10	0.01947	0.00257(18)	4	3	0.00479(79)	1	2

Table 4.1: Values of C_0 in the LLA, in the NLA and in the NLA with LO impact factors for $|\vec{k}_{J_1}| = |\vec{k}_{J_2}| = 35$ GeV at $\sqrt{s} = 14$ TeV, corresponding to the data points in Fig. 4.4. The optimal values of Y_0 and $n_R = \mu_R/\sqrt{|\vec{k}_{J_1}||\vec{k}_{J_2}|}$ for $C_0^{(\mathrm{NLA})}$ are given in the fourth and fifth columns, while those for $C_0^{(\mathrm{NLA/LO\ IF})}$ are given in the last two columns.

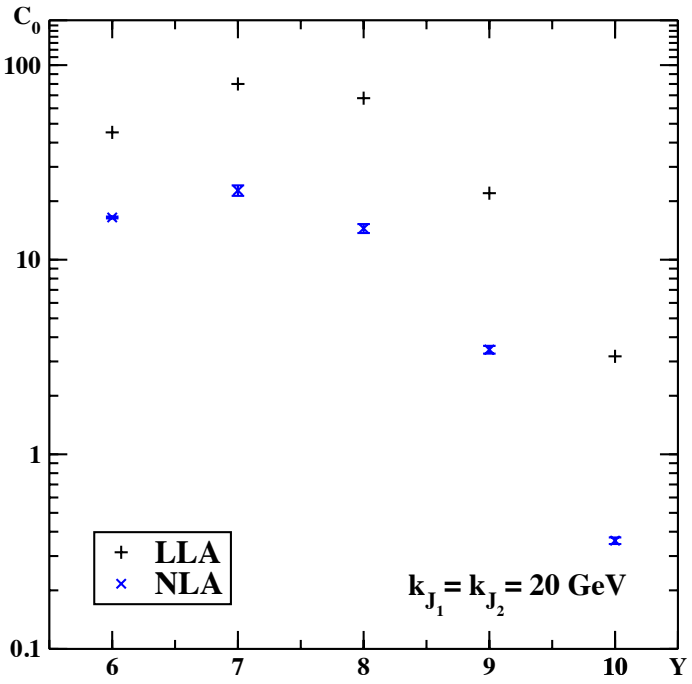

Figure 4.5: Y dependence of C_0 for $|\vec{k}_{J_1}| = |\vec{k}_{J_2}| = 20$ GeV at $\sqrt{s} = 14$ TeV.

Y	$C_0^{(\mathrm{LLA})}$	$C_0^{(\mathrm{NLA})}$	Y_0	n_R
6	45.12	16.49(19)	1	6
7	80.	22.7(14)	1	3
8	67.65	14.48(77)	2	3
9	21.99	3.45(16)	2	3
10	3.187	0.360(14)	3	3

Table 4.2: Values of C_0 in the LLA and in the NLA for $|\vec{k}_{J_1}| = |\vec{k}_{J_2}| = 20$ GeV at $\sqrt{s} = 14$ TeV, corresponding to the data points in Fig. 4.5. The last two columns give the optimal values of Y_0 and $n_R = \mu_R/\sqrt{|\vec{k}_{J_1}||\vec{k}_{J_2}|}$.

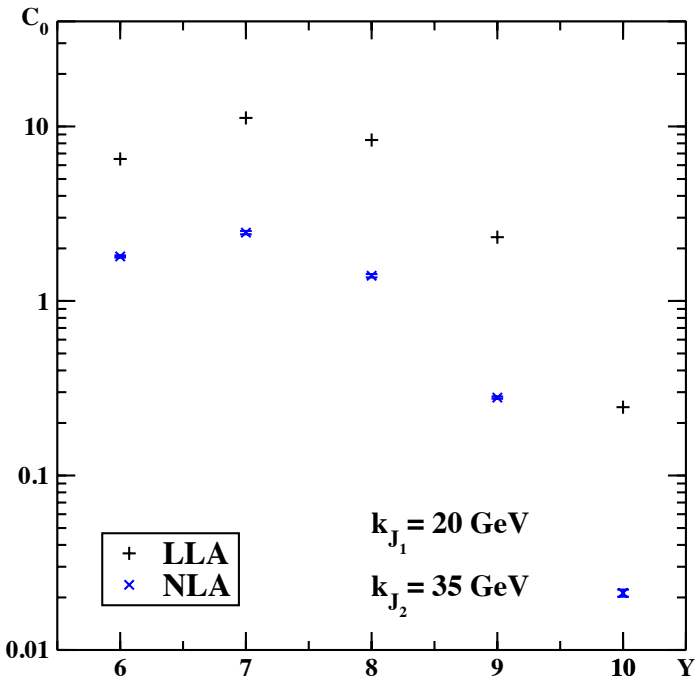

Figure 4.6: Y dependence of C_0 for $|\vec{k}_{J_1}| = 20$ GeV and $|\vec{k}_{J_2}| = 35$ GeV at $\sqrt{s} = 14$ TeV.

Y	$C_0^{(\mathrm{LLA})}$	$C_0^{(\mathrm{NLA})}$	Y_0	n_R
6	6.515	1.800(24)	1	6
7	11.192	2.463(54)	1	5
8	8.361	1.395(30)	2	5
9	2.3214	0.2794(42)	1	8
10	0.2463	0.0212(10)	2	4

Table 4.3: Values of C_0 in the LLA and in the NLA for $|\vec{k}_{J_1}| = 20$ GeV and $|\vec{k}_{J_2}| = 35$ GeV at $\sqrt{s} = 14$ TeV, corresponding to the data points in Fig. 4.6. The last two columns give the optimal values of Y_0 and $n_R = \mu_R/\sqrt{|\vec{k}_{J_1}||\vec{k}_{J_2}|}$.

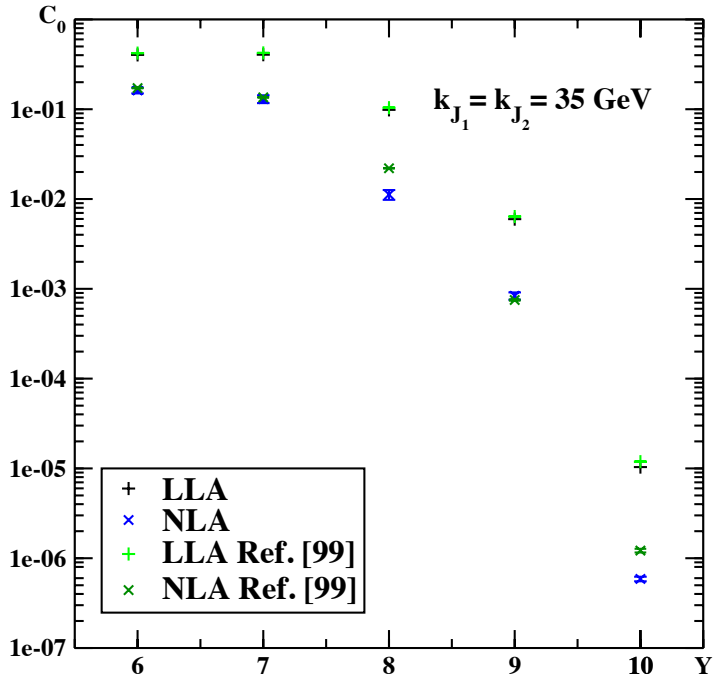

Figure 4.7: Y dependence of C_0 for $|\vec{k}_{J_1}| = |\vec{k}_{J_2}| = 35$ GeV at $\sqrt{s} = 7$ TeV.

Y	$C_0^{(\mathrm{LLA})}$	$C_0^{(\mathrm{NLA})}$	Y_0	n_R
6	0.403	0.162(12)	1	3
7	0.405	0.130(13)	2	3
8	0.0984	0.0112(14)	3	3
9	0.005974	0.000834(79)	4	4
10	$103.62\ 10^{-7}$	$5.88(35)\ 10^{-7}$	5	6

Table 4.4: Values of C_0 in the LLA and in the NLA for $|\vec{k}_{J_1}| = |\vec{k}_{J_2}| = 35$ GeV at $\sqrt{s} = 7$ TeV, corresponding to the data points in Fig. 4.7. The last two columns give the optimal values of Y_0 and $n_R = \mu_R/\sqrt{|\vec{k}_{J_1}||\vec{k}_{J_2}|}$.

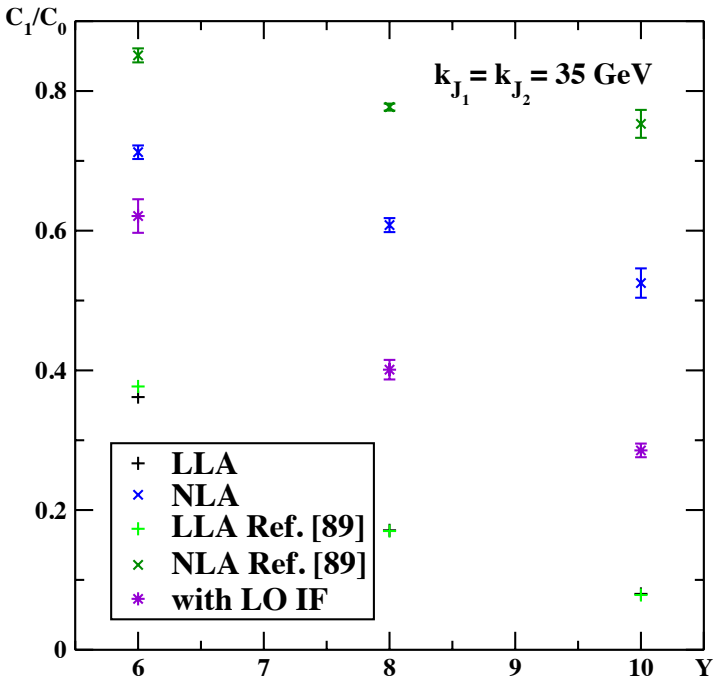

Figure 4.8: Y dependence of C_1/C_0 for $|\vec{k}_{J_1}| = |\vec{k}_{J_2}| = 35$ GeV at $\sqrt{s} = 14$ TeV.

Y	$(C_1/C_0)^{\mathrm{LLA}}$	$(C_1/C_0)^{\mathrm{NLA}}$	Y_0	n_R	$(C_1/C_0)^{\mathrm{NLA/LO\ IF}}$	Y_0	n_R
6	0.3618	0.7124(97)	1	7	0.621(24)	2	10
8	0.171	0.608(10)	2	5	0.401(14)	2	5
10	0.080	0.525(21)	2	5	0.2854(98)	3	5

Table 4.5: Values of $C_1/C_0 = \langle \cos\phi \rangle$ in the LLA, in the NLA and in the NLA with LO impact factors for $|\vec{k}_{J_1}| = |\vec{k}_{J_2}| = 35$ GeV at $\sqrt{s} = 14$ TeV, corresponding to the data points in Fig. 4.8. The optimal values of Y_0 and $n_R = \mu_R/\sqrt{|\vec{k}_{J_1}||\vec{k}_{J_2}|}$ for $(C_1/C_0)^{\mathrm{NLA}}$ are given in the fourth and fifth columns, while those for $(C_1/C_0)^{\mathrm{NLA/LO\ IF}}$ are given in the last two columns.

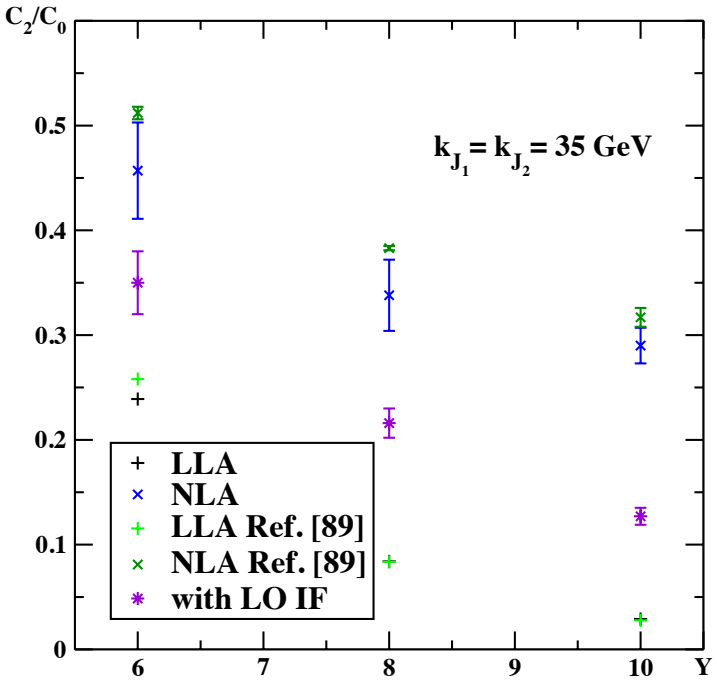

Figure 4.9: Y dependence of C_2/C_0 for $|\vec{k}_{J_1}| = |\vec{k}_{J_2}| = 35$ GeV at $\sqrt{s} = 14$ TeV.

Y	$(C_2/C_0)^{\mathrm{LLA}}$	$(C_2/C_0)^{\mathrm{NLA}}$	Y_0	n_R	$(C_2/C_0)^{\mathrm{NLA/LO\ IF}}$	Y_0	n_R
6	0.239	0.457(46)	1	4	0.350(30)	1	3
8	0.084	0.338(34)	2	3	0.216(14)	2	7
10	0.029	0.290(17)	4	6	0.1271(81)	3	12

Table 4.6: Values of $C_2/C_0 = \langle \cos\phi \rangle$ in the LLA, in the NLA and in the NLA with LO impact factors for $|\vec{k}_{J_1}| = |\vec{k}_{J_2}| = 35$ GeV at $\sqrt{s} = 14$ TeV, corresponding to the data points in Fig. 4.9. The optimal values of Y_0 and $n_R = \mu_R/\sqrt{|\vec{k}_{J_1}||\vec{k}_{J_2}|}$ for $(C_2/C_0)^{\mathrm{NLA}}$ are given in the fourth and fifth columns, while those for $(C_2/C_0)^{\mathrm{NLA/LO\ IF}}$ are given in the last two columns.

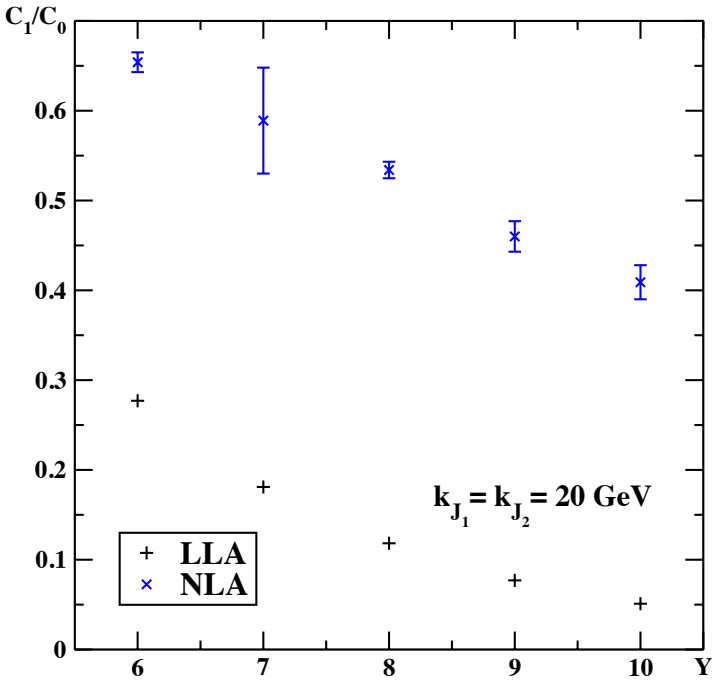

Figure 4.10: Y dependence of C_1/C_0 for $|\vec{k}_{J_1}| = |\vec{k}_{J_2}| = 20$ GeV at $\sqrt{s} = 14$ TeV.

Y	$(C_1/C_0)^{\mathrm{LLA}}$	$(C_1/C_0)^{\mathrm{NLA}}$	Y_0	n_R
6	0.277	0.654(11)	1	10
7	0.181	0.589(59)	2	6
8	0.1183	0.5340(92)	2	5
9	0.077	0.460(17)	1	5
10	0.051	0.409(19)	1	5

Table 4.7: Values of $C_1/C_0 = \langle \cos\phi \rangle$ in the LLA and in the NLA for $|\vec{k}_{J_1}| = |\vec{k}_{J_2}| = 20$ GeV at $\sqrt{s} = 14$ TeV, corresponding to the data points in Fig. 4.10. The last two columns give the optimal values of Y_0 and $n_R = \mu_R/\sqrt{|\vec{k}_{J_1}||\vec{k}_{J_2}|}$.

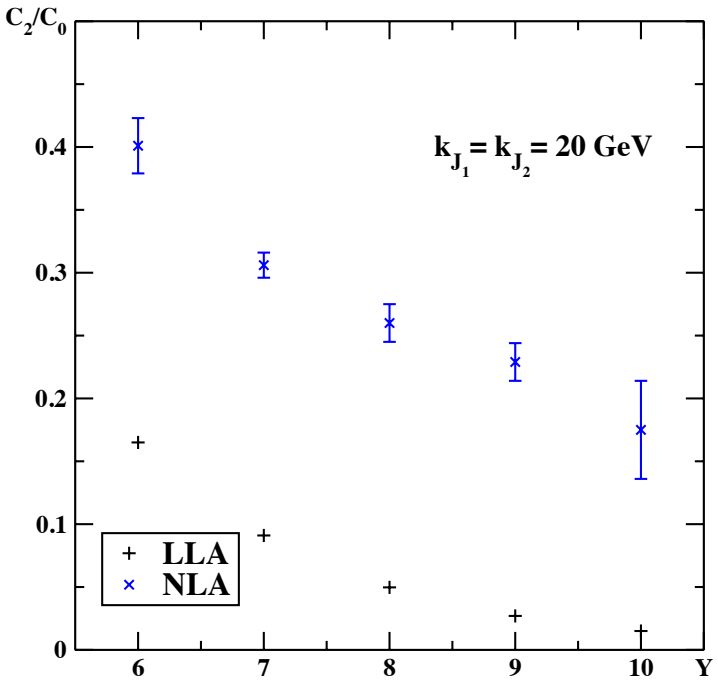

Figure 4.11: Y dependence of C_2/C_0 for $|\vec{k}_{J_1}| = |\vec{k}_{J_2}| = 20$ GeV at $\sqrt{s} = 14$ TeV.

Y	$(C_2/C_0)^{\mathrm{LLA}}$	$(C_2/C_0)^{\mathrm{NLA}}$	Y_0	n_R
6	0.165	0.401(22)	1	12
7	0.091	0.306(10)	1	3
8	0.0497	0.260(15)	2	6
9	0.027	0.229(15)	3	8
10	0.015	0.175(39)	3	4

Table 4.8: Values of $C_2/C_0 = \langle\cos(2\phi)\rangle$ in the LLA and in the NLA for $|\vec{k}_{J_1}| = |\vec{k}_{J_2}| = 20$ GeV at $\sqrt{s} = 14$ TeV, corresponding to the data points in Fig. 4.11. The last two columns give the optimal values of Y_0 and $n_R = \mu_R/\sqrt{|\vec{k}_{J_1}||\vec{k}_{J_2}|}$.

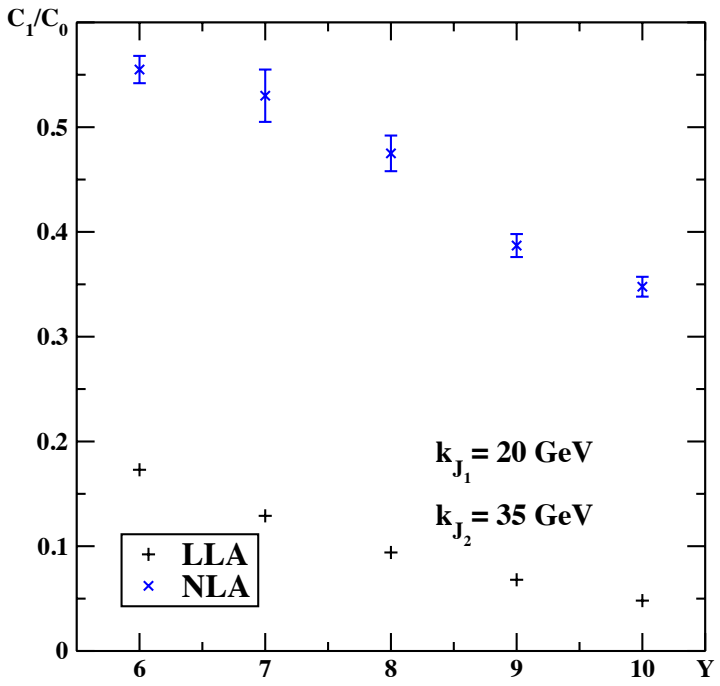

Figure 4.12: Y dependence of C_1/C_0 for $|\vec{k}_{J_1}| = 20$ GeV and $|\vec{k}_{J_2}| = 35$ GeV at $\sqrt{s} = 14$ TeV.

Y	$C_1^{(\mathrm{LLA})}/C_0^{(\mathrm{LLA})}$	$C_1^{(\mathrm{NLA})}/C_0^{(\mathrm{NLA})}$	Y_0	n_R
6	0.173	0.555(13)	1	8
7	0.129	0.530(25)	1	5
8	0.094	0.475(17)	2	5
9	0.068	0.387(11)	1	8
10	0.0481	0.3477(95)	1	9

Table 4.9: Values of $C_1/C_0 = \langle \cos\phi \rangle$ in the LLA and in the NLA for $|\vec{k}_{J_1}| = 20$ GeV and $|\vec{k}_{J_2}| = 35$ GeV at $\sqrt{s} = 14$ TeV, corresponding to the data points in Fig. 4.12. The last two columns give the optimal values of Y_0 and $n_R = \mu_R/\sqrt{|\vec{k}_{J_1}||\vec{k}_{J_2}|}$.

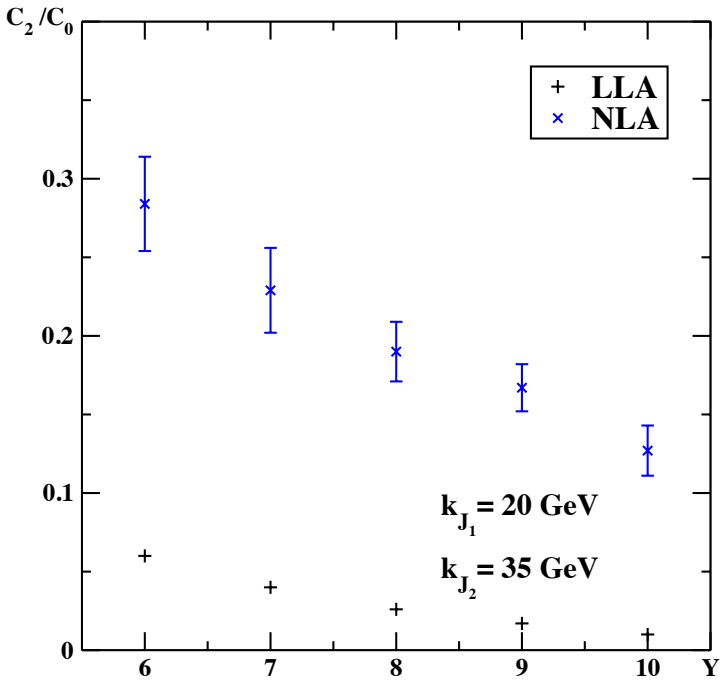

Figure 4.13: Y dependence of C_2/C_0 for $|\vec{k}_{J_1}| = 20$ GeV and $|\vec{k}_{J_2}| = 35$ GeV at $\sqrt{s} = 14$ TeV.

Y	$(C_2/C_0)^{\mathrm{LLA}}$	$(C_2/C_0)^{\mathrm{NLA}}$	Y_0	n_R
6	0.060	0.284(30)	1	3
7	0.040	0.229(27)	1	3
8	0.026	0.190(19)	1	3
9	0.017	0.167(15)	3	3
10	0.010	0.127(16)	1	4

Table 4.10: Values of $C_2/C_0 = \langle\cos(2\phi)\rangle$ in the LLA and in the NLA for $|\vec{k}_{J_1}| = 20$ GeV and $|\vec{k}_{J_2}| = 35$ GeV at $\sqrt{s} = 14$ TeV, corresponding to the data points in Fig. 4.13. The last two columns give the optimal values of Y_0 and $n_R = \mu_R/\sqrt{|\vec{k}_{J_1}||\vec{k}_{J_2}|}$.

Y	$C_0^{(\mathrm{NLA})}$ [Ref. [89]]	$C_0^{(\mathrm{NLA})}$ [here]	$C_0^{(\mathrm{NLA})}$ $Y_0 = 0$, $n_R = 1$
6	0.606	0.613	0.472
7	0.670	0.675	0.469
8	0.289	0.299	0.156
9	0.0474	0.0496	0.0144
10	0.00238	0.00257	−0.00064

Table 4.11: Comparison of our predictions for the observables C_0 in the NLA for $|\vec{k}_{J_1}| = |\vec{k}_{J_2}| = 35$ GeV at $\sqrt{s} = 14$ TeV with those of Ref. [89].

Y	$\langle \cos\phi \rangle^{\mathrm{NLA}}$ [Ref. [89]]	$\langle \cos\phi \rangle^{\mathrm{NLA}}$ [here]	$\langle \cos(\phi) \rangle^{\mathrm{NLA}}$ $Y_0 = 0$, $n_R = 1$
6	0.851	0.7124	1.0866
8	0.777	0.608	1.409
10	0.753	0.525	−2.523

Table 4.12: Comparison of our predictions for the observables $\langle \cos\phi \rangle$ in the NLA for $|\vec{k}_{J_1}| = |\vec{k}_{J_2}| = 35$ GeV at $\sqrt{s} = 14$ TeV with those of Ref. [89].

Y	$\langle \cos(2\phi) \rangle^{\mathrm{NLA}}$ [Ref. [89]]	$\langle \cos(2\phi) \rangle^{\mathrm{NLA}}$ [here]	$\langle \cos(2\phi) \rangle^{\mathrm{NLA}}$ $Y_0 = 0$, $n_R = 1$
6	0.512	0.457	0.612
8	0.383	0.338	0.661
10	0.317	0.290	-1.037

Table 4.13: Comparison of our predictions for the observables $\langle \cos(2\phi) \rangle$ in the NLA for $|\vec{k}_{J_1}| = |\vec{k}_{J_2}| = 35$ GeV at $\sqrt{s} = 14$ TeV with those of Ref. [89].

Y	$C_0^{(\mathrm{NLA})}$ [Ref. [99]]	$C_0^{(\mathrm{NLA})}$ [here]
6	0.172	0.162
7	0.135	0.130
8	0.0220	0.0112
9	0.0007502	0.000834
10	0.00001216	0.000000588

Table 4.14: Comparison of our predictions for the observable C_0 for $|\vec{k}_{J_1}| = |\vec{k}_{J_2}| = 35$ GeV at $\sqrt{s} = 7$ TeV with those of Ref. [99].

Appendix A

Table of Integrals

Fundamental integrals To obtain the results in the Chapter 3, we made use of the following integrals:

$$\bullet \int \frac{d^{D-2}k}{\left(\vec{k}-\vec{q}\right)^2}\frac{1}{\vec{k}^{\,2}+\left(\vec{k}-\vec{q}\right)^2} = \frac{1}{2}\int \frac{d^{D-2}k}{\vec{k}^{\,2}\left(\vec{k}-\vec{q}\right)^2} = \pi^{1+\varepsilon}\frac{\Gamma(1-\varepsilon)\left[\Gamma(1+\varepsilon)\right]^2}{\varepsilon\Gamma(1+2\varepsilon)}\,; \tag{A.1}$$

$$\bullet \int \frac{d^{D-2}k}{\vec{k}^{\,2}}\theta\left(\Lambda^2-\vec{k}^{\,2}\right) = \pi^{1+\varepsilon}\frac{\Gamma(1-\varepsilon)\left[\Gamma(1+\varepsilon)\right]^2}{\varepsilon\Gamma(1+2\varepsilon)}\Lambda^{2\varepsilon}\,. \tag{A.2}$$

Angular average Here we calculate the averaging over the relative angle between the vectors $\vec{k}$ and $\vec{q}-\vec{k}$ used in Eqs. (3.54) and (3.90):

$$\int d^{D-2}k\frac{(1-\beta)\,\vec{k}\cdot\left(\vec{k}-\beta\vec{q}\right)}{\vec{k}^{\,2}\left(\vec{k}-\beta\vec{q}\right)^2} = \int\frac{d^{D-2}k}{\vec{k}^{\,2}}\theta\Big((1-\beta)\,|\vec{k}|-\beta|\vec{q}-\vec{k}|\Big)\,. \tag{A.3}$$

If ϕ is the relative angle between the vectors $\vec{k}$ and $\vec{q}-\vec{k}$, we can write

$$\vec{k} = k\,(\cos\phi,\,\sin\phi) \quad\text{and}\quad \left(\vec{q}-\vec{k}\right) = (q-k)\,(1,0)\;. \tag{A.4}$$

In this way

$$I = \Big\langle\frac{(1-\beta)\,\vec{k}\cdot\left(\vec{k}-\beta\vec{q}\right)}{\vec{k}^{\,2}\left(\vec{k}-\beta\vec{q}\right)^2}\Big\rangle_\phi$$

$$= \frac{1}{2\pi}\int_0^{2\pi} d\phi \frac{1-\beta}{k^2} \frac{(1-\beta)\,k^2 - \beta k\,(q-k)\cos\phi}{\left[(1-\beta)^2\,k^2 + \beta^2\,(q-k)^2 - 2\beta\,(1-\beta)\,k\,(q-k)\cos\phi\right]}$$

and using the complex variables $\omega = e^{\imath\phi}$, we obtain

$$\begin{aligned} I &= \frac{1-\beta}{2\pi k^2}\oint \frac{d\omega}{2\imath\omega} \frac{2\,(1-\beta)\,k^2\omega - \beta k\,(q-k)\,(1+\omega^2)}{(1-\beta)^2\,k^2\omega + \beta^2\,(q-k)^2\,\omega - \beta\,(1-\beta)\,k\,(q-k)\,(1+\omega^2)} \\ &= -\frac{1-\beta}{2k^2}\frac{1}{2\pi\imath}\frac{1}{\beta\,(1-\beta)\,k\,(q-k)} \\ &\times \oint \frac{d\omega}{\omega}\frac{2\,(1-\beta)\,k^2\omega - \beta k\,(q-k) - \beta k\,(q-k)\,\omega^2}{\left(\omega - \frac{(1-\beta)k}{\beta(q-k)}\right)\left(\omega - \frac{\beta(q-k)}{(1-\beta)k}\right)}\,, \end{aligned} \tag{A.5}$$

with $(1-\beta)\,|k| \geq \beta|q-k|$. Using the Residue Theorem we get

$$I = \frac{1}{k^2}\,\theta\Big(\,(1-\beta)\,|k| - \beta|q-k|\,\Big)\,. \tag{A.6}$$

Bibliography

[1] T. Regge, *Nuovo Cim.* **14** (1959) 951.

[2] P.D.B. Collins, *An introduction to Regge Theory and high energy physics*, Cambridge University Press (1977).

[3] V. Barone, E. Predazzi, *High-Energy Particle Diffraction*, Springer (2002).

[4] G.F.P. Chew, S.C. Frautschi, *Phys. Rev. Lett.* **7** (1961) 394.

[5] V.N. Gribov, *Zh. Eksp. Teor. Fiz.* **41** (1961) 667.

[6] I.Ya. Pomeranchuk *Sov. Phys.* **5** (1958) 499.

[7] J.R. Forshaw & D.A. Ross, *Quantum Chromodynamics and the Pomeron*, Cambridge University Press (1997).

[8] M. Froissart, *Phys. Rev.* **123** (1961) 1053.

[9] L.N. Lipatov, *Nucl. Phys.* **B 452** (1995) 369.

[10] L.N. Lipatov, *Phys. Rept.* **286** (1997) 131.

[11] V.S. Fadin, E.A. Kuraev, L.N. Lipatov, *Phys. Lett.* **B 60** (1975) 50.

[12] E.A. Kuraev, L.N. Lipatov, V.S. Fadin, *Sov. Phys.* JETP **44** (1976) 443 [*Zh. Eksp. Teor. Fiz.* **71** (1976) 840].

[13] E.A. Kuraev, L.N. Lipatov, V.S. Fadin, *Sov. Phys.* JETP **45** (1977) 199 [*Zh. Eksp. Teor. Fiz.* **72** (1977) 377].

[14] I.I. Balitsky, L.N. Lipatov, *Sov. J. Nucl. Phys.* **28** (1978) 822 [*Yad. Fiz.* **15** (1972) 781].

[15] V.N. Gribov, L.N. Lipatov, *Sov. J. Nucl. Phys.* **15** (1972) 438 [*Yad. Fiz.* **15** (1972) 781].

[16] V.N. Gribov, L.N. Lipatov, *Sov. J. Nucl. Phys.* **15** (1972) 675 [*Yad. Fiz.* **15** (1972) 1218].

[17] L.N. Lipatov, *Sov. J. Nucl. Phys.* **20** (1975) 94 [*Yad. Fiz.* **20** (1974) 181].

[18] G. Altarelli, G. Parisi, *Nucl. Phys.* **B 126** (1977) 298.

[19] Y.L. Dokshitzer, *Sov. Phys.* JETP **46** (1977) 641 [*Zh. Eksp. Teor. Fiz.* **73** (1977) 1216].

[20] M. Gell-Mann, M.L. Goldberger, F.E. Low, E. Marx, F. Zachariasen, *Phys. Rev.* **B 133** (1964) 145.

[21] B.L. Ioffe, V.S. Fadin, L.N. Lipatov, *Quantum Chromodynamics Perturbative and Nonperturbative Aspects*, Cambridge Monographs on Particle Physics, Nuclear Physics and Cosmology (2010).

[22] S. Mandelstam, *Phys. Rev.* **B 137** (1964) 949.

[23] M.T. Grisaru, H.J. Schnitzer, *Phys. Lett.* **30** (1973) 811.

[24] M.T. Grisaru, H.J. Schnitzer, H.S. Tsao, *Phys. Rev.* **D 8** (1973) 4498.

[25] L.N. Lipatov, *Sov. J. Nucl. Phys.* **23** (1976) 338 [*Yad. Fiz.* **23** (1976) 642].

[26] V.S. Fadin, V.E. Sherman, *Zh. Eksp. Teor. Fiz. Pis'ma* **23** (1976) 599.

[27] V.S. Fadin, V.E. Sherman, *Zh. Eksp. Teor. Fiz. Pis'ma* **72** (1977) 1640.

[28] A.V. Bogdan, V. del Duca, V.S. Fadin, E.W.N. Glover, *JHEP* **0203** (2002) 032.

[29] M.I. Kotsky, L.N. Lipatov, A. Principe, M.I. Vyazovsky, *Nucl. Phys.* **B 648** (2003) 277.

[30] V.S. Fadin BUDKER-INP-1998-55 (1998) 742.

[31] L.N. Lipatov, V.S. Fadin, *Zh. Eksp. Teor. Fiz. Pis'ma* **49** (1989) 311 [JETP *Lett.* **49** (1989) 352] *Yad. Fiz.* **50** (1989) 1141 [*Sov. J. Nucl. Phys.* **50** (1989) 712].

[32] V.S. Fadin, *Zh. Eksp. Teor. Fiz. Pis'ma* **61** (1995) 342.

[33] V.S. Fadin, R. Fiore, A. Quartarolo, *Phys. Rev.* **D 53** (1996) 2729.

[34] V.S. Fadin, M.I. Kotsky, *Yad. Fiz.* **59** (6) (1996) 1080.

[35] V.S. Fadin, R. Fiore, M.I. Kotsky, *Phys. Lett.* **B 359** (1995) 181.

[36] V.S. Fadin, R. Fiore, M.I. Kotsky, *Phys. Lett.* **B 387** (1996) 593.

[37] V.S. Fadin, R. Fiore, M.G. Kozlov, A.V. Reznichenko, *Phys. Lett.* **B 639** (2006) 74.

[38] R.E. Cutkosky, *J. Math. Phys.* **1** (1960) 429.

[39] J. Bartels, *Phys. Rev.* **D 11** (1975) 2977.

[40] J. Bartels, *Phys. Rev.* **D 11** (1975) 2989.

[41] J. Bartels, *Nucl. Phys.* **B 175** (1980) 365.

[42] V.S. Fadin, L.N. Lipatov, *Nucl. Phys.* **B 406** (1993) 259.

[43] V.S. Fadin, R. Fiore, *Phys. Lett.* **B 440** (1998) 359.

[44] L.N. Lipatov, *Nucl. Phys.* **B 365** (1991) 641.

[45] V.S. Fadin, L.N. Lipatov, *Nucl. Phys.* B (Proc. Suppl.) **A 29** (1992) 93.

[46] V.S. Fadin, L.N. Lipatov, *Nucl. Phys.* **B 477** (1996) 767.

[47] V.S. Fadin, M.I. Kotsky, L.N. Lipatov, *Phys. Lett.* **B 415** (1997) 97 [*Yad. Fiz.* **61** (6) (1998) 716].

[48] V.S. Fadin, D.A. Gorbachev, JETP *Letters* **71** (2000) 222.

[49] V.S. Fadin, D.A. Gorbachev, *Pis'ma v ZhETF* **71** (2000) 322 [*Yad. Fiz.* **63** (12) (2000) 1].

[50] V.S. Fadin, R. Fiore, A. Flachi, M.I. Kotsky, *Phys. Lett.* **B 422** (1998) 287.

[51] S. Catani, M. Ciafaloni, F. Hautmann, *Phys. Lett.* **B 242** (1990) 97.

[52] S. Catani, M. Ciafaloni, F. Hautmann, *Nucl. Phys.* **B 366** (1991) 135.

[53] V.S. Fadin, R. Fiore, A. Papa, *Phys. Rev.* **D 60** (1999) 07025.

[54] V.S. Fadin, L.N. Lipatov, *Phys. Lett.* **B 429** (1998) 127.

[55] G. Camici, M. Ciafaloni, *Phys. Lett.* **B 430** (1998) 349.

[56] C.R. Schmidt *Phys. Rev.* **D 60** (1999) 074003.

[57] J.R. Forshaw, D.A. Ross, A. Sabio Vera, *Phys.Lett.* **B 455** (1999) 273.

[58] M. Ciafaloni, D. Colferai, G.P. Salam *JHEP* **9910** (1999) 017.

[59] V.S. Fadin, R. Fiore, M.I. Kotsky, A. Papa, *Phys. Lett.* **D 61** (2000) 094005.

[60] V.S. Fadin, R. Fiore, M.I. Kotsky, A. Papa, *Phys. Lett.* **D 61** (2000) 094006.

[61] M. Ciafaloni, D. Colferai, *Nucl. Phys.* **B 538** (1999) 187.

[62] M. Ciafaloni, G. Rodrigo, *JHEP* **0005** (2000) 042.

[63] J. Bartels, S. Gieseke, C.F. Qiao, *Phys. Rev.* **D 63** (2001) 056014 [*Erratum-ibid.* **D 65** (2002) 079902].

[64] J. Bartels, S. Gieseke, A. Kyrieleis, *Phys. Rev.* **D 65** (2002) 014006.

[65] J. Bartels, D. Colferai, S. Gieseke, A. Kyrieleis, *Phys. Rev.* **D 66** (2002) 094017.

[66] J. Bartels, *Nucl. Phys.* (Proc. Suppl.) (2003) 116.

[67] J. Bartels, A. Kyrieleis, *Phys. Rev.* **D 70** (2004) 114003.

[68] V.S. Fadin, D.Yu. Ivanov, M.I. Kotsky, *Phys. Atom. Nucl.* **65** (2002) 1513 [Yad. Fiz. 65 (2002) 1551].

[69] V.S. Fadin, D.Yu. Ivanov, M.I. Kotsky, *Nucl. Phys.* **B 658** (2003) 156.

[70] D.Yu. Ivanov, M.I. Kotsky, A. Papa, *Eur. Phys. J* **C 38** (2004) 195.

[71] D.Yu. Ivanov, M.I. Kotsky, A. Papa, *Nucl. Phys.* (Proc. Suppl.) 146 (2005) 117.

[72] J. Bartels, D. Colferai, G. Vacca, *Eur. Phys. J.* **C 24** (2002) 83.

[73] J. Bartels, D. Colferai, G. Vacca, *Eur. Phys. J.* **C 29** (2003) 235.

[74] C. Caporale, D.Yu. Ivanov, B. Murdaca, A. Papa, A. Perri, *JHEP* **1202** (2012) 101.

[75] D.Yu. Ivanov, A. Papa, *JHEP* **1205** (2012) 086.

[76] H. Cheng, T.T. Wu, *Expanding Protons: Scattering at High Energies*, MIT Press, Cambridge (1987).

[77] J. Bartels, *Nucl. Phys.* **B 175** (1980) 365.

[78] J. Kwiecinski, M. Praszalowicz, *Phys. Lett.* **B 94** (1980) 413.

[79] R. Kirschner, L.N. Lipatov, L. Szymanowski, *Nucl. Phys.* **B 425** (1994) 579.

[80] E.N. Antonov, L.N. Lipatov, E.A. Kuraev, I.O. Cherednikov, *Nucl. Phys.* **B 721** (2005) 111.

[81] M. Hentschinski, DESY-THESIS-2009-025.

[82] J. Bartels, L.N. Lipatov, A.S. Vera, *Phys. Rev.* **D 80** (2009) 045002.

[83] M. Hentschinski, A. Sabio Vera, *Phys. Rev.* **D 85** (2012) 056006.

[84] G. Chachamis, M. Hentschinski, J. Madrigal Martinez, A. Sabio Vera, *Nucl. Phys.* **B 861** (2012) 133.

[85] M. Hentschinski, B. Murdaca, A. Sabio Vera, arXiv:1206.1622.

[86] M. Hentschinski, B. Murdaca, A. Sabio Vera, in preparation.

[87] A.H. Mueller, W.K. Tang, *Phys. Lett.* **B 284** (1992) 123.

[88] A.H. Mueller, H. Navelet, *Nucl. Phys.* **B 282** (1987) 727.

[89] D. Colferai, F. Schwennsen, L. Szymanowski, S. Wallon, *JHEP* **12** (2010) 026.

[90] S.D. Ellis, Z. Kunszt, D.E. Soper, *Phys. Rev.* **D 40** (1989) 2188.

[91] Z. Kunszt, D.E. Soper, *Phys. Rev.* **D 46** (1992) 192.

[92] G. Dissertori, I. Knowles, M. Schmelling, *Quantum Chromodynamics*, Oxford Science Publications (2003).

[93] M. Ciafaloni, *Phys. Lett.* **B 429** (1998) 363.

[94] D. Ivanov, A. Papa, *Nucl. Phys.* **B 732** (2006) 183.

[95] D. Ivanov, A. Papa, *Eur. Phys. J.* **C 49** (2007) 947.

[96] F. Caporale, A. Papa, A. Sabio Vera, *Eur. Phys. J.* **C 53** (2008) 525.

[97] F. Caporale, D.Yu. Ivanov, A. Papa, *Eur. Phys. J.* **C 58** (2008) 1.

[98] V.S. Fadin, arXiv:hep-ph/9807527.

[99] B. Ducloué, L. Szymanowski, S. Wallon, arXiv:1208.6111.

[100] A. Sabio Vera, *Nucl. Phys.* **B 746** (2006) 1.

[101] A. Sabio Vera, F. Schwennen, *Nucl. Phys.* **B 776** (2007) 170.

[102] C. Marquet, C. Royon, *Phys. Rev.* **D 79** (2009) 034028.

[103] F. Caporale, D.Yu. Ivanov, B. Murdaca, A. Papa, arXiv:1209.6233.

[104] F. Caporale, D.Yu. Ivanov, B. Murdaca, A. Papa, in preparation.

[105] M. Furman, *Nucl. Phys.* **B 197** (1982) 413.

[106] F. Aversa, P. Chiappetta, M. Greco, J.P. Guillet, *Nucl. Phys.* **B 327** (1989) 105.

[107] F. Aversa, P. Chiappetta, M. Greco, J.P. Guillet, *Z. Phys.* **C 46** (1990) 253.

[108] Jäger, M. Stratmann, W. Vogelsang, *Phys. Rev.* **D 70** (2004) 034010.

[109] A.V. Kotikov, L.N. Lipatov, *Nucl. Phys.* **B 582** (2000) 19.

[110] A.V. Kotikov, L.N. Lipatov, *Nucl. Phys.* **B 661** (2003) 19 [*Erratum-ibid.* **B 685** (2004) 405].

[111] S. Cerci, D. d'Enterria, *AIP Conf. Proc.* **1105** (2009) 28.

[112] A.D. Martin, W.J. Stirling, R.S. Thorne, G. Watt, *Eur. Phys. J.* **C 63** (2009) 189.

[113] P.M. Stevenson, *Phys. Lett.* **B 100** (1981) 61.

[114] P.M. Stevenson, *Phys. Rev.* **D 23** (1981) 2916.

Acknowledgments

I would like to express my very great appreciation to my supervisor, Professor Alessandro Papa, not only for the fantastic subject that he proposed, but also for his suggestions, and for helping me discover the fascinating world of physics.
A particular thank you to my collaborator and friend, Dr. Francesco Caporale, who has been a reference point since I started working on my PhD.
My grateful thanks are also extended to Dr. Dmitry Yu. Ivanov for the stimulating conversation.
I would also like to extend my thanks to Dr. Agustin Sabio Vera and Dr. Martin Hentschinski for the hospitality at the Universidad Autónoma de Madrid.

I would also like to thank my friends Caterina, Gianfranco, Ilenia and Valentina, and in particular to Cinzia, Mariaelena and Rocco. A special thank you to Denise and her family.

Finally, thank you to my family and my boyfriend, to whom I dedicate this thesis.